9. SITE 721[1]

Shipboard Scientific Party[2]

HOLE 721A

Date occupied: 3 September 1987

Date departed: 3 September 1987

Time on hole: 13 hr

Position: 16°40.636′N, 59°51.879′E

Water depth (sea level; corrected m, echo-sounding): 1944.8

Water depth (rig floor; corrected m, echo-sounding): 1955.3

Bottom felt (m, drill pipe): 1952.2

Penetration (m): 86.4

Number of cores: 9

Total length of cored section (m): 86.4

Total core recovered (m): 89.28

Core recovery (%): 103.3

Oldest sediment cored:
Depth sub-bottom (m): 86.4
Nature: nannofossil ooze
Age: late Pliocene
Measured velocity (km/s): 1.55

HOLE 721B

Date occupied: 4 September 1987

Date departed: 6 September 1987

Time on hole: 50 hr, 15 min

Position: 16°40.636′N, 59°51.879′E

Water depth (sea level; corrected m, echo-sounding): 1944.8

Water depth (rig floor; corrected m, echo-sounding): 1955.3

Bottom felt (m, drill pipe): 1949.0

Penetration (m): 424.2

Number of cores: 44

Total length of cored section (m): 424.2

Total core recovered (m): 342.8

Core recovery (%): 80.8

Oldest sediment cored:
Depth sub-bottom (m): 424.2
Nature: siltstone, claystone, and mudstone
Age: early Miocene
Measured velocity (km/s): 1.55

HOLE 721C

Date occupied: 6 September 1987

Date departed: 6 September 1987

Time on hole: 20 hr, 25 min

Position: 16°40.636′N, 59°51.879′E

Water depth (sea level; corrected m, echo-sounding): 1944.8

Water depth (rig floor; corrected m, echo-sounding): 1955.3

Bottom felt (m, drill pipe): 1949.1

Penetration (m): 138.0

Number of cores: 15

Total length of cored section (m): 138.0

Total core recovered (m): 133.8

Core recovery (%): 97

Oldest sediment cored:
Depth sub-bottom (m): 138.0
Nature: nannofossil ooze
Age: early Pliocene
Measured velocity (km/s): 1.55

Principal Results: Site 721 is located on the Owen Ridge in the western Arabian Sea. Its objective was to recover a continuous upper Neogene section of pelagic sediments that record changes in the monsoonal circulation system.

The section penetrated at Site 721 ranges from early Miocene to Holocene in age and has been divided into four major lithologic units.

Unit I (0.0–289.0 mbsf) consists exclusively of alternating light and dark layers of foraminifer-bearing to foraminifer-nannofossil ooze-chalk, and nannofossil ooze-chalk of Holocene to late Miocene age. The sediments of this unit reveal strong cyclicity that is indicated by changes in color, bulk density, carbonate content, and particularily well by magnetic susceptibility on whole-round cores.

Unit II (289.0–309.9 mbsf) is a siliceous-bearing nannofossil- to diatomaceous nannofossil chalk of early late Miocene age. Sediments of this unit show evidence of soft sediment deformation throughout. In contrast to Unit I, biogenic opal is an abundant component of Unit II, and both diatoms and radiolarians are preserved in the sediments. Microfossil assemblages in general are characterized by the lack of typical tropical species and the dominance of cool water assemblages.

Unit III (309.9–340.7 mbsf) is comprised of nannofossil chalk of middle Miocene age. Silica preservation is poor in the carbonate-rich chalks (which average about 77% $CaCO_3$). A hiatus (from Zone NN9 to NN5) occurs at the top of this unit (at about 310 mbsf), and as much as 150 m of the middle Miocene section may be missing.

Unit IV (340.7–424.2 mbsf) is characterized by turbiditic intercalations of silts and mud turbidites and contrasts from the dominantly pelagic facies of the overlying units. Clay-bearing nannofossil chalk grades downsection into calcareous silty clay and clayey siltstone of early Miocene age. Preservation of planktonic calcareous and opaline tests is poor and benthic foraminifers from the upper and middle bathyal depths are absent. The increase of pelagic deposits upsection is related to the uplift of the Owen Ridge out of the regime of turbidite deposition.

The sediments at Site 721 indicate that the monsoonal upwelling system of the northern Indian Ocean was active in the late Miocene. Turbidite deposition on the ridge ceased as the ridge rose over the surrounding seafloor during the early Miocene in the wake of tectonic reorganization of spreading centers and transform faults in the Indian Ocean.

[1] Prell, W. L., Niitsuma, N., et al., 1989. *Proc. ODP, Init. Repts.*, 117: College Station, TX (Ocean Drilling Program).
[2] Shipboard Scientific Party is as given in the list of Participants preceding the contents.

BACKGROUND AND OBJECTIVES

Site 721 is located near the crest of the Owen Ridge at 16°40.636′N and 59°51.879′E, at a water depth of 1944.8 m (Fig. 1). The site is positioned above the regional carbonate lysocline to avoid major dissolution changes in the calcareous deposits. The site was selected on Line 40 (2010 hr, 3 June 1986) of the *Robert Conrad* (Leg 27-04) site survey (Fig. 2). Total sediment thickness is about 1.62 s (about 1400 m), and the target depth is at 0.5 s (about 425 m). The upper part of the section (0.34 s, ~290 mbsf) has relatively smooth, low-amplitude parallel reflectors with some structure near 0.22 s (about 180 mbsf). A prominent seismic reflector (see "Seismic Stratigraphy" section, this chapter) with complex structure occurs at 0.34–0.38 s (~290–320 mbsf), and the top of a strongly reflective sequence occurs at 0.47 s (about 410 mbsf). Correlating the recovered section at DSDP Site 224 (Whitmarsh et al., 1974) with the seismic data from the site survey, the upper seismic reflector was thought to be of late Miocene age and the lower reflector to be of middle to early Miocene age. The strongly reflective sequence below the reflector at 0.47 s was interpreted as correlative with the terrigenous detrital clayey silty claystones observed in Site 224. The target depth of Site 721 was calculated to penetrate this terrigenous sequence at about 420 mbsf.

OPERATIONS

The vessel departed Site 720 at 2100 hr on 2 September for the area of the Owen Ridge Sites 721 and 722. Because of the

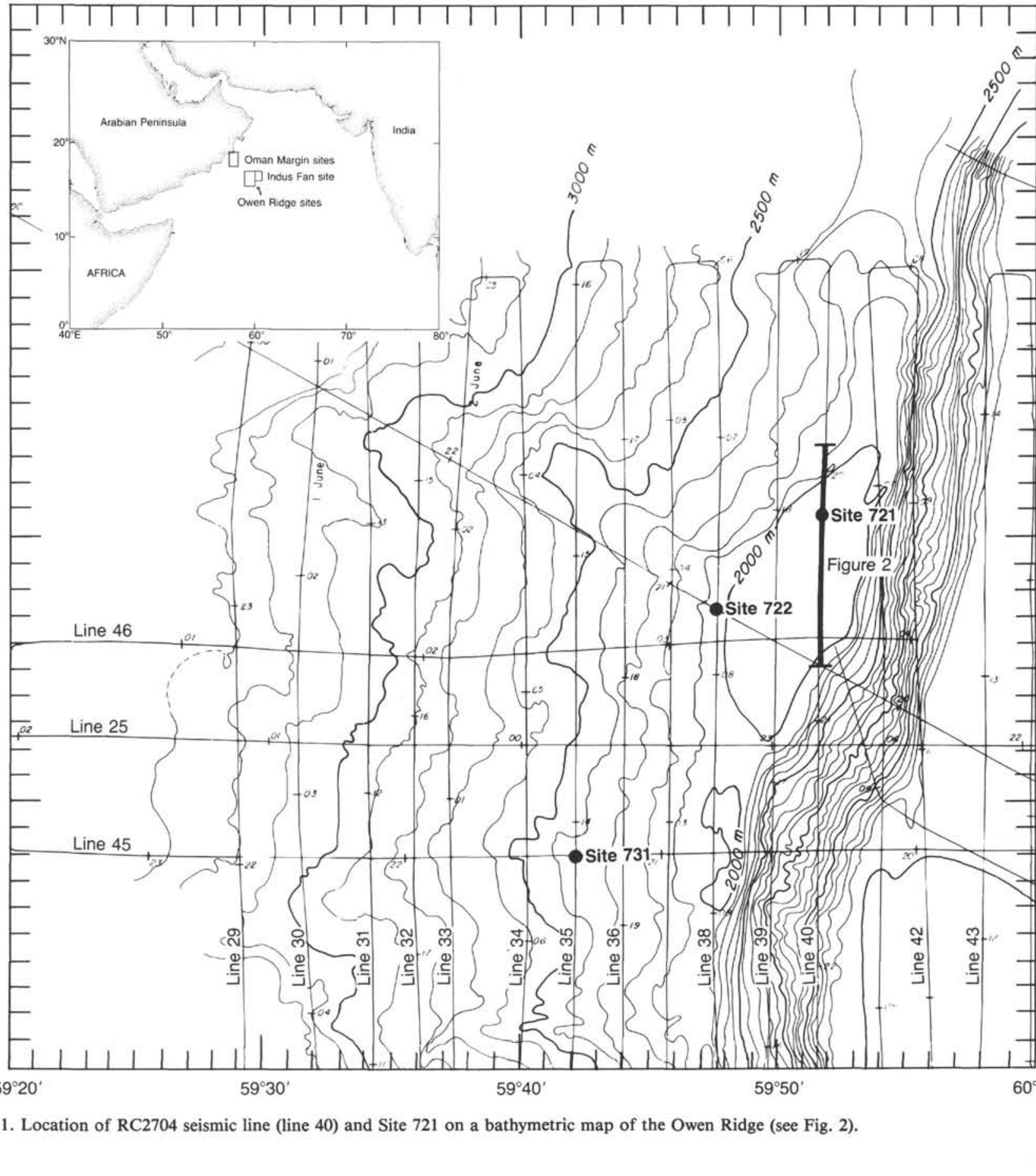

Figure 1. Location of RC2704 seismic line (line 40) and Site 721 on a bathymetric map of the Owen Ridge (see Fig. 2).

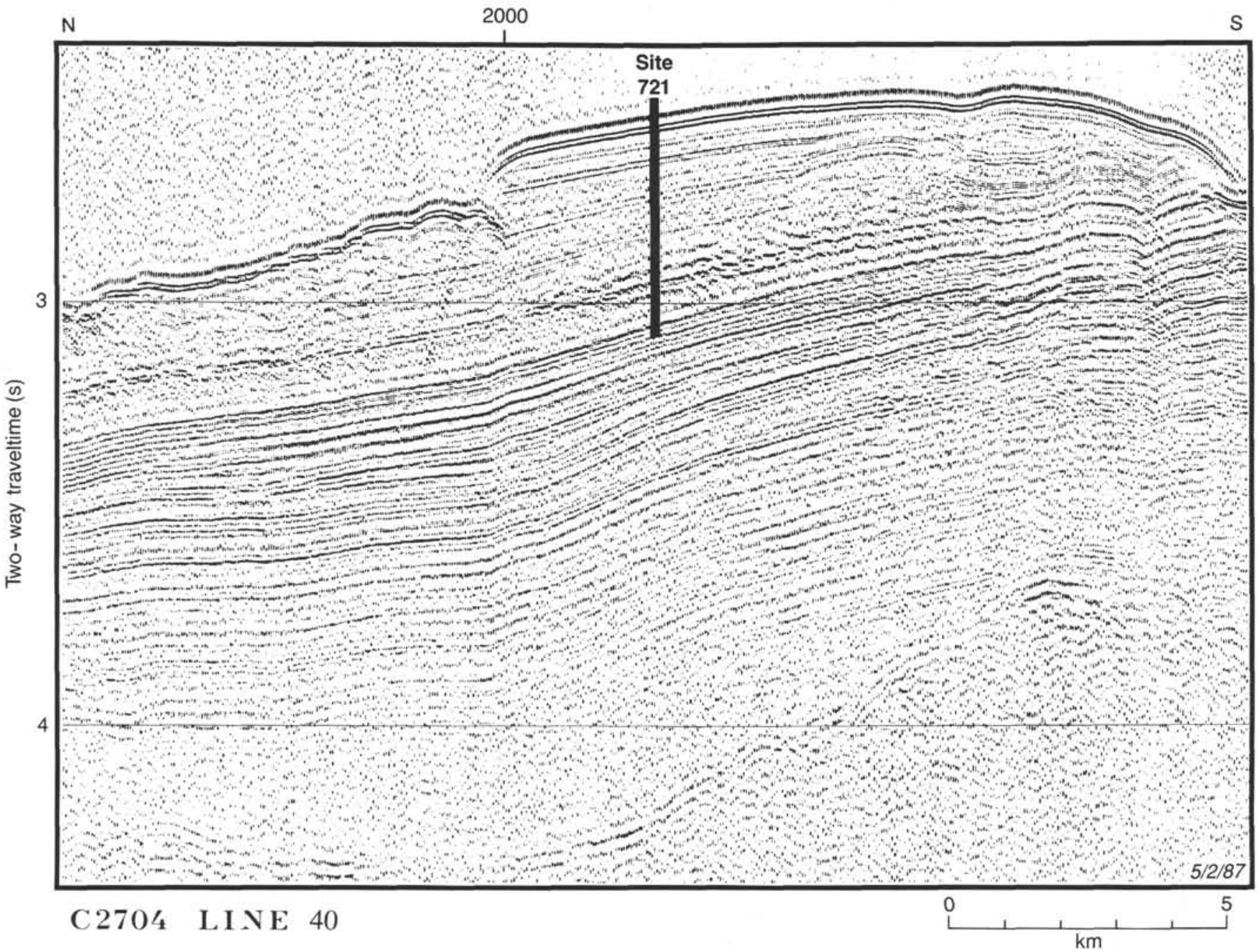

Figure 2. Seismic profile of Site 721 (Line RC2704-40).

proximity of the two sites, it was decided to survey both locations on approach to Site 721, and the seismic gear was deployed upon departure from Site 720. Good GPS coverage ensured accurate positioning throughout the survey and site approach, and a high-resolution positioning chart was obtained for the ship's track (Fig. 3). Upon passage of the target location of Site 722 at 0900 hr on 3 September, a beacon was dropped at the site, and the ship continued approach to Site 721, where the beacon was dropped at 1100 hr. The final position of Site 721 was established as 16°40.636′N and 59°51.879′E. The seismic gear was retrieved and the ship positioned, and the mud line of Hole 721A was established at 1952 m (bottom felt) at 1515 hr on 3 September.

Nine APC cores were drilled with a maximum overpull of 10,000 pounds with excellent recovery (>100%) to a total depth for Hole 721A of 86.4 mbsf (Table 1). Core 117-721A-10H stuck in a clay-rich interval, and the core barrel failed at 140,000 pounds overpull, so that Hole 721A had to be abandoned.

Hole 721B was spudded 20 m west of Hole 721A at 0017 hr on 4 September. Nine APC cores recovered >100% of the cored section to 86.0 mbsf. Because of an increase of overpull to 25,000 pounds, drilling mode was switched to XCB coring from Core 117-721B-10X. Forty-four cores were drilled to the target depth of 424.2 mbsf with an average recovery of 81%. After clearing the mud line, the ship positioned 20 m west of Hole 721B and spudded Hole 721C at 0335 hr on 6 September. Ten APC cores yielded >100% recovery to a depth of 89.9 mbsf, where a maximum overpull of 35,000 pounds necessitated a switch to XCB coring. Overall recovery was 97% in the 138.0 m total depth of Hole 721C. The *in-situ* pore-water sampler was deployed twice in Hole 721C. At 2230 hr on 6 September, the mud line was cleared and the ship relocated to Site 722 without pulling pipe.

LITHOSTRATIGRAPHY

Lithologic Units

Sediments recovered at Site 721 span the time interval from early Miocene to Holocene and are divided into four lithologic units (Table 2, Fig. 4). This subdivision is based on visual core descriptions, smear slide analysis, calcium carbonate content (Table 3, Fig. 5), and biostratigraphic data. Lithologic Unit I is further divided into two subunits.

Unit I (Depth: 0–289.0 mbsf; Age: Holocene to late Miocene)

Core 117-721A-1H to Section 117-721A-9H, CC; Cores 117-721B-1H to 117-721B-30X; Cores 117-721C-1H to 117-721C-15X. Bottom of Unit I not reached in Holes 721A and 721C.

Subunit IA (Depth: 0–261.2 mbsf)

Lithologic Subunit IA extends from 0 to 261.2 mbsf and consists of alternating light and dark layers of foraminifer-bear-

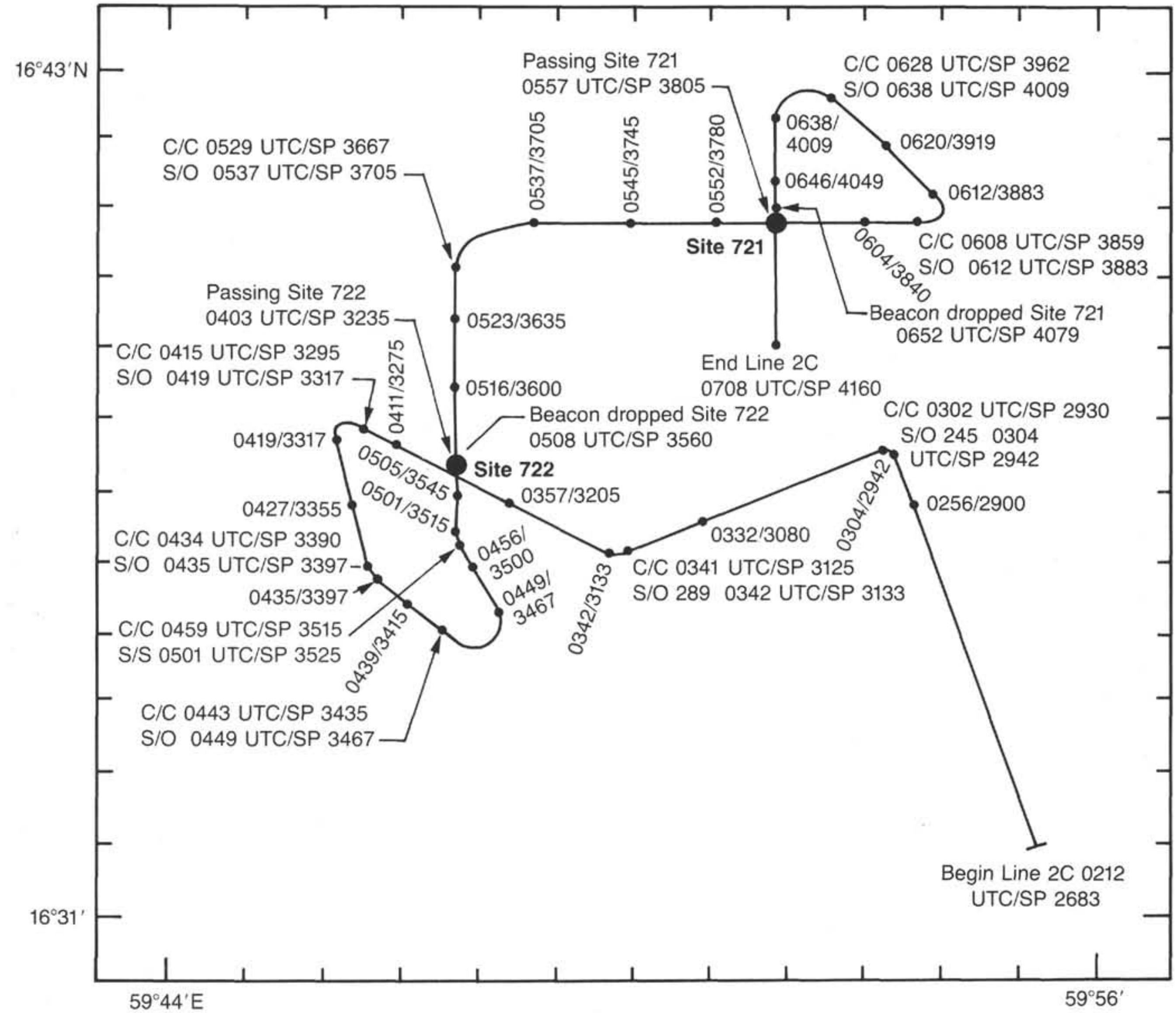

Figure 3. Ship track during approach to Owen Ridge operational area and survey of Sites 721 and 722.

ing nannofossil oozes, foraminifer-nannofossil oozes, and nannofossil oozes, which grade to chalks by 155 mbsf. These beds are between 10 and 200 cm thick. Light beds range in color from light greenish gray (10Y 6/2-7/1) to light gray and light olive gray (5Y 6/2-7/1). Dark beds range from dark greenish gray (10Y 5/-4/) to olive, pale olive, and olive gray (5Y 6/3, 6/4, 5/1, 4/1), and dark beds generally contain 5%-20% more terrigenous silty clay and 5%-20% less biogenic calcium carbonate than do light beds. Generally, the boundaries between these beds are gradational and blurred by bioturbation (Figs. 6-8). Calcium carbonate concentrations range from 38% to 90%, with a mean of 66.0% (Fig. 5, Table 3). Based on smear slide analysis, nannofossils are the dominant sedimentary component. Foraminifers range from 10% to 35% in the first core of each hole to less than 10% for the remainder of lithologic Subunit IA, and biogenic silica rarely occurs in more than trace amounts. Inorganic calcite ranges from 0% to 20%, but is commonly less than 5%. Quartz, dolomite, mica, and accessory minerals are present in trace amounts. Further documentation of the mineralogy can be found in the "Inorganic Geochemistry" section of this chapter. The transition from oozes to chalks (top of Core 117-721B-17X) reflects a change to more indurated sediments downhole.

Drilling of Hole 721A was stopped below 86 mbsf (after coring of 117-721A-9H) because a stiff sediment layer could not be penetrated by the APC. In Holes 721B and 721C this level corresponds to the appearance of a dark olive gray (5Y 3/2) marly nannofossil ooze beginning at 117-721B-10X-1, 35 cm (86.35 mbsf), and 117-721C-10X-4, 20 cm (85 mbsf). The marly ooze is interbedded with nannofossil ooze beds over the next 5-10 m downhole. Based on smear slide analysis, the dark marly layer contains more than 30% terrigenous clay. Calcium carbonate values near 55% (Table 3, Fig. 5) are consistent with higher clay contents for these layers.

Subunit IB (Depth: 261.1-289.0 mbsf)

Subunit IB is composed of foraminifer-bearing nannofossil and nannofossil chalks and extends from 261.2 to 289.0 mbsf. Subunit IB contains microfaults and other disturbance structures not attributable to drilling, which distinguishes it from Subunit IA. The structures are thought to record the emplacement of material at this site by slumping. The material is com-

Table 1. Coring summary, Site 721.

Core no.	Date (Sept. 1987)	Time	Depth (mbsf)	Cored (m)	Recovered (m)	Recovery (%)
117-721A-						
1H	3	1630	0.0-9.8	9.8	9.84	100.0
2H	3	1700	9.8-19.5	9.7	9.84	101.0
3H	3	1735	19.5-29.2	9.7	10.11	104.2
4H	3	1800	29.2-38.9	9.7	10.09	104.0
5H	3	1845	38.9-48.5	9.6	9.45	98.4
6H	3	1915	48.5-57.8	9.3	10.08	108.4
7H	3	2000	57.8-67.3	9.5	9.98	105.0
8H	3	2030	67.3-76.8	9.5	10.04	105.7
9H	3	2115	76.8-86.4	9.6	9.85	102.0
				86.4	89.28	
117-721B-						
1H	4	0045	0.0-9.4	9.4	9.39	99.9
2H	4	0125	9.4-19.1	9.7	9.99	103.0
3H	4	0210	19.1-28.8	9.7	9.91	102.0
4H	4	0300	28.8-38.5	9.7	10.04	103.5
5H	4	0340	38.5-48.1	9.6	10.13	105.5
6H	4	0420	48.1-57.4	9.3	9.98	107.0
7H	4	0500	57.4-66.9	9.5	9.84	103.0
8H	4	0545	66.9-76.4	9.5	10.08	106.1
9H	4	0640	76.4-86.0	9.6	9.89	103.0
10X	4	0815	86.0-95.6	9.6	9.78	102.0
11X	4	0900	95.6-105.2	9.6	8.10	84.4
12X	4	0950	105.2-114.8	9.6	3.73	38.8
13X	4	1035	114.8-124.4	9.6	9.69	101.0
14X	4	1125	124.4-134.1	9.7	9.70	100.0
15X	4	1205	134.1-143.8	9.7	8.62	88.8
16X	4	1240	143.8-153.5	9.7	9.63	99.3
17X	4	1325	153.5-163.2	9.7	9.81	101.0
18X	4	1405	163.2-172.9	9.7	9.77	101.0
19X	4	1440	172.9-182.6	9.7	9.57	98.6
20X	4	1510	182.6-192.3	9.7	8.38	86.4
21X	4	1815	192.3-202.0	9.7	3.68	37.9
22X	4	1900	202.0-211.7	9.7	9.83	101.0
23X	4	1945	211.7-221.3	9.6	5.11	53.2
24X	4	2030	221.3-230.5	9.2	5.29	57.5
25X	4	2115	230.5-240.1	9.6	9.58	99.8

Table 1 (continued).

Core no.	Date (Sept. 1987)	Time	Depth (mbsf)	Cored (m)	Recovered (m)	Recovery (%)
117-721B-						
26X	4	2155	240.1-249.8	9.7	6.26	64.5
27X	4	2235	249.8-259.6	9.8	6.87	70.1
28X	4	2340	259.6-269.4	9.8	9.21	94.0
29X	5	0105	269.4-279.2	9.8	3.92	40.0
30X	5	0215	279.2-289.0	9.8	5.46	55.7
31X	5	0310	289.0-298.8	9.8	9.06	92.4
32X	5	0355	298.8-308.4	9.6	9.79	102.0
33X	5	0450	308.4-318.0	9.6	3.30	34.4
34X	5	0615	318.0-327.7	9.7	7.18	74.0
35X	5	0720	327.7-337.4	9.7	5.28	54.4
36X	5	0915	337.4-347.0	9.6	3.78	39.4
37X	5	1125	347.0-356.6	9.6	9.83	102.0
38X	5	1315	356.6-366.3	9.7	9.45	97.4
39X	5	1500	366.3-375.9	9.6	0.10	1.0
40X	5	1705	375.9-385.6	9.7	9.85	101.0
41X	5	1855	385.6-395.2	9.6	9.86	103.0
42X	5	2020	395.2-404.9	9.7	3.70	38.1
43X	5	2115	404.9-414.5	9.6	0.48	5.0
44X	5	2330	414.5-424.2	9.7	9.88	102.0
				424.2	342.78	
117-721C-						
1H	6	0345	0.0-3.6	3.6	3.63	101.0
2H	6	0420	3.6-13.3	9.7	9.95	102.0
3H	6	0455	13.3-23.0	9.7	9.91	102.0
4H	6	0525	23.0-32.7	9.7	9.78	101.0
5H	6	0555	32.7-42.4	9.7	9.57	98.6
6H	6	0635	42.4-52.0	9.6	9.99	104.0
7H	6	0715	52.0-61.3	9.3	10.01	107.6
8H	6	0755	61.3-70.8	9.5	9.91	104.0
9H	6	0840	70.8-80.3	9.5	9.98	105.0
10H	6	0920	80.3-89.9	9.6	10.01	104.3
11X	6	1045	89.9-99.5	9.6	7.40	77.1
12X	6	1240	99.5-109.1	9.6	9.49	98.8
13X	6	1315	109.1-118.7	9.6	7.21	75.1
14X	6	1355	118.7-128.3	9.6	7.19	74.9
15X	6	1435	128.3-138.0	9.7	9.76	100.0
				138.0	133.79	

Table 2. Lithostratigraphic summary, Site 721.

Lithologic unit	Depth (mbsf)	Cores	Age	$CaCO_3$ ($\bar{X}$ %)
IA Foraminifer-bearing nannofossil, foraminifer-nannofossil, and nannofossil ooze/chalk; alternating light and dark beds	0.0-261.2	721A-1H to -9H, CC 721B-1H to -30X, CC 721C-1H to -15X, CC	Holocene to late Miocene	66.0
IB Foraminifer-bearing nannofossil amd nannofossil chalk; alternating light and dark beds; disturbed beds	261.2-289.0	721B-28X-2, 10 cm to 721B-30X, CC	late Miocene	51.6
II Siliceous-bearing nannofossil, diatomaceous nannofossil, and nannofossil chalk; alternating light and dark beds; disturbed beds	289.0-309.9	721B-31X 721B-33X-2, 0 cm	early late Miocene	43.9
III Nannofossil chalk	309.9-340.7	721B-33X-2, 0 cm 721B-36X, CC, 30 cm	middle Miocene	76.6
IV Interbedded fine-grained turbidites and nannofossil chalk	340.7-424.2	721B-36X, CC, 30 cm 721B-44X, CC	middle to early Miocene	26.8

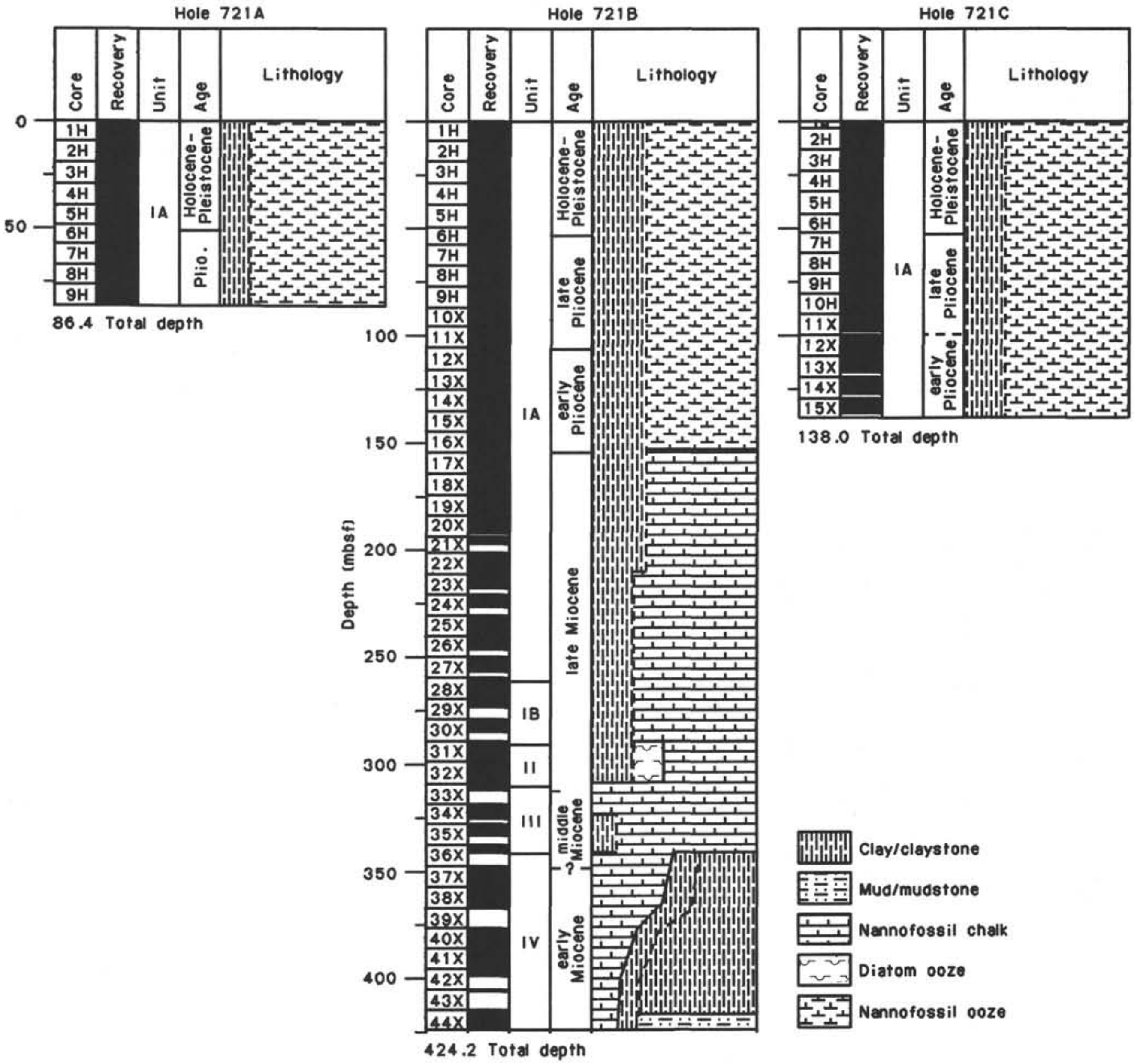

Figure 4. Lithostratigraphic summary, Site 721. Lithology is inferred between recovered intervals.

positionally different from the sediments above and below and the contacts are relatively sharp. The appearance of these features corresponds to an increase in reworked microfossils (see "Biostratigraphy" section, this chapter) which characterizes lithologic Subunit IB and Unit II. However, drilling disturbances are prevalent between 261.2 and 309.9, and it is difficult to distinguish natural disturbances from those caused by drilling.

Unit II (Depth: 289.0–309.9 mbsf; Age: early late Miocene)

Core 117-721B-31 to Section 117-721B-33X-2.

Lithologic Unit II, between 289 and 309.9 mbsf, consists of alternating light and dark layers of siliceous-bearing nannofossil, diatomaceous nannofossil, and nannofossil chalks. It can be distinguished from lithologic Units I and III by the consistent appearance of siliceous microfossils on smear slides. Nannofossils remain the dominant sediment component and smear slides from dark layers contain as much as 20% more siliceous microfossils and 10%–20% more terrigenous clay than do those of light layers. The mean calcium carbonate concentration in lithologic Unit II is lower than in Unit I (Table 2) and reflects the added siliceous component. Lithologic Unit II is characterized by microfaults and disturbance structures similar to those found in Subunit IB. Figure 9 shows one example of these microfaults.

Unit III (Depth: 309.9–340.7 mbsf; Age: middle Miocene)

Samples 117-721B-33X, CC, 10 cm, to 117-721B-36X, CC, 30 cm.

Unit III consists of a greenish gray and light greenish gray (5G 7/1-5G 5/1) to white (2.5Y 8/0) nannofossil chalk. Lithologic Unit III has the highest mean calcium carbonate concentration (76.6%) of the units recognized at Site 721. Slight to moderate bioturbation is evident throughout. The upper and lower boundaries of lithologic Unit III at Site 721 are sharp. The contact between Units IV and III is marked by a change from a grayish brown (2.5Y 5/2) calcareous silty claystone to a greenish gray (5BG 6/1) nannofossil chalk. The Unit III to Unit II contact is identified by a change from greenish gray nanno-

Table 3. Calcium carbonate and organic carbon abundances, Site 721. Asterisk (*) notes samples from Hole 721B not plotted in Figure 5. Depths reported for Hole 721A samples are not comparable to the reported depths for Hole 721B. See Table 17 for depth adjustments.

Hole, core, section, interval (cm)	Depth (mbsf)	Total carbon (%)	Inorganic carbon (%)	Organic carbon (%)	$CaCO_3$ (%)
721A-1H-1, 25-26	0.25	9.40	8.45	0.95	70.4
*721B-1H-1, 50-53	0.50	9.33	9.26	0.07	77.1
721A-1H-1, 75-76	0.75	7.28	6.81	0.47	56.7
721A-1H-1, 125-126	1.25		7.32		61.0
721A-1H-2, 25-26	1.75	9.05	8.04	1.01	67.0
*721B-1H-2, 100-103	2.50	9.07	7.78	1.29	64.8
721A-1H-2, 125-126	2.75		8.25		68.7
721A-1H-3, 25-26	3.25		8.10		67.5
721A-1H-3, 75-76	3.75		8.11		67.6
721A-1H-3, 125-126	4.25		7.15		59.6
721A-1H-4, 25-26	4.75		6.66		55.5
*721B-1H-4, 80-83	5.30	8.93	8.50	0.43	70.8
721A-1H-4, 125-126	5.75		7.70		64.1
*721B-1H-5, 24-27	6.24	9.07	7.86	1.21	65.5
721A-1H-5, 25-26	6.25		9.42		78.5
721A-1H-5, 75-76	6.75		9.46		78.8
721A-1H-5, 125-126	7.25	8.12	7.74	0.38	64.5
721A-1H-6, 25-26	7.75		7.88		65.6
721A-1H-6, 75-76	8.25		8.42		70.1
721A-1H-6, 125-126	8.75		8.19		68.2
721A-1H-6, 144-145	8.94	8.35	7.79	0.56	64.9
721A-1H-6, 145-150	8.95		7.57		63.1
721A-1H-7, 25-26	9.25		7.42		61.8
721A-2H-1, 25-26	10.05		8.98		74.8
*721B-2H-1, 87-90	10.27	9.83	9.37	0.46	78.1
721A-2H-1, 75-76	10.55		9.54		79.5
*721B-2H-2, 17-20	11.07	9.27	7.36	1.91	61.3
721A-2H-2, 25-26	11.55		8.19		68.2
721A-2H-2, 75-76	12.05	8.88	8.63	0.25	71.9
*721B-2H-3, 27-30	12.67	9.27	8.67	0.60	72.2
721A-2H-3, 75-76	13.55		9.42		78.5
721A-2H-3, 125-126	14.05		9.89		82.4
721A-2H-4, 25-26	14.55		7.99		66.6
721A-2H-4, 75-76	15.05		8.41		70.1
721A-2H-4, 125-126	15.55		8.53		71.1
721A-2H-5, 25-26	16.05		7.85		65.4
721A-2H-5, 75-76	16.55		8.73		72.7
721A-2H-5, 125-126	17.05		8.81		73.4
721A-2H-6, 75-76	18.05		8.44		70.3
721A-2H-6, 125-126	18.55		9.14		76.1
721A-2H-6, 149-150	18.79	8.69	8.31	0.38	69.2
721A-3H-1, 25-26	19.75	8.72	8.35	0.37	69.6
721A-3H-1, 125-126	20.75		7.54		62.8
721A-3H-2, 25-26	21.25		7.67		63.9
721A-3H-2, 75-76	21.75		8.38		69.8
*721B-3H-3, 10-13	22.20	8.48	7.74	0.74	64.5
721A-3H-2, 125-126	22.25		6.85		57.1
721A-3H-3, 25-26	22.75		8.73		72.7
721A-3H-3, 75-76	23.25		8.66		72.1
721A-3H-3, 125-126	23.75		8.68		72.3
721A-3H-4, 25-26	24.25		8.29		69.1
721A-3H-4, 75-76	24.75		7.91		65.9
721A-3H-4, 125-126	25.25	8.62	8.25	0.37	68.7
721A-3H-5, 25-26	25.75		8.95		74.6
721A-3H-5, 75-76	26.25		9.49		79.1
*721B-3H-5, 145-150	26.55		8.90		74.1
721A-3H-5, 125-126	26.75		9.32		77.6
721A-3H-6, 25-26	27.25		6.54		54.5
721A-3H-6, 116-117	28.16		6.96		58.0
721A-3H-6, 119-120	28.19	7.13	6.83	0.30	56.9
721A-3H-7, 25-26	28.75		8.41		70.1
721A-3H-7, 75-76	29.25		6.95		57.9
721A-4H-1, 25-26	29.45		7.26		60.5
721A-4H-1, 75-76	29.95		7.15		59.6
721A-4H-1, 125-126	30.45		7.63		63.6
721A-4H-2, 25-26	30.95		8.39		69.9
721A-4H-2, 75-76	31.45		8.44		70.3
721A-4H-2, 125-126	31.95		8.23		68.6
721A-4H-3, 25-26	32.45		7.96		66.3
721A-4H-3, 75-76	32.95		8.19		68.2
721A-4H-3, 125-126	33.45		7.41		61.7
721A-4H-4, 25-26	33.95		9.15		76.2
721A-4H-4, 75-76	34.45		8.79		73.2
721A-4H-4, 125-126	34.95		8.55		71.2
721A-4H-5, 0-1	35.20	8.75	8.09	0.66	67.4
721A-4H-5, 41-42	35.61		7.50		62.5

Table 3 (continued).

Hole, core, section, interval (cm)	Depth (mbsf)	Total carbon (%)	Inorganic carbon (%)	Organic carbon (%)	$CaCO_3$ (%)
721A-4H-5, 75-76	35.95		6.25		52.1
721A-4H-5, 125-126	36.45		8.42		70.1
721A-4H-6, 25-26	36.95		8.70		72.5
721A-4H-6, 75-76	37.45		9.06		75.5
721A-4H-6, 125-126	37.95		8.36		69.6
721A-4H-7, 75-76	38.95		9.76		81.3
721A-5H-1, 25-26	39.15		7.61		63.4
721A-5H-1, 75-76	39.65		7.82		65.1
721A-5H-1, 125-126	40.15		7.45		62.1
721A-5H-2, 25-26	40.65		7.67		63.9
721A-5H-2, 75-76	41.15		9.27		77.2
721A-5H-2, 125-126	41.65		6.55		54.6
721A-5H-3, 25-26	42.15		6.57		54.7
721A-5H-3, 75-76	42.65		8.60		71.6
721A-5H-3, 125-126	43.15		8.01		66.7
721A-5H-4, 25-26	43.65		9.37		78.1
721A-5H-4, 75-76	44.15		7.13		59.4
721A-5H-4, 125-126	44.65		8.54		71.1
721A-5H-4, 149-150	44.89	7.78	6.74	1.04	56.1
721A-5H-5, 25-26	45.15		6.72		56.0
721A-5H-5, 75-76	45.65		8.07		67.2
721A-5H-5, 125-126	46.15		7.67		63.9
721A-5H-6, 25-26	46.65		7.00		58.3
721A-5H-6, 75-76	47.15		8.09		67.4
721A-5H-6, 125-126	47.65		7.04		58.6
721A-6H-1, 25-26	48.75		8.22		68.5
721A-6H-1, 75-76	49.25		6.62		55.1
721A-6H-1, 125-126	49.75		6.70		55.8
721A-6H-2, 25-26	50.25		4.86		40.5
721A-6H-2, 75-76	50.75		5.23		43.6
721A-6H-2, 125-126	51.25		8.24		68.6
721A-6H-3, 25-26	51.75		7.64		63.6
721A-6H-3, 75-76	52.25		4.64		38.7
721A-6H-3, 125-126	52.75		8.55		71.2
721A-6H-4, 25-26	53.25		5.39		44.9
721A-6H-4, 75-76	53.75		7.27		60.6
721A-6H-4, 125-126	54.25		5.65		47.1
721A-6H-5, 25-26	54.75		9.33		77.7
721A-6H-5, 75-76	55.25		5.83		48.6
721A-6H-5, 125-126	55.75		7.72		64.3
721A-6H-6, 25-26	56.25		8.34		69.5
721A-6H-6, 75-76	56.75		6.48		54.0
721A-6H-6, 119-120	57.19	9.61	8.73	0.88	72.7
721A-6H-6, 145-150	57.45		8.43		70.2
721A-6H-7, 25-26	57.75		8.41		70.1
721A-6H-7, 75-76	58.25		7.35		61.2
721A-7H-1, 75-76	58.55		6.00		50.0
721A-7H-1, 125-126	59.05		6.17		51.4
721A-7H-2, 25-26	59.55		5.81		48.4
721A-7H-2, 75-76	60.05		9.82		81.8
721A-7H-2, 125-126	60.55		8.58		71.5
721A-7H-3, 25-26	61.05		8.90		74.1
721A-7H-3, 75-76	61.55		8.57		71.4
721A-7H-3, 125-126	62.05		7.49		62.4
721A-7H-4, 25-26	62.55		7.58		63.1
721A-7H-4, 125-126	63.55		9.84		82.0
721A-7H-5, 25-26	64.05		7.92		66.0
721A-7H-5, 75-76	64.55		8.68		72.3
721A-7H-5, 125-126	65.05		8.57		71.4
721A-7H-5, 149-150	65.29	8.50	7.46	1.04	62.1
721A-7H-6, 25-26	65.55		9.00		75.0
721A-7H-6, 75-125	66.05		7.78		64.8
721A-7H-6, 125-126	66.55		7.95		66.2
721A-7H-7, 25-26	67.05		8.90		74.1
721A-7H-7, 70-71	67.50		9.26		77.1
721A-8H-1, 25-26	67.55		10.04		83.6
721A-8H-1, 75-76	68.05		9.44		78.6
721A-8H-1, 125-126	68.55		7.96		66.3
721A-8H-2, 25-26	69.05		7.82		65.1
721A-8H-2, 75-76	69.55		8.53		71.1
721A-8H-2, 125-126	70.05		8.38		69.8
721A-8H-3, 25-26	70.55		8.73		72.7
721A-8H-3, 75-76	71.05		8.50		70.8
721A-8H-3, 125-126	71.55		7.68		64.0
721A-8H-4, 25-26	72.05		6.90		57.5

Table 3 (continued).

Hole, core, section, interval (cm)	Depth (mbsf)	Total carbon (%)	Inorganic carbon (%)	Organic carbon (%)	$CaCO_3$ (%)
721A-8H-4, 75-76	72.55		8.16		68.0
721A-8H-4, 125-126	73.05		7.21		60.1
721A-8H-5, 25-26	73.55		9.34		77.8
721A-8H-5, 75-76	74.05		7.12		59.3
721A-8H-5, 125-126	74.55		7.98		66.5
721A-8H-5, 149-150	74.79	9.93	8.48	1.45	70.6
721A-8H-6, 25-26	75.05		8.28		69.0
721A-8H-6, 75-76	75.55		8.97		74.7
721A-8H-6, 125-126	76.05		8.85		73.7
721A-8H-7, 25-26	76.55		8.27		68.9
*721B-9H-1, 25-26	76.65		4.89		40.7
721A-9H-1, 25-26	77.05		7.79		64.9
*721B-9H-1, 75-76	77.15		7.03		58.6
721A-9H-1, 75-76	77.55		8.05		67.1
*721B-9H-1, 125-126	77.65		6.36		53.0
721A-9H-1, 125-126	78.05		8.23		68.6
*721B-9H-2, 25-26	78.15		9.00		75.0
721A-9H-2, 25-26	78.55		9.14		76.1
*721B-9H-2, 75-76	78.65		7.22		60.1
721A-9H-2, 75-76	79.05		8.35		69.6
*721B-9H-2, 125-126	79.15		7.57		63.1
*721B-9H-2, 144-145	79.34	9.95	8.00	1.95	66.6
721A-9H-2, 125-126	79.55		8.86		73.8
*721B-9H-3, 25-26	79.65		7.87		65.6
721A-9H-3, 25-26	80.05		7.61		63.4
721A-9H-3, 75-76	80.55		7.98		66.5
*721B-9H-3, 125-126	80.65		8.82		73.5
721A-9H-3, 125-126	81.05		7.53		62.7
*721B-9H-4, 25-26	81.15		9.34		77.8
721A-9H-4, 25-26	81.55		7.55		62.9
*721B-9H-4, 75-76	81.65		5.99		49.9
721A-9H-4, 75-76	82.05		5.48		45.7
*721B-9H-4, 125-126	82.15		8.54		71.1
*721B-9H-4, 145-150	82.35		8.03		66.9
721A-9H-4, 125-126	82.55		8.04		67.0
*721B-9H-5, 25-26	82.65		4.83		40.2
721A-9H-5, 25-26	83.05		8.87		73.9
*721B-9H-5, 75-76	83.15		7.28		60.6
721A-9H-5, 75-76	83.55		7.89		65.7
721A-9H-5, 125-126	84.05		7.63		63.6
*721B-9H-6, 25-26	84.15		8.50		70.8
721A-9H-6, 25-26	84.55		7.96		66.3
*721B-9H-6, 75-76	84.65		7.95		66.2
721A-9H-6, 75-76	85.05		7.39		61.6
*721B-9H-6, 125-126	85.15		8.58		71.5
721A-9H-6, 117-118	85.47		6.03		50.2
721A-9H-6, 119-120	85.49	9.95	6.27	3.68	52.2
*721B-9H-7, 25-26	85.65		7.94		66.1
721A-9H-6, 145-150	85.75		6.32		52.7
721A-9H-7, 25-26	86.05		7.86		65.5
*721B-10X-1, 25-26	86.25		8.09		67.4
*721B-10X-1, 75-76	86.75		6.89		57.4
*721B-10X-1, 125-126	87.25		5.89		49.1
*721B-10X-2, 25-26	87.75		8.86		73.8
*721B-10X-2, 75-76	88.25		8.13		67.7
*721B-10X-2, 125-126	88.75		6.52		54.3
*721B-10X-3, 25-26	89.25		8.88		74.0
*721B-10X-3, 75-76	89.75		7.05		58.7
*721B-10X-3, 125-126	90.25		7.28		60.6
*721B-10X-4, 75-76	91.25		8.39		69.9
721B-10X-4, 125-126	91.75		7.35		61.2
721B-10X-4, 149-150	91.99	10.58	9.62	0.96	80.1
721B-10X-5, 25-26	92.25		8.27		68.9
721B-10X-5, 75-76	92.75		7.55		62.9
721B-10X-5, 125-126	93.25		7.06		58.8
721B-10X-6, 25-26	93.75		8.63		71.9
721B-10X-6, 75-76	94.25		7.27		60.6
721B-10X-6, 125-126	94.75		8.42		70.1
721B-10X-7, 25-26	95.25		9.09		75.7
721B-11X-1, 25-26	95.85		7.95		66.2
721B-11X-1, 75-76	96.35		8.21		68.4
721B-11X-1, 125-126	96.85		9.02		75.1
721B-11X-2, 25-26	97.35		7.58		63.1
721B-11X-2, 75-76	97.85		8.36		69.6
721B-11X-2, 125-126	98.35		7.14		59.5
721B-11X-2, 149-150	98.59	9.95	6.88	3.07	57.3
721B-11X-3, 25-26	98.85		8.07		67.2
721B-11X-3, 75-76	99.35		8.07		67.2

Table 3 (continued).

Hole, core, section, interval (cm)	Depth (mbsf)	Total carbon (%)	Inorganic carbon (%)	Organic carbon (%)	$CaCO_3$ (%)
721B-11X-3, 125-126	99.85		8.99		74.9
721B-11X-4, 25-26	100.35		6.66		55.5
721B-11X-4, 75-76	100.85		7.90		65.8
721B-11X-4, 125-126	101.35		9.27		77.2
721B-11X-5, 25-26	101.85		7.13		59.4
721B-11X-5, 75-76	102.35		9.60		80.0
721B-11X-5, 125-126	102.85		8.13		67.7
721B-11X-6, 23-24	103.33		8.88		74.0
721B-12X-1, 25-26	105.45		7.01		58.4
721B-12X-1, 75-76	105.95		7.35		61.2
721B-12X-1, 125-126	106.45		7.91		65.9
721B-12X-1, 144-145	106.64	9.94	8.38	1.56	69.8
721B-12X-1, 145-150	106.65		8.77		73.1
721B-12X-2, 25-26	106.95		8.23		68.6
721B-12X-2, 75-76	107.45		8.71		72.6
721B-12X-2, 125-126	107.95		8.84		73.6
721B-12X-CC, 25-26	108.70		9.32		77.6
721B-13X-1, 25-26	115.05		6.41		53.4
721B-13X-1, 75-76	115.55		6.12		51.0
721B-13X-1, 125-126	116.05		9.33		77.7
721B-13X-2, 25-26	116.55		5.53		46.1
721B-13X-2, 75-76	117.05		8.61		71.7
721B-13X-2, 125-126	117.55		6.91		57.6
721B-13X-3, 25-26	118.05		7.67		63.9
721B-13X-3, 75-76	118.55		6.66		55.5
721B-13X-3, 125-126	119.05		6.94		57.8
721B-13X-4, 25-26	119.55		7.56		63.0
721B-13X-4, 75-76	120.05		7.70		64.1
721B-13X-4, 125-126	120.55		7.13		59.4
721B-13X-4, 149-150	120.79	8.63	8.03	0.60	66.9
721B-13X-5, 25-26	121.05		8.87		73.9
721B-13X-5, 75-76	121.55		6.63		55.2
721B-13X-5, 125-126	122.05		6.99		58.2
721B-13X-6, 25-26	122.55		8.24		68.6
721B-13X-6, 75-76	123.05		8.44		70.3
721B-13X-6, 125-126	123.55		8.74		72.8
721B-14X-1, 25-26	124.65		7.56		63.0
721B-14X-1, 75-76	125.15		8.36		69.6
721B-14X-1, 125-126	125.65		8.44		70.3
721B-14X-1, 149-150	125.89	7.75	6.38	1.37	53.2
721B-14X-2, 25-26	126.15		6.89		57.4
721B-14X-2, 75-76	126.65		7.28		60.6
721B-14X-2, 125-126	127.15		6.61		55.1
721B-14X-3, 25-26	127.65		8.83		73.6
721B-14X-3, 75-76	128.15		4.87		40.6
721B-14X-3, 125-126	128.65		7.92		66.0
721B-14X-4, 25-26	129.15		9.84		82.0
721B-14X-4, 75-76	129.65		6.69		55.7
721B-14X-4, 125-126	130.15		7.71		64.2
721B-14X-5, 25-26	130.65		9.56		79.6
721B-14X-5, 75-76	131.15		6.34		52.8
721B-14X-5, 125-126	131.65		8.88		74.0
721B-14X-6, 25-26	132.15		8.77		73.1
721B-14X-6, 75-76	132.65		7.74		64.5
721B-14X-6, 125-126	133.15		7.63		63.6
721B-14X-7, 25-26	133.65		8.67		72.2
721B-15X-1, 25-26	134.35		8.87		73.9
721B-16X-1, 125-126	145.05		7.05		58.7
721B-16X-2, 25-26	145.55		8.07		67.2
721B-16X-2, 75-76	146.05		8.14		67.8
721B-16X-2, 125-126	146.55		7.81		65.1
721B-16X-3, 25-26	147.05		8.92		74.3
721B-16X-3, 75-76	147.55		7.56		63.0
721B-16X-3, 125-126	148.05		9.43		78.6
721B-16X-4, 25-26	148.55		9.65		80.4
721B-16X-4, 75-76	149.05		8.88		74.0
721B-16X-4, 125-126	149.55		8.60		71.6
721B-16X-5, 25-26	150.05		9.23		76.9
721B-16X-5, 75-76	150.55		8.81		73.4
721B-16X-5, 125-126	151.05		7.57		63.1
721B-16X-5, 149-150	151.29	8.48	7.78	0.70	64.8
721B-16X-6, 25-26	151.55		7.60		63.3
721B-16X-6, 75-76	152.05		8.08		67.3
721B-16X-6, 125-126	152.55		8.95		74.6
721B-16X-7, 25-26	153.05		7.73		64.4
721B-17X-1, 25-26	153.75		6.15		51.2
721B-17X-1, 75-76	154.25		9.46		78.8
721B-17X-1, 125-126	154.75		7.35		61.2

Table 3 (continued).

Hole, core, section, interval (cm)	Depth (mbsf)	Total carbon (%)	Inorganic carbon (%)	Organic carbon (%)	$CaCO_3$ (%)
721B-17X-2, 25-26	155.25		8.77		73.1
721B-17X-2, 75-76	155.75		6.62		55.1
721B-17X-2, 125-126	156.25		9.19		76.6
721B-17X-3, 25-26	156.75		6.81		56.7
721B-17X-3, 75-76	157.25		6.44		53.7
721B-17X-3, 125-126	157.75		7.86		65.5
721B-17X-4, 25-26	158.25		8.56		71.3
721B-17X-4, 75-76	158.75		9.11		75.9
721B-17X-4, 125-126	159.25		7.42		61.8
721B-17X-5, 25-26	159.75		6.70		55.8
721B-17X-5, 75-76	160.25		9.24		77.0
721B-17X-5, 125-126	160.75		6.59		54.9
721B-17X-5, 149-150	160.99	9.14	8.57	0.57	71.4
721B-17X-6, 75-76	161.75		8.39		69.9
721B-17X-6, 125-126	162.25		8.24		68.6
721B-17X-7, 25-26	162.75		10.44		87.0
721B-18X-1, 25-26	163.45		6.05		50.4
721B-18X-1, 75-76	163.95		9.57		79.7
721B-18X-1, 125-126	164.45		8.45		70.4
721B-18X-2, 25-26	164.95		5.60		46.7
721B-18X-2, 75-76	165.45		7.75		64.6
721B-18X-2, 125-126	165.95		6.84		57.0
721B-18X-3, 25-26	166.45		7.69		64.1
721B-18X-3, 75-76	166.95		7.81		65.1
721B-18X-3, 125-126	167.45		7.11		59.2
721B-18X-4, 25-26	167.95		6.75		56.2
721B-18X-4, 75-76	168.45		6.03		50.2
721B-18X-4, 125-126	168.95		7.82		65.1
721B-18X-5, 25-26	169.45		7.38		61.5
721B-18X-5, 75-76	169.95		7.77		64.7
721B-18X-5, 119-120	170.39	8.26	6.77	1.49	56.4
721B-18X-5, 145-150	170.65		9.67		80.6
721B-18X-6, 25-26	170.95		6.45		53.7
721B-18X-6, 75-76	171.45		8.93		74.4
721B-18X-6, 125-126	171.95		7.45		62.1
721B-18X-7, 25-26	172.45		7.01		58.4
721B-18X-CC, 25-26	172.78		8.03		66.9
721B-19X-1, 25-26	173.15		6.83		56.9
721B-19X-1, 75-76	173.65		8.30		69.0
721B-19X-1, 125-126	174.15		7.78		64.8
721B-19X-2, 25-26	174.65		8.68		72.3
721B-19X-2, 75-76	175.15		6.36		53.0
721B-19X-2, 125-126	175.65		7.88		65.6
721B-19X-3, 25-26	176.15		7.04		58.6
721B-19X-3, 75-76	176.65		7.46		62.1
721B-19X-3, 125-126	177.15		7.98		66.5
721B-19X-4, 25-26	177.65		5.73		47.7
721B-19X-4, 75-76	178.15		7.20		60.0
721B-19X-4, 125-126	178.65		7.73		64.4
721B-19X-5, 25-26	179.15		8.43		70.2
721B-19X-5, 75-76	179.65		7.13		59.4
721B-19X-5, 125-126	180.15		8.54		71.1
721B-19X-5, 149-150	180.39	9.23	7.26	1.97	60.5
721B-19X-6, 25-26	180.65		8.76		73.0
721B-19X-6, 75-76	181.15		8.98		74.8
721B-19X-6, 125-126	181.65		6.86		57.1
721B-20X-1, 25-26	182.85		6.93		57.7
721B-20X-1, 75-76	183.35		7.56		63.0
721B-20X-1, 125-126	183.85		8.65		72.1
721B-20X-2, 25-26	184.35		8.66		72.1
721B-20X-2, 75-76	184.85		9.52		79.3
721B-20X-2, 125-126	185.35		8.13		67.7
721B-20X-3, 25-26	185.85		9.39		78.2
721B-20X-3, 75-76	186.35		7.49		62.4
721B-20X-3, 125-126	186.85		8.93		74.4
721B-20X-4, 25-26	187.35		6.73		56.1
721B-20X-4, 75-76	187.85		7.55		62.9
721B-20X-4, 125-126	188.35		8.77		73.1
721B-20X-5, 25-26	188.85		8.32		69.3
721B-20X-5, 75-76	189.35		6.42		53.5
721B-20X-5, 125-126	189.85		8.60		71.6
721B-20X-5, 149-150	190.09	8.23	7.31	0.92	60.9
721B-20X-6, 25-26	190.35		6.72		56.0
721B-21X-1, 25-26	192.55		7.20		60.0
721B-21X-1, 75-76	193.05		6.70		55.8
721B-21X-1, 125-126	193.55		9.04		75.3
721B-21X-2, 0-1	193.80	8.91	8.63	0.28	71.9
721B-21X-2, 25-26	194.05		7.40		61.6

Table 3 (continued).

Hole, core, section, interval (cm)	Depth (mbsf)	Total carbon (%)	Inorganic carbon (%)	Organic carbon (%)	$CaCO_3$ (%)
721B-21X-2, 75-76	194.55		7.59		63.2
721B-21X-2, 125-126	195.05		6.33		52.7
721B-22X-1, 25-26	202.25		7.56		63.0
721B-22X-1, 75-76	202.75		7.27		60.6
721B-22X-1, 125-126	203.25		6.55		54.6
721B-22X-2, 25-26	203.75		10.09		84.1
721B-22X-2, 75-76	204.25		8.37		69.7
721B-22X-2, 125-126	204.75		8.58		71.5
721B-22X-3, 0-1	205.00	9.84	9.06	0.78	75.5
721B-22X-3, 25-26	205.25		6.60		55.0
721B-22X-3, 75-76	205.75		7.44		62.0
721B-22X-3, 125-126	206.25		9.53		79.4
721B-22X-4, 25-26	206.75		5.95		49.6
721B-22X-4, 75-76	207.25		10.28		85.6
721B-22X-4, 125-126	207.75		8.23		68.6
721B-22X-5, 25-26	208.25		7.92		66.0
721B-22X-5, 75-76	208.75		8.77		73.1
721B-22X-5, 119-120	209.19		7.30		60.8
721B-22X-5, 145-150	209.45		10.09		84.1
721B-22X-6, 25-26	209.75		9.40		78.3
721B-22X-6, 75-76	210.25		8.60		71.6
721B-22X-6, 125-126	210.75		7.09		59.1
721B-22X-7, 25-26	211.25		8.70		72.5
721B-23X-1, 25-26	211.95		7.83		65.2
721B-23X-1, 125-126	212.95		8.50		70.8
721B-23X-2, 25-26	213.45		6.36		53.0
721B-23X-2, 75-76	213.95		8.83		73.6
721B-23X-2, 125-126	214.45		7.89		65.7
721B-23X-3, 25-26	214.95		10.30		85.8
721B-23X-3, 75-76	215.45		6.95		57.9
721B-24X-1, 25-26	221.55		8.58		71.5
721B-24X-1, 75-76	222.05		10.80		90.0
721B-24X-1, 120-121	222.50		8.21		68.4
721B-24X-2, 25-26	223.05		6.11		50.9
721B-24X-2, 75-76	223.55		9.32		77.6
721B-24X-2, 112-113	223.92		8.98		74.8
721B-24X-2, 140-150	224.20		8.81		73.4
721B-24X-3, 0-1	224.30	8.69	8.13	0.56	67.0
721B-24X-3, 25-26	224.55		5.21		43.4
721B-24X-3, 75-76	225.05		6.11		50.9
721B-24X-3, 125-126	225.55		4.61		38.4
721B-24X-4, 25-26	226.05		8.40		70.0
721B-25X-1, 25-26	230.75		7.16		59.6
721B-25X-1, 75-76	231.25		7.19		59.9
721B-25X-1, 125-126	231.75		6.74		56.1
721B-25X-2, 25-26	232.25		9.05		75.4
721B-25X-2, 75-76	232.75		7.92		66.0
721B-25X-2, 122-123	233.22		8.54		71.1
721B-25X-3, 25-26	233.75		10.46		87.1
721B-25X-3, 75-76	234.25		8.94		74.5
721B-25X-3, 125-126	234.75		7.78		64.8
721B-25X-4, 25-26	235.25		8.72		72.6
721B-25X-4, 75-76	235.75		7.89		65.7
721B-25X-4, 125-126	236.25		8.16		68.0
721B-25X-5, 0-1	236.50	8.93	8.56	0.37	71.3
721B-25X-5, 25-26	236.75		8.41		70.1
721B-25X-5, 75-76	237.25		8.26		68.8
721B-25X-5, 125-126	237.75		8.37		69.7
721B-25X-6, 25-26	238.25		9.48		79.0
721B-25X-6, 75-76	238.75		8.12		67.6
721B-25X-6, 125-126	239.25		7.38		61.5
721B-26X-1, 25-26	240.35		8.46		70.5
721B-26X-1, 75-76	240.85		7.74		64.5
721B-26X-1, 125-126	241.35		7.68		64.0
721B-26X-2, 25-26	241.85		7.81		65.1
721B-26X-2, 75-76	242.35		9.53		79.4
721B-26X-2, 125-126	242.85		7.74		64.5
721B-26X-2, 125-126	242.85		7.74		64.5
721B-26X-3, 25-26	243.35		7.40		61.6
721B-26X-3, 75-76	243.85		8.74		72.8
721B-26X-3, 125-126	244.35		7.23		60.2
721B-26X-3, 149-150	244.59	6.02	5.80	0.22	48.3
721B-26X-4, 25-26	244.85		9.37		78.1
721B-26X-4, 75-76	245.35		6.16		51.3
721B-26X-4, 125-126	245.85		7.59		63.2
721B-26X-CC, 25-26	246.13		7.40		61.6
721B-27X-1, 75-76	250.55		6.37		53.1
721B-27X-1, 125-126	251.05		10.52		87.6

Table 3 (continued).

Hole, core, section, interval (cm)	Depth (mbsf)	Total carbon (%)	Inorganic carbon (%)	Organic carbon (%)	$CaCO_3$ (%)
721B-27X-2, 25-26	251.55		6.88		57.3
721B-27X-2, 75-76	252.05		6.53		54.4
721B-27X-2, 125-126	252.55		9.52		79.3
721B-27X-3, 25-26	253.05		8.76		73.0
721B-27X-3, 75-76	253.55		6.68		55.6
721B-27X-3, 117-118	253.97		10.36		86.3
721B-27X-3, 119-120	253.99	8.44	8.19	0.25	68.2
721B-27X-3, 145-150	254.25		10.80		90.0
721B-27X-4, 25-26	254.55		7.92		66.0
721B-27X-4, 75-76	255.05		7.37		61.4
721B-27X-4, 125-126	255.55		6.73		56.1
721B-27X-5, 25-26	256.05		8.77		73.1
721B-27X-CC, 25-26	256.48		7.88		65.6
721B-28X-1, 25-26	259.85		7.02		58.5
721B-28X-1, 75-76	260.35		8.04		67.0
721B-28X-1, 125-126	260.85		7.62		63.5
721B-28X-2, 25-26	261.35		6.54		54.5
721B-28X-2, 75-76	261.85		4.70		39.2
721B-28X-2, 125-126	262.35		7.68		64.0
721B-28X-3, 25-26	262.85		4.09		34.1
721B-28X-3, 75-76	263.35		5.25		43.7
721B-28X-4, 25-26	264.35		8.10		67.5
721B-28X-4, 75-76	264.85		5.61		46.7
721B-28X-4, 125-126	265.35		8.47		70.6
721B-28X-5, 0-1	265.60	7.43	6.63	0.80	55.2
721B-28X-5, 25-26	265.85		4.89		40.7
721B-28X-5, 125-126	266.85		5.60		46.7
721B-28X-6, 25-26	267.35		5.72		47.7
721B-28X-CC, 25-26	268.59		4.19		34.9
721B-29X-1, 25-26	269.65		8.68		72.3
721B-29X-1, 75-76	270.15		7.37		61.4
721B-29X-1, 125-126	270.65		4.48		37.3
721B-29X-2, 0-1	270.90	7.89	7.46	0.43	62.1
721B-29X-2, 25-26	271.15		5.82		48.5
721B-29X-2, 75-76	271.65		5.90		49.2
721B-29X-2, 125-126	272.15		6.83		56.9
721B-29X-3, 25-26	272.65		6.24		52.0
721B-29X-CC, 25-26	273.08		2.47		20.6
721B-30X-1, 25-26	279.45		6.50		54.2
721B-30X-1, 75-76	279.95		8.96		74.6
721B-30X-1, 125-126	280.45		9.21		76.7
721B-30X-2, 25-26	280.95		6.30		52.5
721B-30X-2, 75-76	281.45		5.71		47.6
721B-30X-2, 114-115	281.84	6.36	6.22	0.14	51.8
721B-30X-2, 140-150	282.10		11.26		93.8
721B-30X-3, 25-26	282.45		3.55		29.6
721B-30X-3, 75-76	282.95		3.59		29.9
721B-30X-3, 125-126	283.45		7.35		61.2
721B-30X-4, 25-26	283.95		3.29		27.4
721B-30X-CC, 25-26	284.52		5.97		49.7
721B-31X-1, 25-26	289.25		3.25		27.1
721B-31X-1, 75-76	289.75		6.68		55.6
721B-31X-1, 125-126	290.25		6.99		58.2
721B-31X-2, 28-29	290.78		3.32		27.7
721B-31X-2, 75-76	291.25		4.90		40.8
721B-31X-2, 125-126	291.75		7.64		63.6
721B-31X-3, 25-26	292.25		3.59		29.9
721B-31X-3, 125-126	293.25		2.76		23.0
721B-31X-3, 149-150	293.49	5.02	4.17	0.85	34.7
721B-31X-4, 25-26	293.75		8.63		71.9
721B-31X-4, 77-78	294.27		4.22		35.2
721B-31X-4, 125-126	294.75		7.70		64.1
721B-31X-5, 14-15	295.14		4.26		35.5
721B-31X-5, 75-76	295.75		4.45		37.1
721B-31X-5, 125-126	296.25		8.80		73.3
721B-31X-6, 25-26	296.75		1.39		11.6
721B-31X-6, 75-76	297.25		2.80		23.3
721B-32X-1, 25-26	299.05		6.13		51.1
721B-32X-1, 75-76	299.55		6.39		53.2
721B-32X-1, 125-126	300.05		6.29		52.4
721B-32X-2, 25-26	300.55		3.11		25.9
721B-32X-2, 75-76	301.05		7.81		65.1
721B-32X-2, 125-126	301.55		6.64		55.3
721B-32X-2, 149-150	301.79	5.06	3.59	1.47	29.9
721B-32X-3, 25-26	302.05		2.75		22.9
721B-32X-3, 75-76	302.55		7.76		64.6
721B-32X-3, 125-126	303.05		2.90		24.2
721B-32X-4, 25-26	303.55		8.13		67.7
721B-32X-4, 75-76	304.05		3.58		29.8
721B-32X-4, 125-126	304.55		5.93		49.4
721B-32X-5, 25-26	305.05		7.89		65.7
721B-32X-5, 75-76	305.55		5.51		45.9
721B-32X-5, 125-126	306.05		4.63		38.6
721B-32X-6, 25-26	306.55		1.42		11.8
721B-32X-6, 75-76	307.05		7.18		59.8
721B-32X-6, 125-126	307.55		3.36		28.0
721B-32X-7, 25-26	308.05		4.19		34.9
721B-33X-1, 24-25	308.64		3.43		28.6
721B-33X-1, 75-76	309.15		7.02		58.5
721B-33X-1, 112-113	309.52		2.89		24.1
721B-33X-1, 114-115	309.54	4.66	3.06	1.60	25.5
721B-33X-1, 140-150	309.80		8.31		69.2
721B-33X-2, 24-25	310.14		5.76		48.0
721B-33X-2, 75-76	310.65		9.93		82.7
721B-33X-2, 124-125	311.14		6.04		50.3
721B-33X-CC, 24-25	311.49		10.82		90.1
721B-34X-1, 5-6	318.05		9.03		75.2
721B-34X-1, 54-55	318.54		10.50		87.5
721B-34X-1, 145-146	319.45		7.10		59.1
721B-34X-2, 5-6	319.55		7.53		62.7
721B-34X-2, 54-55	320.04		10.97		91.4
721B-34X-2, 126-128	320.76		9.78		81.5
721B-34X-3, 5-6	321.05		3.83		31.9
721B-34X-3, 70-71	321.70		10.83		90.2
721B-34X-3, 134-135	322.34		10.99		91.6
721B-34X-4, 0-1	322.50	10.81	10.81	0.00	90.1
721B-34X-4, 14-15	322.64		10.87		90.6
721B-34X-4, 71-72	323.21		10.75		89.6
721B-34X-4, 126-127	323.76		8.35		69.6
721B-34X-5, 10-11	324.10		10.44		87.0
721B-34X-5, 45-46	324.45		8.91		74.2
721B-35X-1, 25-26	327.95		10.79		89.9
721B-35X-1, 125-126	328.95		11.91		99.2
721B-35X-2, 25-26	329.45		7.37		61.4
721B-35X-2, 75-76	329.95		5.87		48.9
721B-35X-2, 125-126	330.45		11.07		92.2
721B-35X-2, 145-150	330.65	4.06	4.06	0.00	33.8
721B-35X-3, 25-26	330.95		9.05		75.4
721B-35X-3, 75-76	331.45		9.70		80.8
721B-36X-1, 25-26	337.65		10.13		84.4
721B-36X-1, 75-76	338.15		10.36		86.3
721B-36X-1, 114-115	338.54	10.92	10.55	0.37	87.9
721B-36X-1, 140-150	338.80		10.43		86.9
721B-36X-2, 25-26	339.15		10.58		88.1
721B-36X-2, 75-76	339.65		5.26		43.8
721B-36X-2, 125-126	340.15		8.80		73.3
721B-36X-3, 25-26	340.65		6.66		55.5
721B-37X-1, 25-26	347.25		0.91		7.6
721B-37X-1, 75-76	347.75		3.98		33.2
721B-37X-1, 125-126	348.25		5.53		46.1
721B-37X-2, 25-26	348.75		7.12		59.2
721B-37X-2, 75-76	349.25	1.47		12.3	
721B-37X-2, 125-126	349.75		6.89		57.4
721B-37X-3, 25-26	350.25		2.93		24.4
721B-37X-3, 125-126	351.25		4.21		35.1
721B-37X-3, 149-150	351.49	1.00	0.93	0.07	7.8
721B-37X-4, 25-26	351.75		2.44		20.3
721B-37X-4, 75-76	352.25		5.06		42.2
721B-37X-4, 125-126	352.75		6.57		54.7
721B-37X-5, 25-26	353.25		6.44		53.7
721B-37X-5, 125-126	354.25		5.43		45.2
721B-37X-6, 25-26	354.75		3.39		28.2
721B-37X-6, 25-26	354.75		3.39		28.2
721B-37X-6, 39-40	354.89	1.02	0.97	0.05	8.1
721B-37X-6, 40-42	354.90	1.11	1.10	0.01	9.2
721B-37X-6, 42-43	354.92	1.11	1.06	0.05	8.8
721B-37X-6, 46-47	354.96	6.45	6.43	0.02	53.6
721B-37X-6, 75-76	355.25	5.47		45.6	
721B-37X-6, 126-127	355.76		0.75		6.3
721B-40X-5, 114-115	383.04		0.66		5.5
721B-40X-5, 114-115	383.04	0.56	0.50	0.06	4.2
721B-41X-5, 114-115	392.74	0.56	0.50	0.06	4.2
721B-41X-5, 149-150	393.09	5.05	4.86	0.19	40.5
721B-42X-2, 149-150	398.19	2.69	2.57	0.12	21.4
721B-44X-5, 114-115	421.64	1.42	1.31	0.11	10.9
721B-44X-5, 140-150	421.90		1.24		10.3

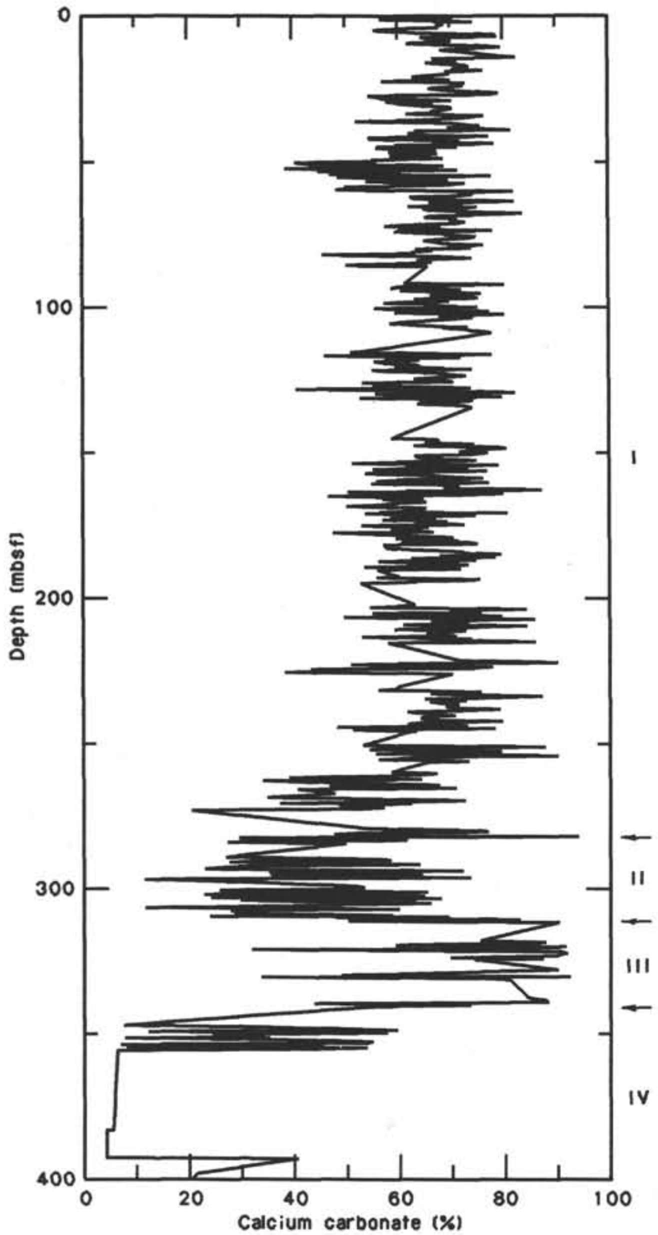

Figure 5. Calcium carbonate profile, Site 721. Hole 721A samples cover 0–86 mbsf, and Hole 721B samples correspond to the interval from 92–422 mbsf. Because the recorded depths in Hole 721A are 3–5 m shallower than corresponding depths in 721B, an artificial gap exists between 86 and 92 mbsf downhole. The arrows denote lithologic boundaries, and the numbers correspond to lithologic units.

fossil chalk to olive (5Y 4/3) siliceous bearing nannofossil chalk. These lithologic changes are evident on seismic reflection profiles (see "Seismic Stratigraphy" section, this chapter).

Unit IV (Depth: 340.7–424.2 mbsf; Age: middle Miocene to early Miocene)

Sample 117-721B-36X, CC, 30 cm, to Section 117-721B-44, CC.

Unit IV contains marly nannofossil and nannofossil chalks that overlie fining-upward turbidite sequences (5–300 cm thick) of clayey siltstones to silty claystones. The basal layers of the turbidites fine upward through Unit IV from mudstones in Core 117-721B-44X to silty claystones in Core 117-721B-36X. The deposits have low organic carbon and calcium carbonate values

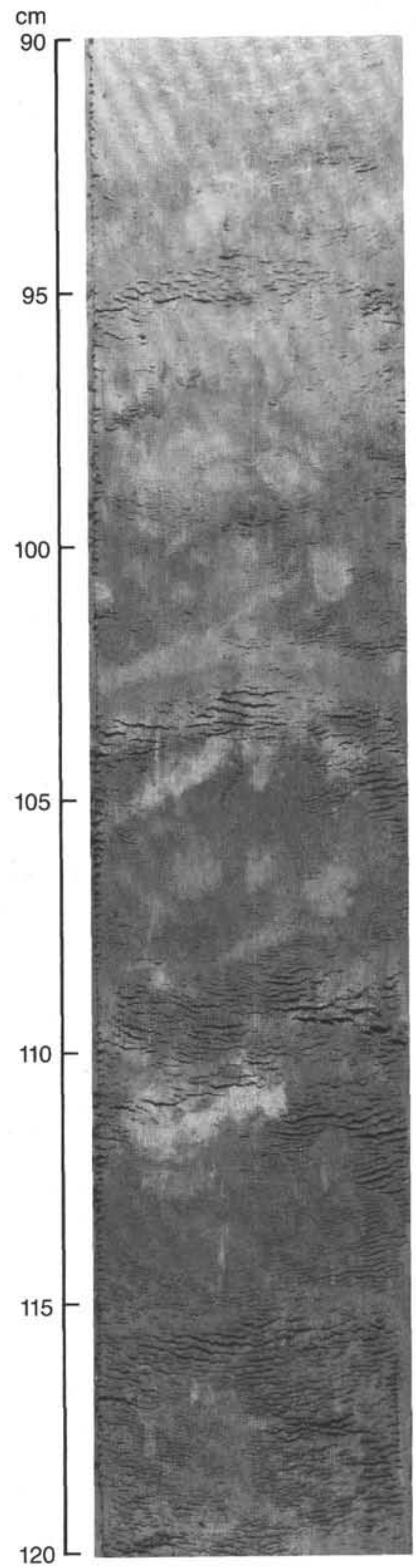

Figure 6. Burrow structures at boundary between light and dark layers in Unit I (Section 117-721B-17X-1, 90–120 cm). Note blurring of boundary by bioturbation.

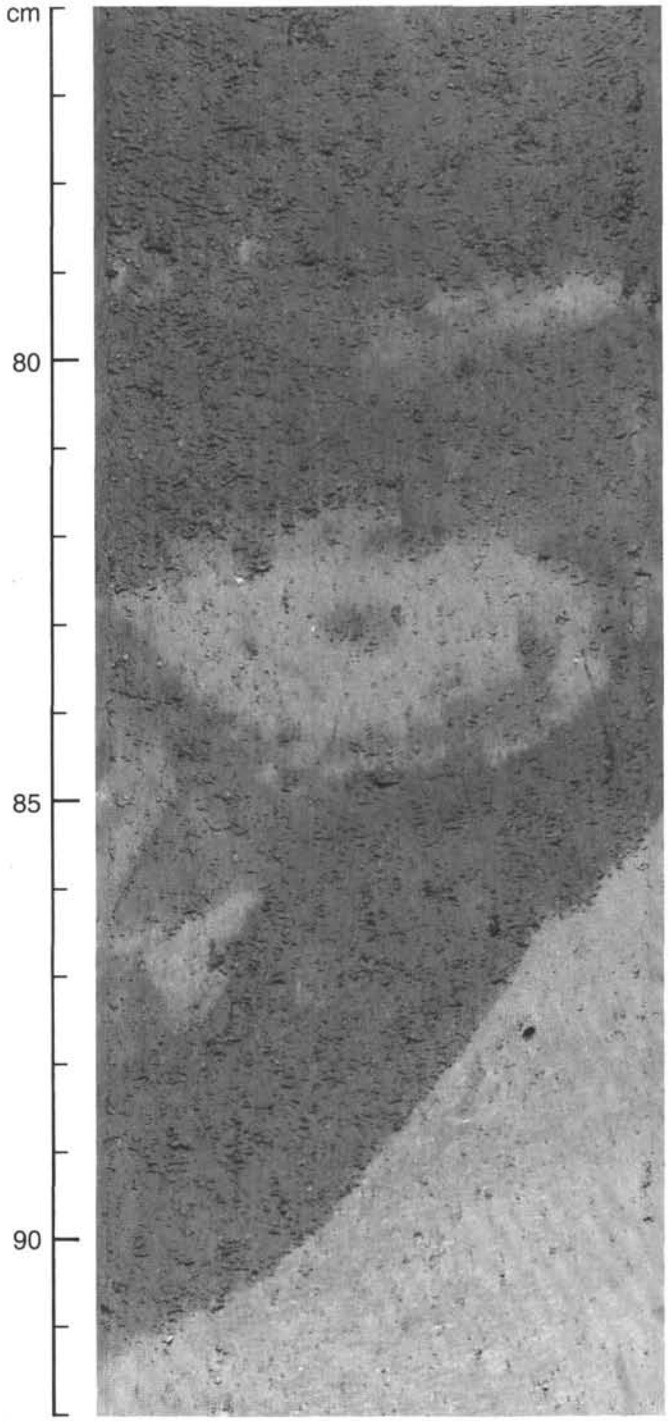

Figure 7. Transition between light and dark layers in Unit I (Section 117-721B-3H-6, 76–92 cm). Note mixing of dark material into light colored material by burrowing.

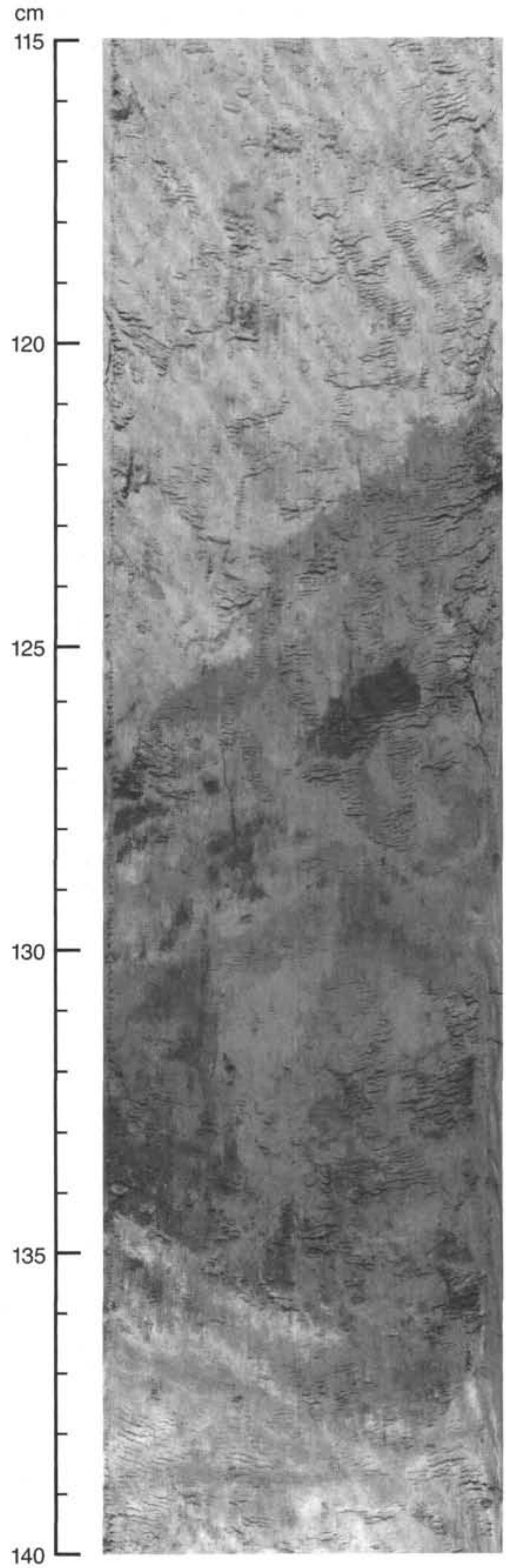

Figure 8. Inclined contact of dark material and light layer. Possible slump feature in Subunit IB (Section 117-721B-29X-2, 115–140 cm).

(Table 3) and some turbidites contain thin (0.1–2 mm) sand- to silt-sized pyrite bands (Fig. 10). These pyrite bands contain euhedral grains and framboids which imply an authigenic source. Because the grains are concentrated mostly in layers near the base of turbidites, we cannot discard the possibility that the bands result from winnowing of previously deposited sediments which contain pyrite as their sole coarse component.

The basal layers range from dark gray (N 4/0) and dark greenish gray (5G 4/1) to dark reddish gray (5YR 4/2). Above

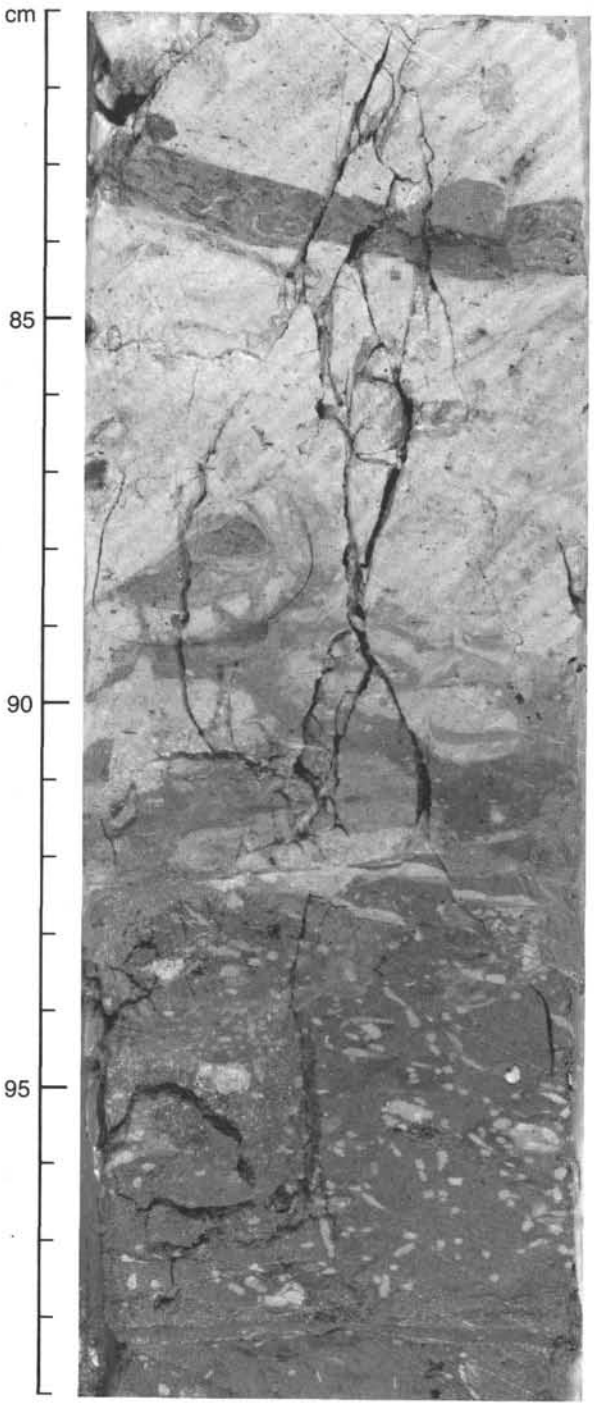

Figure 9. Disturbed section in lithologic Unit II (Section 117-721B-32X-6, 81–99 cm) showing microfault between 85 and 90 cm. Large fractures are attributed to coring disturbance.

the basal layers, olive (5Y 4/3), dark brown (10YR 3/3), and greenish brown (10YR 5/2) silty claystones and clayey siltstones predominate which in turn grade upward to greenish gray (5GY 5/1, 5BG 4/1, and 5BG 5/1) calcareous silty claystones. These claystones are frequently capped by olive (5Y 5/3), brown (10YR 5/3), and pale brown (10YR 6/2) marly nannofossil chalks and light gray (5Y 7/1) nannofossil chalks. The calcareous silty claystone and chalks are slightly to moderately bioturbated. The sharp contact which characterizes the change from pelagic deposition (nannofossil chalk) to the turbidites is shown in Figure 11.

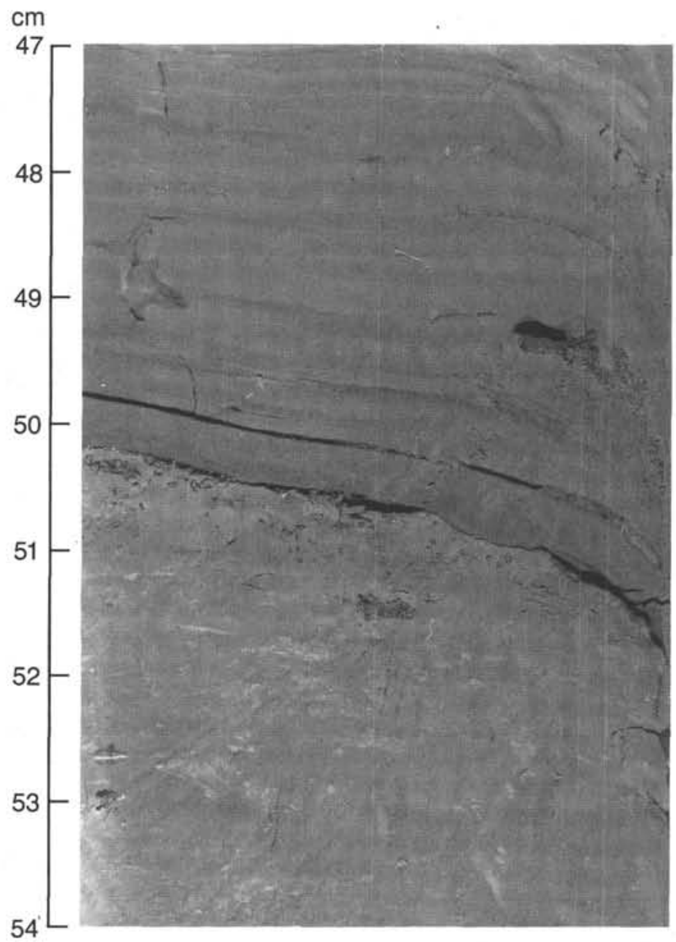

Figure 10. Pyrite grains at base of turbidite deposit (Section 117-721B-41X-6, 51 cm), in pocket at 49 cm, in thin layer near 48.5 cm.

Discussion

The lithologic units identified at Site 721 exhibit distinct characteristics that are attributed to changes in surface plankton productivity and tectonic uplift of the Owen Ridge. Lower Miocene deposits encountered in lithologic Unit IV are fine-grained (clayey silt and silty clay) turbidites with intercalated nannofossil chalks. The source of the fine-grained turbidites is unknown, but we interpret the fining-upward sequence of clayey silts and silty clays to reflect the uplift of the Owen Ridge out of the zone of turbidity current deposition. As the lower Miocene turbidite sequences below seismic reflector C (see "Seismic Stratigraphy" section, this chapter) were uplifted, the fine-grained turbidite deposits became more common in addition to thicker pelagic interbeds. This sequence is expected as the site is lifted above the zone of bedload transport. Seismic reflection profiles (see "Seismic Stratigraphy" section, this chapter) show the expected off-lapping reflectors during this interval and the timing is consistent with early Miocene uplift of the Owen Ridge discussed by Whitmarsh et al. (1974) and Whitmarsh (1979). By middle Miocene, the site was elevated above the zone of turbidite deposition and Unit III, a nannofossil chalk, reflects pelagic deposition. Site 721 contains a record of much higher resolution of the lower Miocene uplift of the Owen Ridge than was available previously.

An unconformity at 310 mbsf separates Units II and III. This contact corresponds to a 5-m.y. hiatus in the sediment record (see "Biostratigraphy" section, this chapter) and separates nannofossil chalks from siliceous-bearing nannofossil chalks.

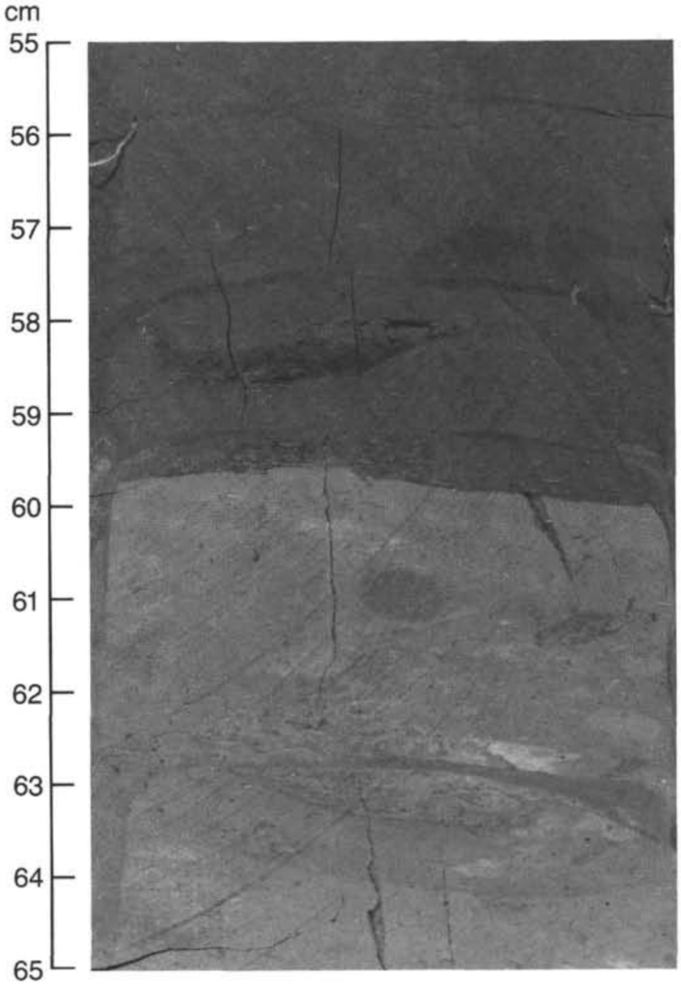

Figure 11. Contact between light colored pelagic nannofossil chalk and turbidite in Unit IV (Section 117-721B-41X-6, 60 cm).

The upper Miocene sediments deposited above the hiatus contain reworked microfossils in addition to microfault and possible slump-related structures (Figs. 8 and 9). These data are consistent with postdepositional disturbance of sediments in lithologic Unit II and Subunit IB. On the scale of seismic images, the reflectors which correspond to Unit II and Subunit IB also exhibit this disturbance (see "Seismic Stratigraphy" section, this chapter).

Upper Miocene sediments in Unit II represent a dramatic change in the plankton assemblage where, in addition to nannofossils, biogenic silica becomes abundant and both diatoms and radiolarians are preserved in the sediments. Unfortunately, the initiation of opaline sedimentation in the middle to late Miocene, which may reflect the onset of monsoonal upwelling (Whitmarsh et al., 1974), is not recorded in Hole 721B because of the unconformity between Units II and III. However, Hole 722B, in close proximity to Site 721, contains a more complete section that includes this interval and will be used to document this transition (see "Site 722" chapter, this volume).

Upper Miocene to Holocene deposits are dominantly alternating light and dark layers of foraminifer-bearing, foraminifer-nannofossil, and nannofossil oozes with a mean calcium carbonate content of 66% and a range from 40% to 90%. The color alternations in the upper Miocene to Holocene sediments reflect changes in calcium carbonate concentration and terrigenous clay abundance. Similar sediment cycles, which are evident from the Miocene to the Holocene, have been identified in other regions (i.e., Gardner, 1982; Pisias and Prell, 1985). The primary cause of these cycles has been attributed to carbonate productivity and/or preservation changes and changes in the eolian (terrigenous silty clay) input. However, post-cruise studies, which will quantify the accumulation of carbonate and terrigenous components and provide estimates of carbonate dissolution, are necessary to differentiate between each of these factors.

A preliminary analysis for cyclicity of the light and dark bedding was made on the top 100 m of Hole 721B. Colors, coded as +1 for light, 0 for medium, and −1 for dark, were assessed at 10 cm intervals from the core photos. The resulting series, which represents color changes (Fig. 12), was analyzed with Walsh spectral analysis (Weedon, 1986) to determine the dominant periods of variation. The spectra reveal well-defined peaks corresponding to cycles of 0.52, 0.64, 0.95, 1.51, 4.09, 7.87, and 17.06 m (Fig. 13). Assuming a constant sedimentation rate

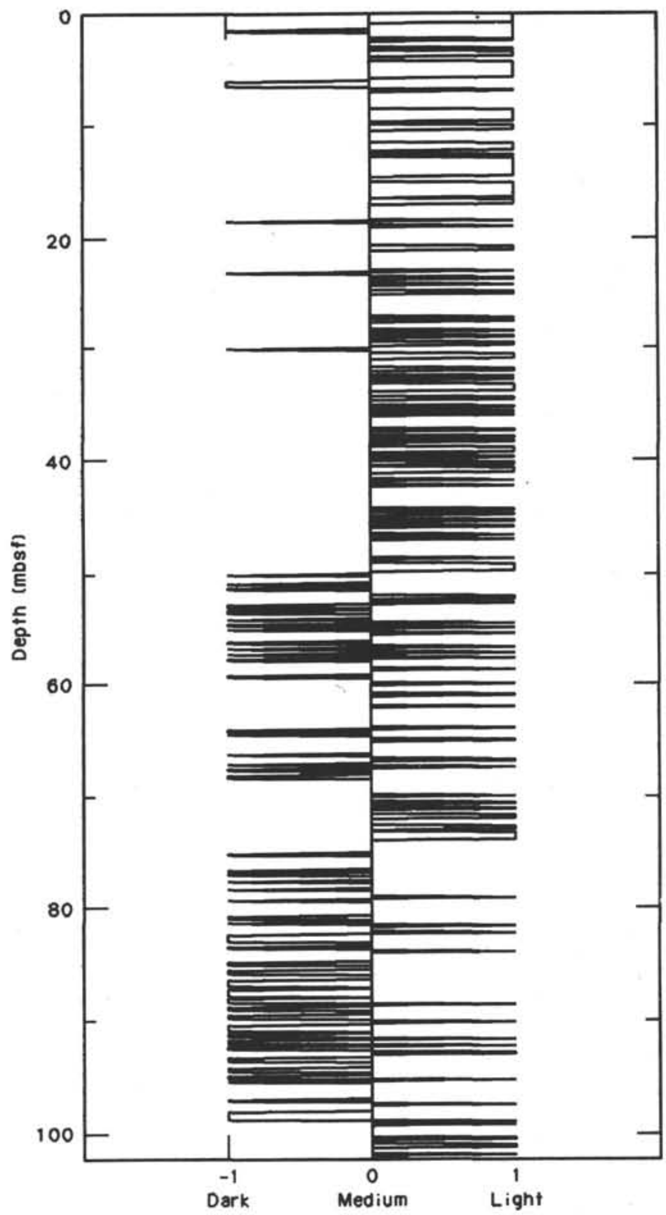

Figure 12. Diagram showing alternating light and dark layers at 10-cm intervals in the top 100 m of Hole 721B.

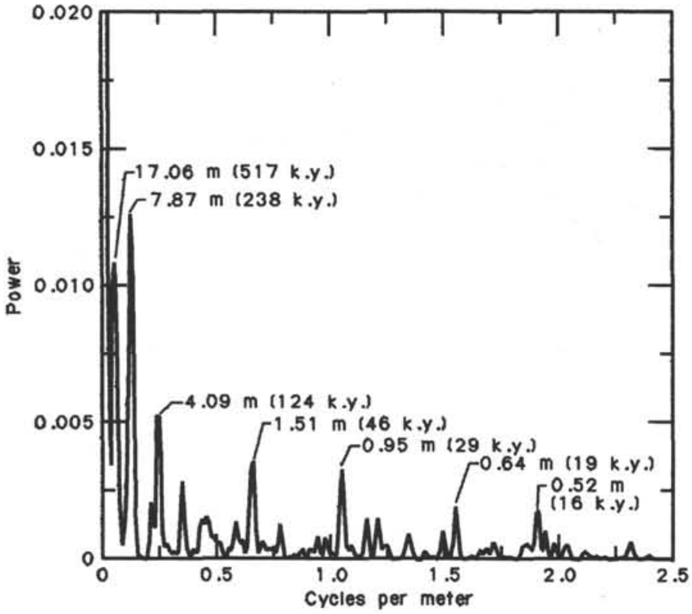

Figure 13. Walsh power spectrum of thickness variations in light and dark layers. Dominant periods are noted. Conversion to k.y. is based on a constant sedimentation rate of 33 m/m.y., and the plot represents the time since 3.10 Ma.

of 33 m/m.y. (see "Accumulation Rates" section, this chapter), these cycles correspond to 16, 19, 29, 46, 124, 238, and 517 k.y., respectively. The cycles with periods close to 410, 100, 40, and 21 k.y. correspond to the known variations in the earth's orbital parameters (Milankovitch frequencies). The high correspondence between orbital variations which influence climate and the sedimentary cycles implies that the compositional changes causing the light and dark layering may reflect climatic variations. These preliminary results are encouraging. Post-cruise studies will identify the components responsible for the color changes and their response to climatic fluctuations, and establish a high-resolution age model to document more precisely the periods of variation.

BIOSTRATIGRAPHY

Introduction

To investigate the evolution of monsoonal upwelling and the tectonic uplift history of the Owen Ridge, three holes were drilled at the top of the Owen Ridge at Site 721 to provide a partly overlapping and composite section down to the lower Miocene. A plot of faunal datum levels and paleomagnetic reversals vs. depth below the seafloor is presented in Figure 14; for a detailed listing of these data points, see Tables 4 and 5.

Planktonic foraminifers are abundant, highly diverse, and well-preserved in Hole 721A and the upper part of Hole 721B. The lower part of Hole 721B, however, contains low-diversity and sparse assemblages. Benthic foraminifers are abundant, highly diverse, and well-preserved throughout almost all of the cores. Calcareous nannofossils are abundant throughout the cores. However, below the top of lithologic Unit III (310 mbsf) the state of preservation of coccoliths is poor. Radiolarians are abundant and well-preserved in almost all samples down to the bottom of lithologic Unit II. Diatoms start to increase in number in the middle part of lithologic Subunit IA (around 125 mbsf) downhole and become abundant from the lower part of Subunit IA (around 220 mbsf).

The zonation of the various fossil groups is summarized in Figures 15, 16, and 17. A hiatus is inferred between lithologic Unit II and Unit III. The bottom of lithologic Unit II belongs to nannofossil Zone NN9 (upper middle Miocene to lower upper Miocene). The nannofossils in the uppermost part of lithologic Unit III belong to Zone NN5 (uppermost lower Miocene to middle Miocene). The planktonic foraminifers also show a similar hiatus between Zone N15 (middle to upper Miocene) at the bottom of lithologic Unit II and Zones N7 to N8 (uppermost lower Miocene) at the top of lithologic Unit III. Most of the middle Miocene sediments are not recorded.

The nannofossil flora and radiolarian fauna of Site 721 are characterized by the absence of some typical tropical species since the late Miocene. Remarkable changes in nannoflora occur at the top of the Miocene (around 140 mbsf) and in radiolarian fauna in the upper Miocene (around 220 mbsf). Planktonic foraminifers indicate an increased upwelling intensity from the lowermost upper Miocene (around 260 mbsf). Two horizons of faunal change are recognized; one is just above the unconformity (308 mbsf) in the middle Miocene and another is in the middle part of Unit I (around 135 mbsf) in the lowermost Pliocene. The faunal and floral events in combination with the observed increase in diatom abundance downhole represent strong environmental changes during the earliest late Miocene, which may be related to stronger upwelling intensity and/or global cooling events.

Planktonic Foraminifers

Hole 721A and the upper part of Hole 721B in general contain highly diverse, well-preserved foraminiferal faunas. The lower interval (Samples 117-721B-28X, CC, 269.4 mbsf, to 117-721B-44X, CC, 424.2 mbsf) yields low-diversity assemblages and only sparse specimens of planktonic foraminifers. The lowest concentrations are confined to a turbidite sequence (Samples 117-721B-37X, CC, 356.6 mbsf, to 117-721B-44X, CC, 424.2 mbsf), where only reworked specimens were found. Zonal boundaries are tentatively assigned based on shipboard analyses of the core-catcher samples. Samples were not investigated from Hole 721C.

In Cores 117-721A-1H to -7H and 117-721B-1H to -7H (0–67.3 mbsf in Hole 721A and 0–66.9 mbsf in Hole 721B) the faunas are of Pleistocene age, which is corroborated by the presence of sparse *Globorotalia truncatulinoides* specimens. The upper three cores contain rare *Globigerinella calida calida* and *Globigerinella digitata* specimens, and thus represent Zone N23. A coiling change in the tests of *Pulleniatina obliquiloculata* was observed between Cores 117-721A-3H and -4H, and 117-721B-3H and -4H (29.2–38.9 mbsf in Hole 721A and 28.8–38.5 mbsf in Hole 721B) and is thought to correlate with the Jaramillo subchronozone (0.9 Ma; Saito et al., 1975). Planktonic foraminifers were completely absent from Sample 117-721A-8H, CC (76.8 mbsf) and *Globorotalia truncatulinoides* could not be identified in Sample 117-721B-8H, CC (76.4 mbsf). The last appearance of *Globigerinoides obliquus* was observed in Sample 117-721A-8H, CC (76.8 mbsf) and in Sample 117-721B-8H, CC (76.4 mbsf).

Zone N21 could not be identified because of the absence of *Globorotalia tosaensis* in this interval of the hole. The first appearance of *Sphaeroidinella dehiscens*, which marks the N18/N19–20 zonal boundary, could not be assigned, because specimens of this species are absent or rare. The recognition of the N17/N18 and N16/N17 zonal boundaries are difficult because these boundaries are defined by transitional forms in the evolutionary morphological series of subspecies of *Globorotalia tumida*. However, the first appearance of *Globorotalia tumida tumida* (N17/N18 boundary) seems to lie approximately between Samples 117-721B-21X, CC (202.0 mbsf), and 117-721B-22X, CC (211.7 mbsf). This datum also defines the base of the Pliocene (Berggren et al., 1985a). The position of the N16/N17 boundary has been estimated to lie between Samples 117-721B-

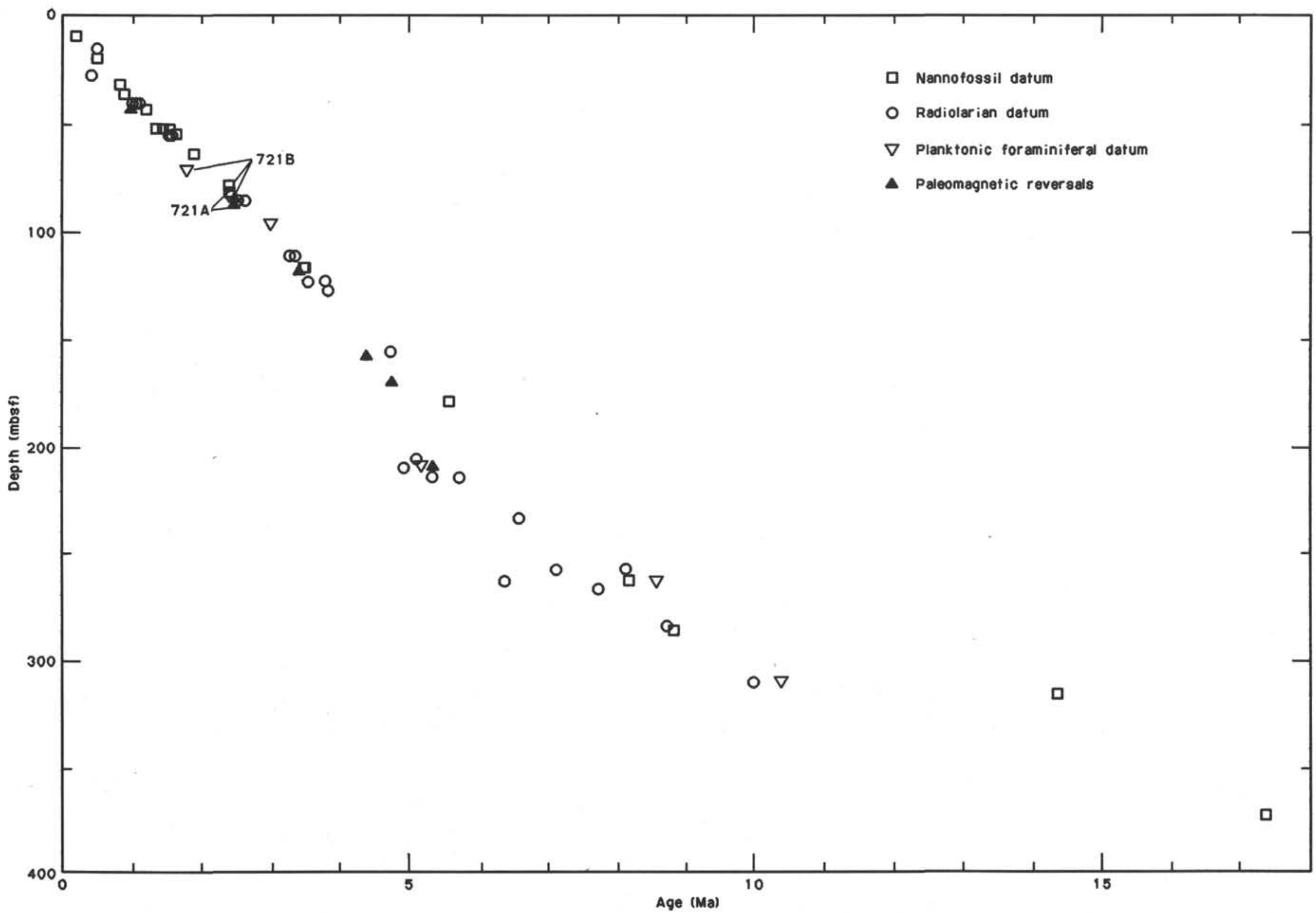

Figure 14. Stratigraphic datum vs. depth plot for Site 721. For the upper part, approximately above 80 mbsf, datum levels from Hole 721A are used, whereas datum levels from Hole 721B are used for the lower part below 80 mbsf. For a detailed listing of events, see Tables 4 and 5.

Table 4. Stratigraphic listing of faunal events and paleomagnetic reversals for Hole 721A.

Event	Core Level	Depth (mbsf)	Age (Ma)	Source of age	Notes
B *Emiliania huxleyi*	1H-4, 115–117	8.40	0.19	3	
	1H-5, 115–117	9.90			
B *Collosphaera tuberosa*	1H-CC	12.55	0.40–0.59	1	Cores MD81-369, RC14-22, and VM24-35; DSDP 214 data probably less accurate.
	2H-4, 85–87	17.90			
T *Pseudoemiliania lacunosa*	2H-4, 115–117	18.20	0.49	3	
	2H-5, 115–117	19.70			
T *Stylatractus universus*	2H-CC	22.25	0.37–0.47	1	
	3H-CC	31.95			
T *Reticulofenestra* sp. A (acme)	3H-6, 115–117	30.87	0.82	3	
	3H-CC	31.95			
B *Gephyrocapsa parallela*	4H-2, 115–117	34.60	[a]0.89	4	
	4H-3, 115–117	36.10			
T *Anthocyrtidium angulare*	4H-4, 85–87	37.30	0.94–1.04	1	
	4H-CC	41.65			
B *Lamprocyrtis nigriniae*	4H-4, 85–87	37.30	1.02–1.07	1	
	4H-CC	41.65			
T *Lamprocyrtis neoheteroporos*	4H-4, 85–87	37.30	1.09–1.13	1	
	4H-CC	41.65			
B Jaramillo	4H-7, 35–37	41.30	0.98	6	
	5H-1, 115–117	42.80			
T *Gephyrocapsa* "large"[b]	4H-CC	41.65	[a]1.10	4	
	5H-1, 115–117	42.80			
T *Helicosphaera sellii*	5H-5, 115–117	48.80			No good published age; event may be diachronous.
	5H-6, 115–117	50.30			
B *Gephyrocapsa* "large"[b]	5H-6, 115–117	50.30	[a]1.36	4	
	5H-CC	51.25			
T *Calcidiscus macintyrei*	5H-6, 115–117	50.30	1.45	6	
	5H-CC	51.25			
B *Gephyrocapsa oceanica*	5H-6, 115–117	50.30	[a]1.57	4	
	5H-CC	51.25			
T *Pterocanium prismatium*	5H-CC	52.25	1.52–1.56	1	
	6H-4, 85–87	56.60			
B *Anthocyrtidium angulare*	5H-CC	51.25	1.52–1.64	1	
	6H-4, 85–87	56.60			
B *Gephyrocapsa caribbeanica*	6H-1, 115–117	52.40	[c]1.66	4, 8	
	6H-2, 115–117	53.90			
T *Discoaster brouweri*	7H-1, 115–117	61.70	1.90	6	
	7H-2, 115–117	63.20			
T *Discoaster pentaradiatus*	8H-CC	79.55	2.40	6	
	9H-1, 115–117	80.70			
B *Theocalyptra davisiana*	8H-CC	79.55	2.42–2.44	1	
	9H-4, 85–87	84.90			
Matuyama/Gauss	9H-2, 146–148	82.51	2.47	6	
	9H-3, 35–37	82.90			

Note: Depths in Hole 721A reflect the addition of 2.75 m at the top of the hole to account for loss due to coring (see "Interhole Correlation" section, this chapter).T = upper limit and B = lower limit. Sources of ages are: 1 = Johnson et al., in press; 3 = oxygen isotope data for Site 723 (N. Niitsuma, unpubl. data); 4 = Takayama and Sato, 1987; 6 = Berggren et al., 1985b; 8 = Sato et al., in press.

[a] North Atlantic data.

[b] Long axis greater than 6 μm.

[c] North Atlantic age consistent with Italian-type section.

23X, CC (221.3 mbsf) and 117-721B-24X, CC (230.5 mbsf). The first appearance of *Neogloboquadrina acostaensis* defines the N15/N16 boundary which could be recognized in Sample 117-721B-27X, CC (259.6 mbsf). Because foraminifers are rare in this interval, this boundary is considered unreliable.

A sharp faunal break occurs between Zones N15 and N16, which is characterized by a dramatic increase in the abundance of *Globigerina bulloides*, *Globorotalia menardii*, and the appearance of the *Neogloboquadrina acostaensis-humerosa-dutertrei* group. This faunal event may represent an increased upwelling intensity during the earliest late Miocene, because the modern representatives are known to be upwelling indicators (Bé, 1977).

Samples 117-721B-28X, CC (269.4 mbsf), to 117-721B-30X, CC (289.0 mbsf), have tentatively been assigned to Zone N15, based on the absence of *Neogloboquadrina acostaensis*. No foraminifers were present in Sample 117-721B-31X, CC, and no zonal indicator could be found in Sample 117-721B-32X, CC. The co-occurrence of *Globorotalia birnageae* and *Globorotalia mayeri/siakensis* (Zones N7–8) in Samples 117-721B-33X, CC (318.0 mbsf), to 117-721B-36X, CC (347.0 mbsf), indicate a late early Miocene age; hence a discontinuity exists between Samples 117-721B-32X, CC (308.4 mbsf), and 117-721B-33X, CC (318.0 mbsf).

Planktonic foraminifers are absent in the remainder of the recovered section or are reworked.

Benthic Foraminifers

The benthic foraminiferal fauna (Corliss, 1979; Mead, 1985) was studied at Site 721 in the core-catcher samples of Hole 721A down to 86.4 mbsf (117-721A-1H, CC, through -9H, CC) and in the core-catcher samples of Hole 721B for the depths below 86.0 mbsf (117-721B-9H, CC, through -44X, CC). The abundance ranges from abundant to common in the uppermost interval (down to 240.1 mbsf). The interval from 249.8 to 347.0 mbsf contains few benthic foraminifers, whereas the lowermost interval (356.6–424.2 mbsf) contains few or no benthic foraminifers. The diversity is high in the upper part of the recovered se-

Table 5. Stratigraphic listing of faunal events and paleomagnetic reversals for Hole 721B.

Event	Core level	Depth (mbsf)	Age (Ma)	Source of age	Notes
T *Globigerinoides extremus*	7H-4, 65–67	63.21	[a]1.8	6	
	8H-CC	76.40			
T *Discoaster pentaradiatus*	8H-CC	76.97	2.40	6	
	9H-1, 115–117	77.55			
B *Lamprocyrtis neoheteroporos*	9H-4, 85–87	81.75	2.51–2.53	1	Cores MD81-369, RC14-22 and VM34-35;
	9H-CC	86.00			DSDP 214 data probably less accurate.
T *Stichocorys peregrina*	9H-4, 85–87	81.75	2.62–2.64	1	
	9H-CC	86.00			
Matuyama/Gauss	9H-6, 115–117	85.05	2.47	6	
	10X-1, 35–37	86.35			
T *Sphaeroidinellopsis* sp.	10X-4, 65–67	91.15	3.0	6	
	11X-2, 65–67	97.75			
T *Phormostichoartus fistula*	11X-CC	105.20	3.26–3.28	1	
	12X-CC	114.80			
T *Lychnodictyum audax*	11X-CC	105.20	3.33–3.35	1	
	12X-CC	114.80			
T *Sphenolithus abies*	12X-CC	114.80	3.47	6	
	13X-1, 115–117	115.95			
T *Reticulofenestra pseudoumbilica*	12X-CC	114.80	3.50	6	
	13X-1, 115–117	115.95			
Gauss/Gilbert	13X-2, 35–37	116.65	3.40	6	
	13X-2, 115–117	117.45			
T *Phormostichoartus doliolum*	13X-4, 85–87	120.15	3.53–3.55	1	
	13X-CC	124.40			
B *Amphirhopalum ypsilon*	13X-4, 85–87	120.15	3.77–3.79	1	
	13X-CC	124.40			
T *Spongodiscus ambus*	13X-4, 85–87	120.15			Irregular distribution at top of range.
	13X-CC	124.40			
B *Spongaster tetras tetras*	13X-CC	124.40	3.83–3.85	1	
	14X-4, 85–87	129.75			
T *Didymocyrtis penultima*	14X-4, 85–87	129.75			
	14X-CC	134.10			
T *Solenosphaera omnitubus*	16X-CC	153.50	4.7–4.8	2	
	17X-4, 85–87	158.85			
T Sidufjall	17X-2, 115–117	156.15	4.40	6	
	17X-4, 115–117	159.15			
T *Stichocorys delmontensis*	17X-CC	163.20			
	18X-4, 85–87	168.55			
B Thvera	18X-3, 115–117	167.35	4.77	6	
	18X-6, 115–117	171.85			
T *Discoaster quinqueramus*	19X-3, 115–117	177.05	5.6	6	Age appears to be erroneous.
	19X-4, 115–117	178.55			
T *Siphostichartus corona*	21X-CC	202.00	5.0–5.1	2	
	22X-4, 85–87	207.35			
B *Globorotalia tumida tumida*	22X-2, 65–67	204.15	5.2	6	
	22X-CC	211.70			

quence and deteriorates downhole. The preservation shows the same pattern as the diversity, with well-preserved fauna occurring in the upper part. Preservation becomes good further down, and below 385.6 mbsf the fauna is badly preserved and shows signs of reworking.

Eggerella bradyi, *Globocassidulina subglobosa*, *Melonis barleeanum*, and *Pullenia bulloides* are the only species that occur consistently in high relative abundances throughout the sequence; occurrences of other species are restricted to parts of the sequence. A slight faunal change in the benthic foraminiferal fauna appears to occur somewhere between Sample 117-721B-14X, CC (134.1 mbsf), and 117-721B-16X, CC (153.5 mbsf). The most abundant species in the uppermost part (above 76.8 mbsf) are *Cassidulina carinata* and *Uvigerina auberiana*, which together make up about 40% of the benthic foraminiferal fauna in these samples. Species like *Cassidulina carinata* and *Hoeglundina elegans* are not present below this interval.

The species *Sigmoilinopsis schlumbergeri* occurs consistently above 221.3 mbsf and is absent below.

A sharp faunal change occurs approximately at the level of Sample 117-721B-32X, CC (308.4 mbsf), or slightly above. *Cibicidoides wuellerstorfi*, *Melonis pompiloides*, *Uvigerina auberiana*, and *Uvigerina peregrina* do not occur below this level, whereas *Anomalinoides semicribratus* and *Vulvulina spinosa* occur with high relative abundances below this level; the former species has a known stratigraphic range from middle Eocene (P12) through middle Miocene (N12; van Morkhoven et al., 1986). *Ehrenbergina hystrix* disappears just above and *Globocassidulina decorata* just below this level. This faunal change coincides with the apparent break in sedimentation seen both in the planktonic foraminiferal and nannofossil records.

Calcareous Nannofossils

Abundant and well-preserved nannofossils are found throughout the Quaternary sequences in Holes 721A to 721C. Samples 117-721B-1H, CC (9.4 mbsf), and 117-721C-1H, CC (3.6 mbsf), contain *Emiliania huxleyi* and can be correlated with the upper Pleistocene to Holocene Zone NN21. Because *Emiliania huxleyi* and *Pseudoemiliania lacunosa* are absent in Sample 117-721A-1H-5, 115–117 cm, down to Sample 117-721A-2H-4, 115–117 cm (12.55–18.20 mbsf), and 117-721C-2H, CC (13.3 mbsf), they are assigned to the Pleistocene Zone NN20. The presence of *P. lacunosa* and the absence of discoasters place Samples 117-721A-2H, 115–117 cm, through 117-721A-7H-1, 115–117 cm (19.70–61.70 cm), and Samples 117-721B-2H, CC (19.1 mbsf), through 117-721B-7H, CC (66.9 mbsf), in Zone NN19. Within Zone NN19 the following calcareous nannofossil datums which were recognized in the North Atlantic Ocean (Perch-Nielsen,

Table 5 (continued).

Event	Core level	Depth (mbsf)	Age (Ma)	Source of age	Notes
Gilbert/Chronozone 5	22X-4, 115–117	207.65	5.35	6	
	22X-5, 35–37	208.35			
T *Botryostrobus bramlettei*	22X-4, 85–87	207.35	4.9–5.0	2	Should be higher.
	22X-CC	211.70			
T *Acrobotrys tritubus*	22X-CC	211.70	5.3–5.4	2	
	23X-C, 85–87	215.55			
T *Stichocorys johnsoni*	22X-CC	211.70	[b]5.7–5.8	2	
	23X-3, 85–87	215.55			
S. delmontensis	24X-CC	230.50	6.1–6.7	2	
S. peregrina	25X-4, 85–87	235.85			
B *Spongodiscus ambus*	25X-CC	240.10			
	26X-4, 85–87	245.45			
T *Diartus hughesi*	27X-4, 85–87	255.15	7.1–7.2	2	Considerable reworking of this species.
	27X-CC	259.60			
T *Diartus petterssoni*	27X-4, 85–87	255.15	8.1–8.2	2	Considerable reworking of this species.
	27X-CC	259.60			
B *Solenosphaera omnitubus*	27X-CC	259.60	6.3–6.5	2	
	28X-4, 85–87	264.95			
B *Stichocorys peregrina*	27X-CC	259.60			
	28X-4, 85–87	264.95			
B *Discoaster quinqueramus*	28X-1, 105–106	260.65	8.2	6	
	28X-2, 107–109	262.17			
B *Neogloboquadrina acostaensis*	28X-2, 65–67	261.75	8.6	6	
	28X-4, 65–67	264.75			
B *Acrobotrys tritubus*	28X-4, 85–87	264.95	7.7–7.8	2	Rare in Site 721.
	28X-CC	269.40			
B *Diartus hughesi*	29X-CC	279.20	8.7–8.8	2	
	30X-CC	289.00			
T *Discoaster hamatus*	30X-3, 115–117	283.37	8.85	6	
	30X-CC	289.00			
T *Globorotalia mayeri*	32X-CC	308.40	[c]10.4	6	
	33X-2, 65–67	310.55			
B *Discoaster hamatus*	33X-1, 115–116	309.55	10.0	6	
	33X-2, 115–116	311.05			
T *Sphenolithus heteromorphus*	33X-2, 115–116	311.05	14.4	6	
	33X-CC	318.00			
T *Sphenolithus belemnos*	38X-CC	366.30	17.4	6	
	39X-CC	375.90			

Note: T = upper limit of event and B = lower limit. Sources of ages are: 1 = Johnson et al., in press; 2 = Johnson and Nigrini, 1985; and 6 = Berggren et al., 1985b.
[a] *G. obliquus extremus* cited in Berggren et al., 1985b.
[b] *E.* cf. *diaphanes* cited in Johnson and Johnson and Nigrini, 1985.
[c] *G. siakensis* cited in Berggren et al., 1985.

1985; Takayama and Sato, 1987) are recognized in descending order in Holes 721B and 721C: (1) top of acme of *Reticulofenestra* sp. A, 0.83 Ma, 117-721B-3H, CC, 117-721A-3H, CC; (2) First Appearance Datum (FAD) *Gephyrocapsa parallela*, 0.89 Ma, 117-721C-4H, CC; (3) Last Appearance Datum (LAD) *Helicosphaera sellii*, 1.19 Ma, 117-721B-5H, CC;(4) FAD *Gephyrocapsa oceanica*, 1.57 Ma, 117-721B-6H, CC; (5) FAD *Gephyrocapsa caribbeanica*, 1.66 Ma, 117-721B-6H, CC.

The Pliocene/Pleistocene boundary, which is designated by the bottom of *Gephyrocapsa caribbeanica* is placed somewhere between Samples 117-721A-6H-1, 115–117 cm, and 117-721A-6H-2, 115–117 cm (52.40–53.90 mbsf), and Samples 117-721B-6H, CC, and 117-721B-7H, CC. The top of *Discoaster brouweri*, which marks the NN19/NN18 boundary occurs between Samples 117-721A-7H-1, 115–117 cm, and 117-721A-7H-2, 115–117 cm (61.70–63.20 mbsf). The top of *Discoaster pentaradiatus* occurs between 117-721A-8H, CC, and 117-721A-8H, CC, and 117-721A-9H-1, 115–117 cm. Samples below the top of *D. pentaradiatus* are assigned to Zone NN17. Sample 117-721B-8H, CC (76.4 mbsf), contains only one discoaster species, *D. brouweri*, and is therefore assigned to Zone NN18. The assemblages in Samples 117-721B-9H, CC (86.0 mbsf), through 117-721B-11X, CC (105.2 mbsf), are characterized by the occurrences of *D. brouweri* and *D. pentaradiatus*. Abundant occurrences of *Reticulofenestra pseudoumbilica* are first observed in Sample

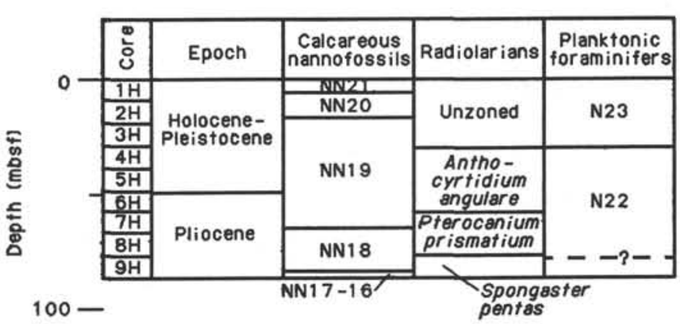

Figure 15. Correlation of planktonic microfossil zones in Hole 721A.

117-721B-12X, CC (114.8 mbsf). Therefore, the samples mentioned above are placed in Zones NN17 to NN16. Notably, *Discoaster surculus* and *D. tamalis* are not found in these samples. In the absence of ceratoliths Samples 117-721B-12X, CC (114.8 mbsf), through 117-721B-14X, CC (134.1 mbsf), are tentatively placed in lower Pliocene Zones NN15 and NN14. The next two samples, 117-721B-15X, CC (143.8 mbsf), and 117-721B-16X, CC (153.5 mbsf) are assigned to Zones NN13 and NN12 (lower Pliocene to uppermost Miocene) because of the absence of both *Discoaster asymmetricus* and *D. quinqueramus*. As ceratoliths are rare, the distinction between the two zones is uncertain.

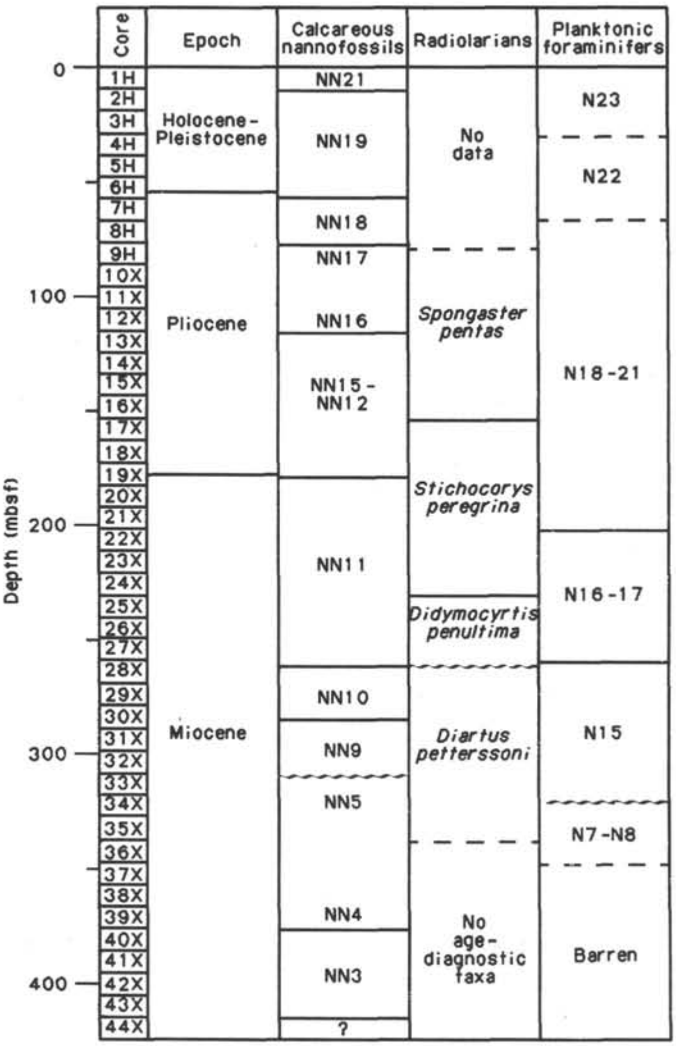

Figure 16. Correlation of planktonic microfossil zones in Hole 721B.

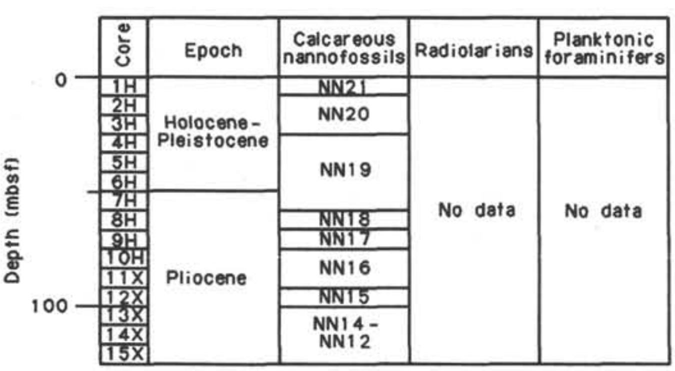

Figure 17. Correlation of planktonic microfossil zones in Hole 721C.

Sample 117-721B-17X, CC (163.2 mbsf), contains rare specimens of *Ceratolithus armatus* and can be assigned to Zone NN12. Below this core the nannoflora changes progressively with a gradual increase in the number of species and specimens of discoasters. The interval from Sample 117-721B-18X, CC (172.9 mbsf), down to 117-721B-27X, CC (259.6 mbsf), contains *Discoaster quinqueramus* together with *D. berggrenii*, *D. surculus*, *D. pentaradiatus*, and *D. variabilis* and belongs to the upper Miocene (Zone NN11). The occurrence of *Discoaster hamatus* suggests that Samples 117-721B-30X, CC (289.0 mbsf), through 117-721B-32X, CC (308.4 mbsf), can be correlated with Zone NN9. Therefore, Samples 117-721B-28X, CC (269.4 mbsf), and 117-721B-29X, CC (279.2 mbsf), belong to Zone NN10.

A remarkable change in species composition and the state of preservation of calcareous nannofossils occurs between Samples 117-721B-32X, CC (308.4 mbsf), and 117-721B-33X, CC (318.0 mbsf). In contrast to the previous samples, sediments below this horizon contain abundant *Cyclicargolithus floridanus*, and the preservation of coccoliths is poor. Though *Helicosphaera ampliaperta* is not found in this hole (it is known to be rare or absent in some regions of the South Atlantic and the Pacific; Perch-Nielsen, 1985), the occurrence of *Sphenolithus heteromorphus* suggests that Samples 117-721B-33X, CC, (318.0 mbsf), through 117-721B-40X, CC (385.6 mbsf), belong to lower and middle Miocene Zones NN5 and NN4. Therefore, Zones NN8 through NN6 are missing; a middle Miocene hiatus is inferred at this site. From Sample 117-721B-33X, CC (318.0 mbsf), down to the bottom of this hole, age-diagnostic species are absent, and no biostratigraphic age assignments can be made.

Nannofossil assemblages in Hole 721C are similar to those observed in Hole 721B. In this hole, however, sporadic occurrences of *Discoaster surculus* are recognized. Based on these occurrences of *D. surculus*, Samples 117-721C-10X, CC (89.9 mbsf), and 117-721C-11X, CC (99.5 mbsf), are assigned to the upper Pliocene (Zone NN16).

As mentioned above, asteroliths and ceratoliths are comparatively rare in the Pliocene sequences at this site. For example, *Discoaster surculus* is known to prefer warm waters (Aubry, 1984) and is extremely rare and *D. tamalis* is absent. *Ceratolithus cristatus, C. rugosus*, and *Amaurolithus tricorniculatus* are missing. In addition, *Coccolithus pelagicus,* which is the typical cold-water species, is dominant. Throughout the Quaternary section, *Pseudoemiliania lacunosa* and *Rhabdosphaera* are rare. The Pliocene and Quaternary flora may suggest an initiation of upwelling in this area at the end of Miocene.

Radiolarians

Shipboard analysis of radiolarians consisted of examination of all core-catcher samples from 721A and Samples 117-721B-9H, CC (86.0 mbsf), to 117-721B-44X, CC (424.2 mbsf). Additional intermediate samples were examined during shore-based studies. Radiolarians are abundant, robust, and well-preserved in all samples examined except for Samples 117-721A-2H, CC (19.5 mbsf), 117-721A-3H, CC (29.2 mbsf), and 117-721A-6H, CC (57.8 mbsf), where they are few and only moderately well-preserved. From 117-721B-33X, CC (318.0 mbsf), to 117-721B-44X, CC (424.2 mbsf), radiolarians are virtually absent. Most samples below 117-721A-7H, CC (67.3 mbsf), contain some reworked middle Miocene taxa. Samples from Hole 721A and the upper part of Hole 721B (down to about 117-721B-23X, CC, 221.3 mbsf) are particularly heavy-shelled and large and contain some forms not commonly found in tropical sediments; they may reflect a response to upwelling conditions. Conversely, some typically tropical forms are absent or very rare. Diatoms are noticeable in Sample 117-721B-13X, CC (124.4 mbsf), and gradually increase in abundance downhole until they become quite abundant in Sample 117-721B-23X, CC (221.3 mbsf).

Sample 117-721A-1H, CC (9.8 mbsf) probably belongs to the upper part of the *Collosphaera tuberosa* Zone. Samples 117-721A-2H, CC (19.5 mbsf), through 117-721A-4H-4, 85–87 cm (37.25 mbsf), belong to the *Amphirohopalum ypsilon* Zone. Samples 117-721A-4H, CC (38.9 mbsf), through 117-721A-6H, CC (57.8 mbsf), belong to the *Anthocyrtidium angulare* Zone. It follows that Sample 117-721A-6H-4, 85–87 cm (56.60 mbsf), belongs to the *Pterocanium prismatium* Zone, but this determination is based on only two specimens in the sample. *Pterocanium prismatium* is extremely rare in all other material examined from this site. A similar virtual absence of this species was noted by Nigrini (1974) at DSDP Site 223. Sample 117-721A-9H, CC (89.15 mbsf), belongs to the *Spongaster pentas* Zone.

Sample 117-721B-9H, CC (86.0 mbsf), also belongs to the *Spongaster pentas* Zone, and the zone persists through Sample 117-721B-16X, CC (153.3 mbsf). Samples 117-721B-17X, CC (163.2 mbsf), through 117-721B-24X, CC (230.5 mbsf), lie within the *Stichocorys peregrina* Zone. Since only a single specimen of *Spongaster pentas* was observed in the material from Sample 117-721B-15X, CC (143.8 mbsf), and *Spongaster berminghami* and *Pterocanium prismatium* are absent, the zonal boundary was approximated to the last appearance of *Solenosphaera omnitubus*. The transition from *Stichocorys delmontensis* to *Stichocorys peregrina*, marking the top of the *Didymocyrtis penultima* Zone, occurs between Samples 117-721B-24X, CC (230.5 mbsf) and 117-721B-25X-4, 85–87 cm, CC (235.85 mbsf). However, considerable reworking of *S. delmontensis* may have influenced the placement of this zonal boundary. Between Samples 117-721B-27X-4, 85–87 cm, and 117-721B-27X, there appears to be a hiatus, and the *Didymocyrtis antepenultima* Zone is entirely missing. The material from Sample 117-721B-27X, CC (259.6 mbsf), lies within the *Diartus petterssoni* Zone, which continues through Sample 117-721B-32X, CC (308.4 mbsf). The rest of the recovered material is virtually barren of radiolarians.

PALEOMAGNETISM

Magnetostratigraphy

Magnetostratigraphy of the Site 721 sediments was studied by measuring discrete samples on the MINISPIN spinner magnetometer. The samples were obtained from Cores 117-721A-1H to -9H, and Cores 117-721B-9H to -32X. We also measured additional samples from Cores 117-721B-4H and -5H to examine horizons of the Brunhes/Matuyama Chronozone boundary and the Jaramillo Subchronozone. Stepwise alternating field (AF) demagnetization was carried out on a pilot sample from most of the cores. Some results of the AF demagnetization tests are shown in Figures 18–20. These results show that several samples had soft magnetic components, which can be erased by AF demagnetization up to 5 mT. These components include coring-induced remanence, which showed steep inclination. The magnetization cleaned by peak AF of 10 or 15 mT tends to be decreased toward the origin of the Zijderveld diagram by subsequent demagnetization. The higher coercivity component was, therefore, assumed to represent characteristic magnetization of the sediments. Other samples were routinely demagnetized at peak AF of 10 or 15 mT. Magnetic intensities after the demagnetization ranges from 0.02 to 1.8 mA/m. Figure 21 shows a histogram of inclinations obtained after the routine demagnetization. While the inclination values are distributed in a relatively wide range, the modes of normal and reversed polarity are concordant with those expected from geocentric axial dipole field at the site (30.0°).

A total of 11 oriented cores were obtained from Site 721 by using a APC and a multishot core orientation tool (Cores 117-721A-5H to -10H and 117-721B-5H to -9H). The orientation data and mean magnetic declinations of discrete samples are listed in Table 6. Declination values estimated from the orientation data are widely scattered, and are generally inconsistent with the expected geomagnetic direction (0° or 180°). The reason for this deflection is not clear at present.

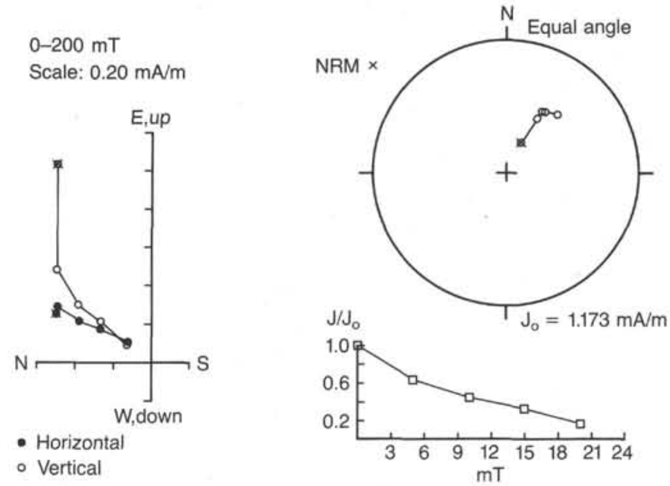

Figure 19. Result of stepwise AF demagnetization for Sample 117-721A-9H-1, 115–117 cm.

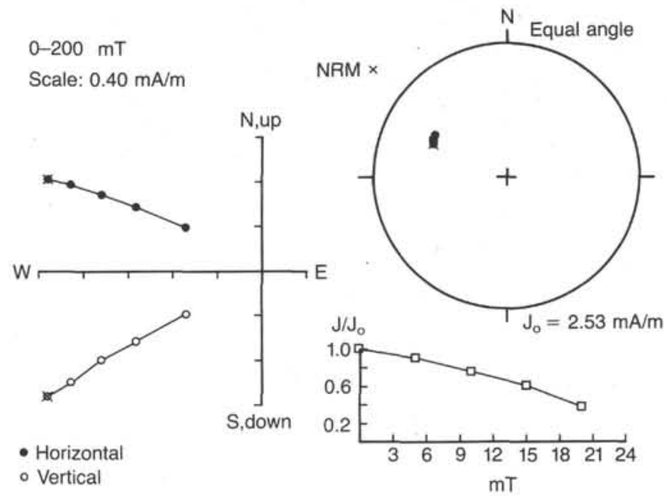

Figure 20. Result of stepwise AF demagnetization for Sample 117-721A-10X-1, 115–117 cm.

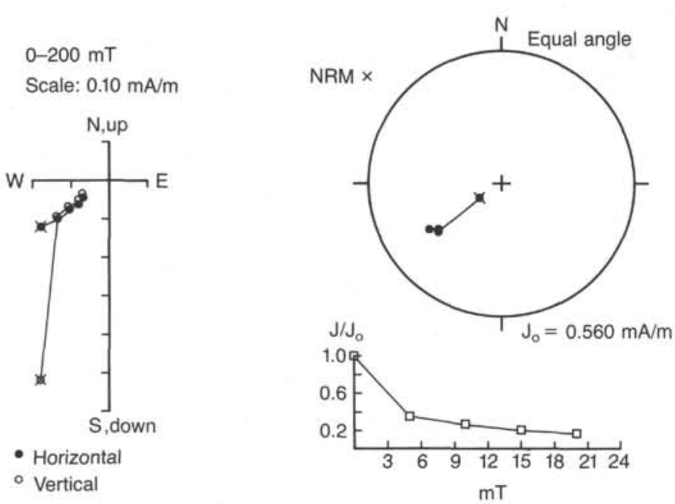

Figure 18. Result of stepwise AF demagnetization for Sample 117-721A-4H-1, 115–117 cm.

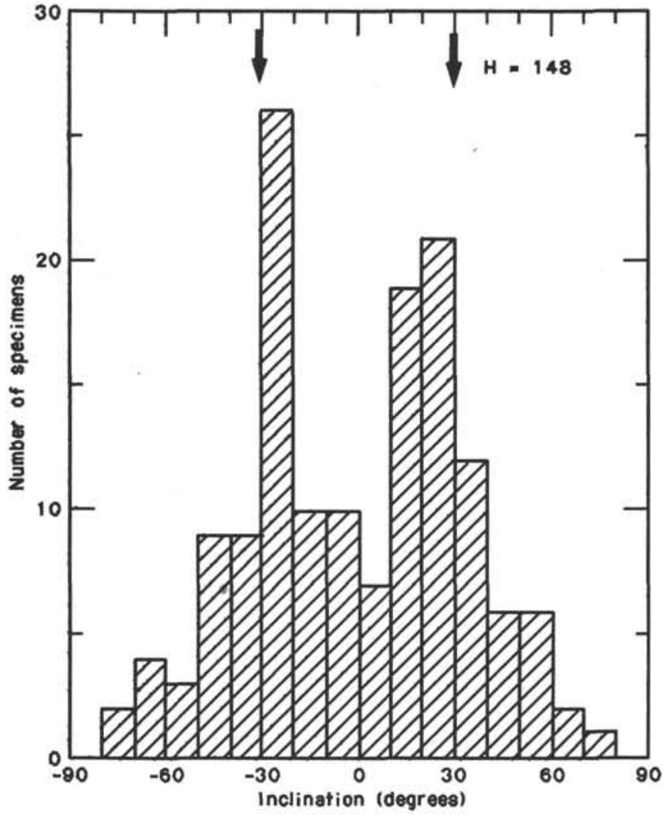

Figure 21. Histogram of magnetic inclination values from Site 721. Arrows shows the values expected from the geocentric axial dipole field (30.6°).

Table 6. Magnetic declinations of samples from oriented cores, Holes 721A and 721B.

Core	Orientation (degrees)	Measured (degrees)	Corrected (degrees)	Expected (degrees)
721A-5H	185	276 (R)	91	180
721A-6H	235	206 (R)	331	180
721A-7H	250	66 (R)	176	180
721A-8H	255	124 (R)	229	180
721A-9H	300	277 (R)	337	180
721B-5H	132	87 (N?)	315	0

Note: Orientation is azimuth of the double-line of a core tube measured from geomagnetic north by a multishot orientation tool. Measured declination is obtained as mean of paleomangetic declination relative to the double-line, and N and R indicate normal and reversed polarity estimated from inclination values. Corrected values are estimates of "true" declination of remanent magnetization, which are expected to be around 0° or 180°.

Figure 22 shows plots of directions and intensities of remanent magnetization of the samples from Hole 721A. The inclination plots in this figure show a reversed polarity zone existing between 39 and 80 mbsf of Hole 721A. Because a reversely magnetized sample was found at 36.35 mbsf, we assigned the polarity change at 39 mbsf to the beginning of the Jaramillo Subchronozone (C1r-1/C1r; 0.98 Ma). Results from the correlative horizons of Site 721B are shown in Figure 23. The polarity zone boundary at 80 mbsf of Hole 721A was also observed on the concordant horizon of Hole 721B (at 86 mbsf). Based on calcareous nannofossil data (see "Biostratigraphy" section, this chapter), this horizon is assigned to the Matuyama/Gauss boundary (C2r/C2A, 2.47 Ma). This interpretation implies that the Olduvai Subchronozone (C2) was not detected at Site 721.

Lack of records of short polarity interval records, such as Olduvai and Brunhes-Jaramillo, suggests a possibility that the Site 721 sediments have acquired remanent magnetization by averaging the geomagnetic field for intervals as long as 10^5 yr. This duration, corresponding to a thickness of about 3 m, is much longer than previously assumed as the interval of postdepositional detrital remanent magnetization (postdepositional DRM). A short hiatus in sedimentation or overprint of chemical remanent magnetization (CRM) may explain the deficiency of paleomagnetic record in some parts.

Results obtained from the Hole 721B sediments between 0 and 310 mbsf are shown in Figure 24. Using these results and additional data from the shore-based work, we determined horizons of magnetic polarity changes and assigned them to a magnetic polarity timescale as listed in Table 7. Most samples from the sections below about 250 mbsf had quite weak magnetization less than 0.04 mA/m. Their CSD (circular standard deviation) values are relatively high, suggesting difficulty of high-precision measurements of these samples. Magnetozones were therefore not identified in the lower part.

Magnetic Susceptibility

All recovered sections of Holes 721A, 721B, and 721C were measured at 5-cm intervals with a total of 1833, 6006, and 2490 measurements on Holes 721A, 721B, and 721C, respectively.

Paleomagnetic and biostratigraphic data of Hole 721A suggest that the oldest recovered sediments are late Pliocene in age (~2.5 Ma). The susceptibility data indicate lower values than observed at Site 720 (Fig. 25). The data generally vary between 25 and 125 X 10^{-6} volume S.I. units. Inspection of the data indicates cyclic fluctuations of susceptibility at a depth scale of ~1 m (Fig. 26). Using an approximate 3.5 cm/k.y. sedimentation rate for Hole 721A, this suggests a periodicity which is very close to the 23 k.y. and 19 k.y periods of precessional insolation fluctuations. Although this higher frequency variability appears to dominate the record, lower frequencies are apparent as well. Additional periodicities of ~1-2 m, ~3-4 m, and ~12-14 m suggest the presence of 41 k.y., 100 k.y., and 400 k.y. periodicities, tentatively correlated with orbital periodicities of obliquity and eccentricity. A possible cause of these cyclic variations in susceptibility is discussed below.

Paleomagnetic and biostratigraphic analyses indicate that the sequence recovered in Hole 721B extends to the early Miocene (~17 Ma) and that a hiatus between ~10-14 Ma occurs at ~310 mbsf. Comparison of the susceptibility data for Holes 721A and 721B indicate that the APC cores can be correlated on a point-for-point basis (Fig. 26). Note that the susceptibility data for each hole have virtually identical profiles. Detailed interhole correlations based on these data and lithologic marker layers are presented in the "Interhole Correlation" section (this chapter). The effect of rust contamination of the XCB core tops can be seen in Figure 27, which appears as ~10-m-spaced susceptibility spikes. Rust contamination was found to largely obliterate the upper ~1-2 m of the susceptibility record of each XCB core. Despite the rust contamination, the rapid and cyclical fluctuations apparent particularly in the APC cores are clearly present in many of the XCB cores as well to at least ~260 mbsf (upper Miocene). Below this depth, higher and less regular variations occur. In part, this may be due to the generally poor quality of the recovered sediments, which were often very disturbed. However, this change is coincident with a sharp lithologic boundary between the overlying nannofossil ooze (lithologic Subunit IA) and the underlying chalk sediments (lithologic Subunit IB; see "Lithostratigraphy" section, this chapter).

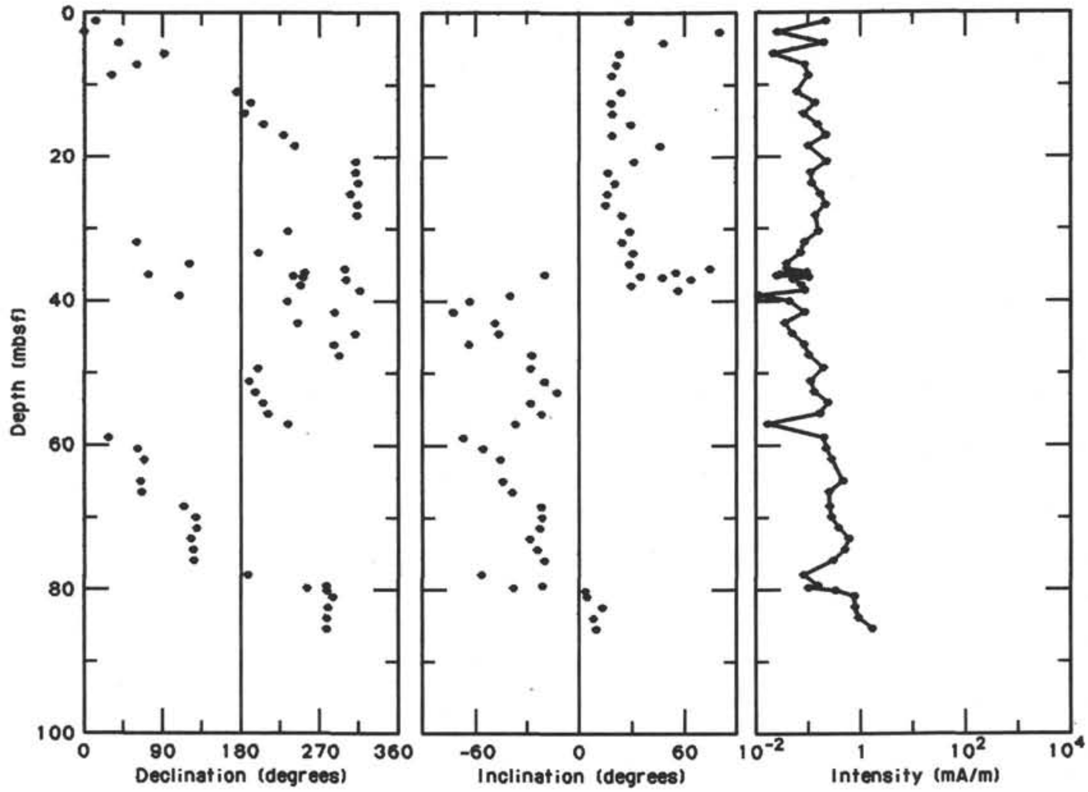

Figure 22. Plots of magnetic declination (relative values), inclination, and intensity against depth of Hole 721A, obtained after AF demagnetization.

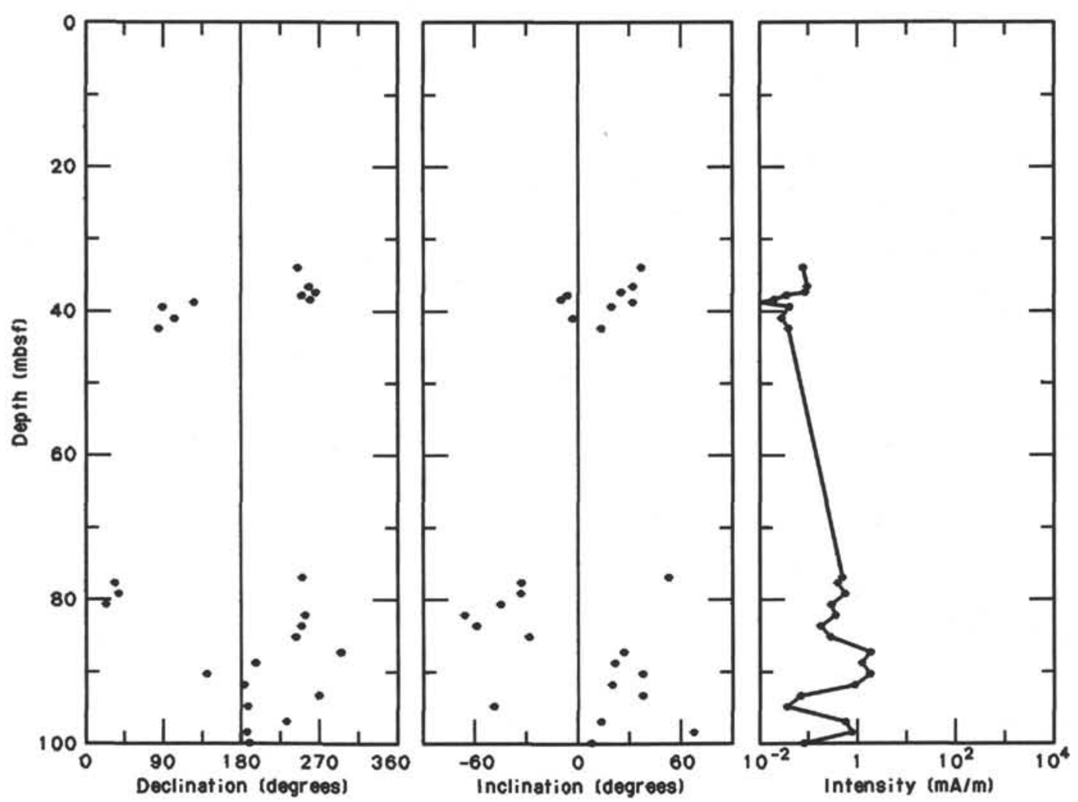

Figure 23. Plots of magnetic declination (relative values), inclination, and intensity against depth of Hole 721B, obtained after AF demagnetization.

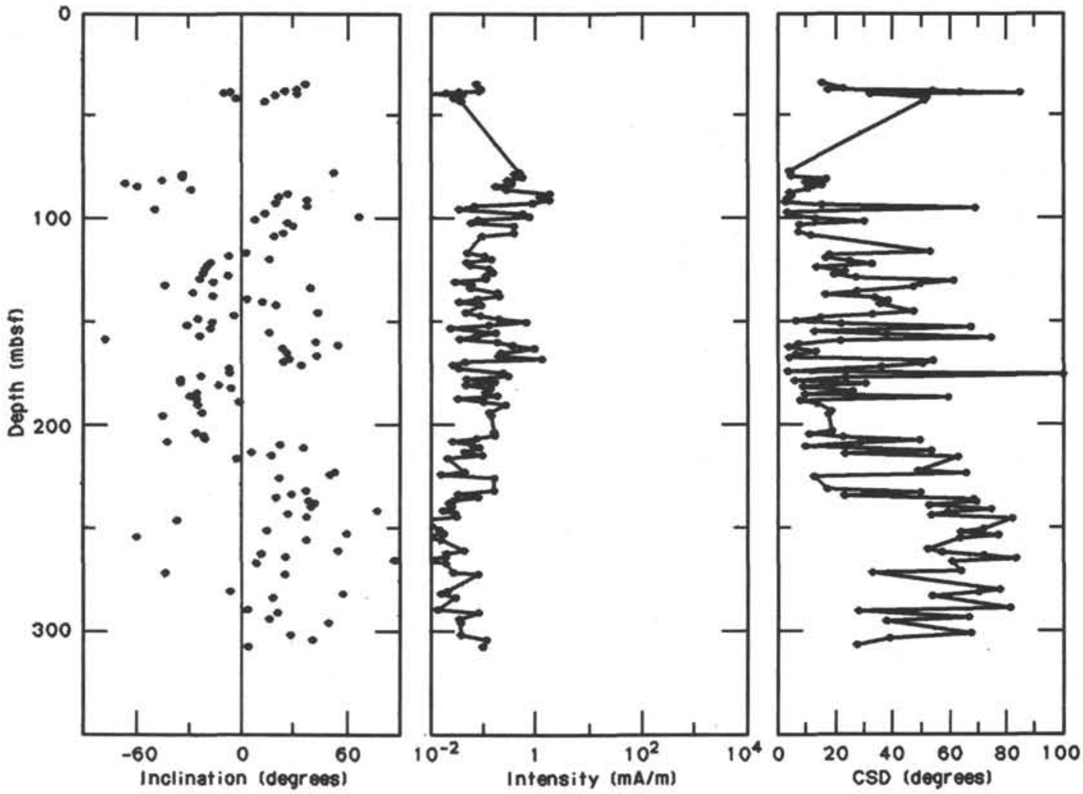

Figure 24. Plots of magnetic inclination, intensity, and CSD value against depth of Hole 721B between 0 and 310 mbsf, obtained after AF demagnetization.

Table 7. Magnetostratigraphic boundaries in Holes 721A and 721B.[a]

Hole, sample (cm)	Depth (mbsf)	Chronozone	Age (Ma)
721A-4H-7, 35 to 5H-1, 115	[b]38.55-40.05	Jaramillo/Matuyama (C1r-1/C1r)	0.98
721A-9H-2, 146 to 9H-3, 35	[b]79.76-80.15	Matuyama/Gauss (C2r/C2A)	2.47
721B-9H-6, 115 to 10X-1, 35	85.05-86.35	Matuyama/Gauss (C2r/C2A)	2.47
721B-13X-2, 35 to 13X-2, 115	116.65-117.45	Gauss/Gilbert (C2A/C2Ar)	3.40
721B-17X-2, 115 to 17X-4, 115	156.15-159.15	Top of Sidufjall (C3.2r/C3.2r1)	4.40
721B-18X-3, 115 to 18X-6, 115	167.35-171.85	Bottom of Thvera (C3A/C3Ar)	4.77
721B-22X-4, 115 to 22X-5, 35	207.65-208.35	Gilbert/5 (C3r/C3A)	5.35

[a] Based on the data with CSD less than 40. Boundary ages are after Berggren et al. (1985).
[b] Correlation with Hole 721B indicates that 2.75 m is missing from the top of Hole 721A. The corrected (true) sub-bottom depths for these events can be calculated by adding 2.75 m to the reported depths.

The shift from the carbonate sediments of lithologic Subunit IB to the more siliceous sediments of lithologic Unit II occurs at 289 mbsf, and is recorded as a significant decrease in the susceptibility data over the interval represented by lithologic Unit II (289–309.9 mbsf). A nannofossil chalk (lithologic Unit III) extends from 309.9 to ~341 mbsf and rests unconformably below lithologic Unit II (see "Biostratigraphy" section, this chapter). Other than a slight increase in the mean susceptibility, this hiatus and change in lithology is not identified in the susceptibility data. However, the boundary of Unit III and Unit IV at 341 mbsf, comprised of terrigenous, clay-bearing, nannofossil chalk, is dramatically indicated by an increase of nearly 2 decades of susceptibility. Visually, the cores of lithologic Unit IV were a reddish, buff color containing numerous mud turbidites, so the increase in susceptibility was not surprising. From ~412 mbsf to the base of Hole 721B, core descriptions indicate a significant increase in the sand-sized terrigenous component. This is consistent with the dramatic increase in susceptibility observed below ~412 mbsf, which may be due to both an increase in concentration and size of the ferrimagnetic grains.

Hole 721C was APC-cored to Core 117-721C-10H at 89.9 mbsf and XCB cored to termination at 138.0 mbsf. The fine-scale variations observed in Holes 721A and 721B are also apparent in Hole 721C (Figs. 26 and 28). Unfortunately, poor XCB recovery and rust contamination compromise these correlations below ~90 mbsf, despite the relatively good recovery.

X-Ray Diffraction Results

In an effort to understand what may be responsible for the cyclic fluctuations observed in the upper 90 m of the three holes, we took discrete 3.0-cm^3 samples from susceptibility maxima and minima over the 0.0–13.0 mbsf interval of Hole 721C. This was done to determine which sedimentary components may be covarying with the susceptibility record. The samples were freeze-dried and ground to a fine powder for X-ray-diffraction (XRD) and carbonate analyses, which were performed

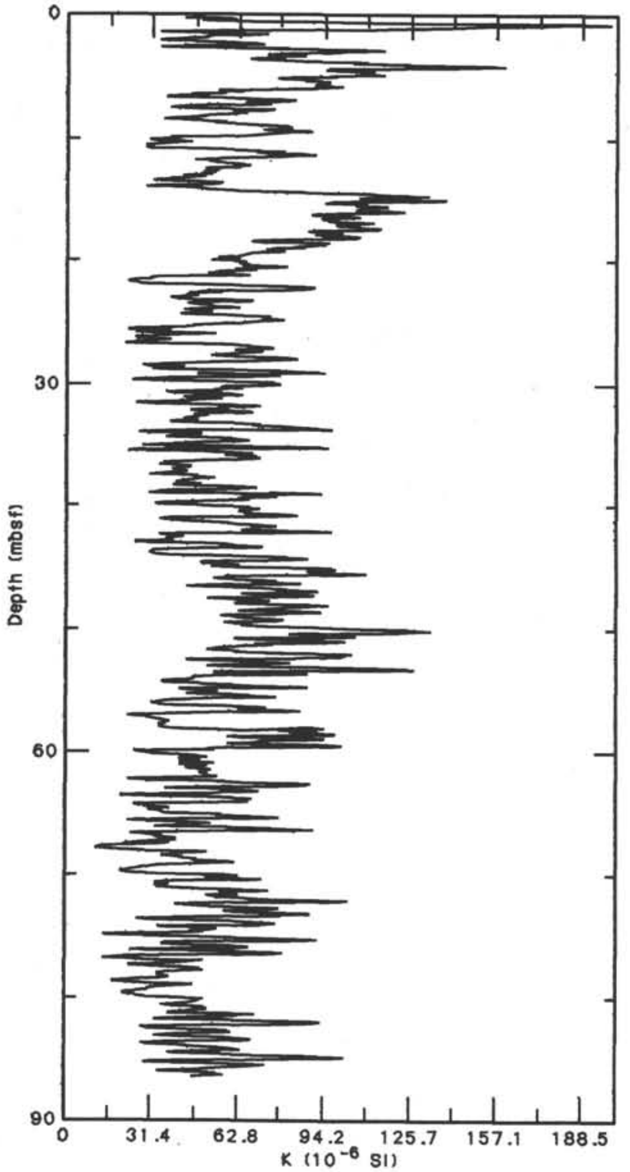

Figure 25. Volume magnetic susceptibility for Hole 721B.

by the shipboard geochemists. Once the XRD data were collected, the carbonate, quartz, dolomite, plagioclase feldspar, and combined kaolinite-chlorite peak areas (total counts) were extracted (Table 8). The carbonate percentages are also shown in Table 8.

Results from these analyses show a general inverse relationship between susceptibility and carbonate. Although this finding is common, the apparent cause of this relationship is interesting. Figure 29 shows plots of quartz, dolomite, plagioclase feldspar, and kaolinite-chlorite against susceptibility. In each case, a well-defined positive correlation exists, particularly for quartz and dolomite. This relation between quartz and dolomite was observed in other Site 721 samples as well (see "Inorganic Geochemistry" section, this chapter). If the mineral species are plotted against quartz a positive correlation emerges, suggesting that the increasing quartz brings with it increasing amounts of the other terrigenous minerals (Fig. 30). If the quartz and dolomite minerals can be interpreted as eolian tracers, then the inverse susceptibility-carbonate relation is most likely one of terrigenous (eolian) dilution of carbonate. However, in the absence of accumulation rate data, it is difficult to determine whether the susceptibility signal is one of terrigenous or carbonate dilution.

ACCUMULATION RATES

Sedimentation rates for Site 721 are based on the mean depth and age of magneto- and biostratigraphic datum levels identified in Holes 721A and 721B (Tables 4 and 5; Fig. 31). Because of uncertainties in the shipboard paleomagnetic data (see "Explanatory Notes" chapter, this volume), we favor the nannofossil biostratigraphic datums for the determination of the sedimentation rates at Leg 117 sites. For the interval from 0 to 3.5 m.y., we used seven nannofossil datums with ages based on oxygen isotope stratigraphy (Niitsuma, unpubl. data) and from Berggren et al. (1985) to determine variations in the mean sedimentation (Tables 4, 5, and 9). These same biohorizons are used to determine the mean sedimentation rate at other Leg 117 sites to permit the comparison of sediment accumulation of hemipelagic deposits on the Oman Margin and the more pelagic sediments on the Owen Ridge.

Four lithologic units are identified at Site 721 which reflect the changing depositional environment at the site due to the uplift of the Owen Ridge, and variations in surface plankton productivity (see "Lithostratigraphy" section, this chapter). Because of poor age control in the turbidite sequence of lithologic Unit IV, no estimate of sedimentation rate can be made at this time.

Lithologic Unit III, a nannofossil chalk deposited in the early to middle Miocene, is characterized by a relatively low mean sedimentation rate of 19 m/m.y. This low rate reflects pelagic sedimentation above the zone of turbidite deposition but still in waters corrosive to calcium carbonate (see "Lithostratigraphy" section, this chapter).

At Site 721, a hiatus spanning approximately 4 m.y. separates lithologic Units II and III. A more complete section representing the transition from Unit III to II in the late middle Miocene can be found in nearby Site 722 (see "Site 722" chapter, this volume). Sediments deposited between 261.2 and 309.9 mbsf at Site 721 (liothologic Units IB and II) at a mean rate of 21 m/m.y. appear disturbed and probably do not reflect continuous sediment accumulation (see "Lithostratigraphy" section, this chapter). The large scatter in age estimates for particular depths within this section, especially near 260 mbsf (Fig. 31), reflect this disturbance. The mean sedimentation rates calculated for comparable sections in nearby Site 722 are much higher than at Site 721 (42–54 m/m.y. vs. 21 m/m.y.) suggesting that Site 722 contains a more complete record of continuous sedimentation in ther middle to late Miocene than is found at Site 721.

Nannofossil oozes in the lower part of lithologic Unit I, which was deposited at the end of the Miocene and the beginning of the Pliocene (169–208 mbsf), are characterized by a high mean sedimentation rate (67 m/m.y.; Fig. 31). The high sedimentation rate may reflect an increase in particle flux associated with an increase in productivity and/or an increase in eolian input, an increase in calcite preservation at the site moves to less corrosive waters, or a change in the tectonic setting of the site such that more of the primary flux accumulated. The cause of this increase cannot be determined at this time.

During the last 3.5 m.y. (the upper part of lithologic Unit I), the mean sedimentation rate at Site 721 varied between 31 and 48 m/m.y. with an average of 33 m/m.y. (Fig. 31; Table 9). These are similar to the rates at Owen Ridge Sites 722 and 731 over this same time interval and of pelagic sedimentation in other areas, but are two to five times lower than rates during comparable time intervals from hemipelagic deposits on the Oman Margin (see "Site 723" through "Site 730" chapters, this volume).

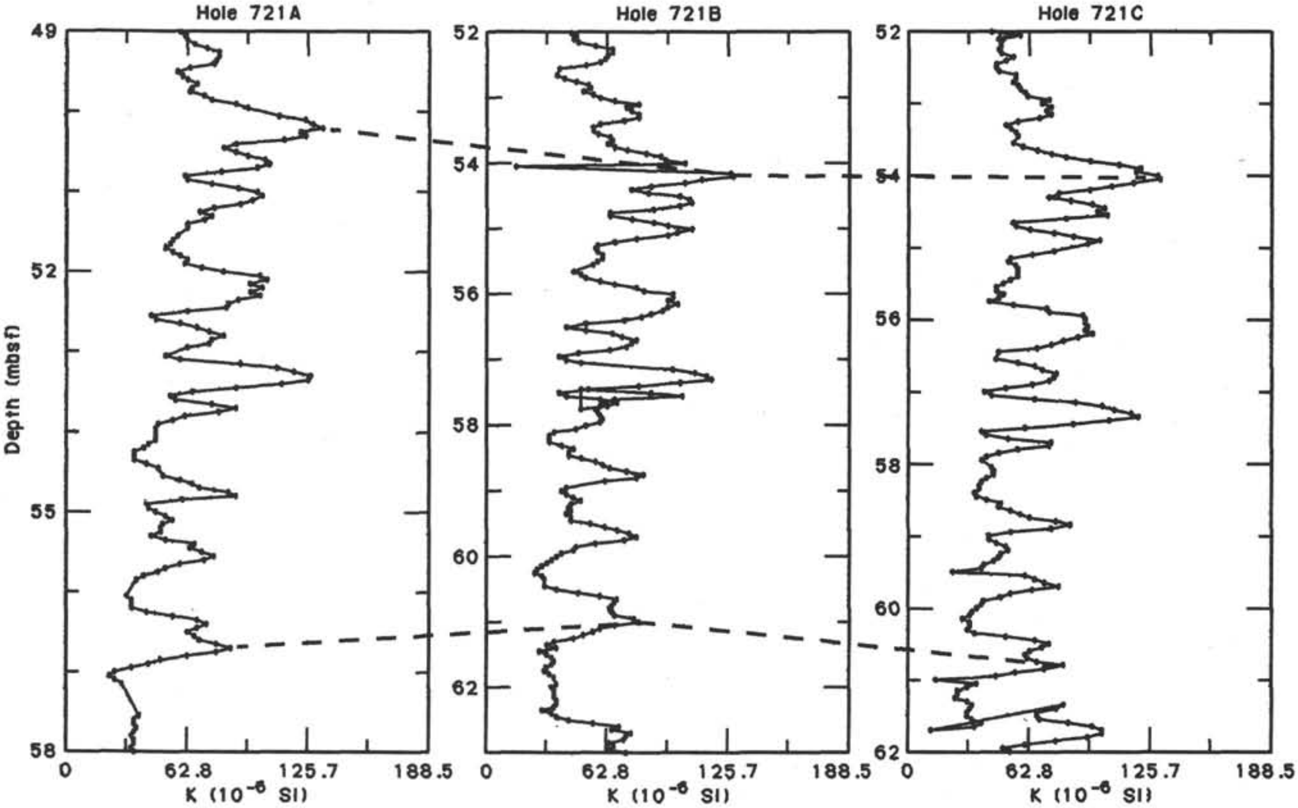

Figure 26. Comparisons of volume magnetic susceptibility of correlative ~ 1-m sections of Holes 721A, 721B, and 721C. Dashed lines denote correlative horizons.

The mass accumulation rates of calcium carbonate, noncarbonate (100 - $CaCO_3$). and organic carbon are calculated from the average values between selected datums (Table 9: Fig. 32). These data allowed an independent examination of the temporal variability in each component. The accumulation rates of calcium carbonate and noncarbonate at Site 721 mostly mirror the sedimentation rates, and calcium carbonate accumulation is generally twice that of noncarbonate in Pliocene-Pleistocene deposits. The present rate of calcite accumulation (~3 g/cm^2/k.y.) is 1.5 times lower than the mean annual flux of calcium carbonate measured in a sediment trap from the mid-water column in the Panama Basin, a comparable high-productivity region (Honjo, 1982). The high rate of calcium carbonate accumulation near the Miocene/Pliocene boundary equals present rates measured in the Panama Basin sediment traps. These rates are characteristic of areas having a high production of calcium carbonate shells of coccolithophores and foraminifers.

PHYSICAL PROPERTIES

Introduction

Physical properties measured on discrete samples of sediments recovered from Site 721 include index properties (wet-bulk density, porosity, water content, and grain density), compressional-wave velocity, and vane shear strength (Tables 10 and 11). Wet-bulk density and compressional-wave velocity were measured on all whole-round core sections that were at least 80 cm in length using the GRAPE and *P*-wave logging apparatus. All techniques and equipment used are described in the "Explanatory Notes" chapter, this volume.

Relatively high overall recovery rate allowed for a high sampling frequency at this site. With this large data set, transitions in the physical properties profiles clearly mark the boundaries between the four lithostratigraphic units that were recognized at Site 721.

Index Properties

Lithologic Unit I

Within the foraminifer-bearing nannofossil ooze and nannofossil ooze/chalk of lithologic Subunit IA (0-261.2 mbsf), the profiles of porosity and water content show very gradual monotonic decreases with depth, with the exception of two zones where the gradients are reversed (Fig. 33). Average values of porosity and water content measure 65% and 45%, respectively, near the seafloor and decrease to about 63% and 43%, respectively, at a depth of 90 mbsf. Between 90 and 110 mbsf a local porosity/water content maximum (and wet-bulk density minimum) was measured as a result of a 10%-15% increase in the concentration of clay minerals. Although this perturbation of the profiles is minimal on the profiles of discrete measurements (Fig. 33), it is a prominent feature on the wet-bulk-density profiles measured by the GRAPE (Fig. 34). Between 110 and 225 mbsf the porosity and water content profiles resume their gradual decreasing trends downhole. Below this level to the base of lithologic Subunit IA at 261.2 mbsf, porosity and water content increase slightly, perhaps in response to the general decrease in calcium carbonate content (see "Lithostratigraphy" section, this chapter; Fig. 5).

Porosity values determined from calcareous sediments (greater than 30% calcium carbonate) from several DSDP sites in the central Pacific (Hamilton, 1976) show a slightly more rapid decrease with depth than the gradient determined at Site 721. The principal deviation from Hamilton's curve occurs in the upper 150 m of lithologic Unit I. In this interval of similar lithofacies, Hamilton reports average porosities of 75%-65% (uncorrected

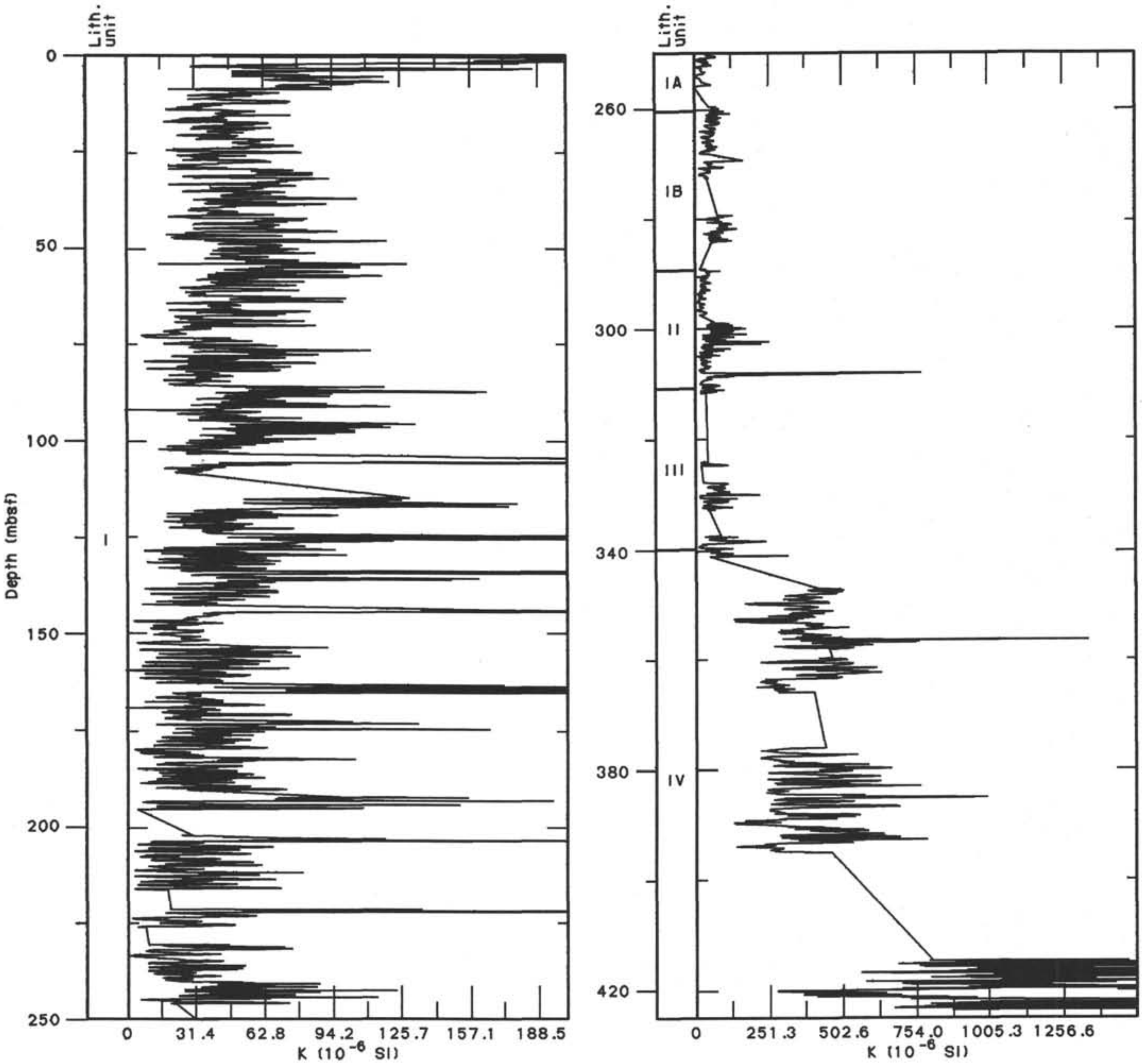

Figure 27. Volume magnetic susceptibility for Hole 721B. Note the susceptibility scale change at 250 mbsf.

for sediment expansion) as compared to the values of 65%–63% measured in the section at Site 721.

The grain densities throughout lithologic Subunit IA vary from a minimum of approximately 2.40 g/cm³ to a maximum of 2.75 g/cm³, but the values remain close to 2.60 g/cm³ at all depths. Given the nearly constant average grain density of Subunit IA, changes in wet-bulk density primarily reflect changes in water content. Throughout Subunit IA, wet-bulk density increases slightly with depth from 1.65 g/cm³ to 1.70 g/cm³ at 225 mbsf as a result of increasing overburden pressure. As also noted in the porosity and water content profiles, the wet-bulk density profile reverses slope near 225 mbsf, and values decrease to 1.65 g/cm³ at 261.2 mbsf. Within the foraminifer-bearing nannofossil ooze and chalk of Subunit IB (261.2–289.0 mbsf) the profiles of index properties display the normal gradient observed in the upper portions of Subunit IA (Fig. 33).

Lithologic Unit II

The siliceous-nannofossil chalk of Lithologic Unit II (289.0–309.9 mbsf) is markedly more porous than the adjacent sediments due to the increased abundance of diatoms frustules and the presence of radiolarians (see "Lithostratigraphy" section, this chapter). The structural attributes of the siliceous microfossils produce an open sediment fabric and higher porosity. Porosities vary from 66% to 75% with a corresponding variation in the water contents (44%–54%) that reflect the inherent high water content of this siliceous unit. The wet-bulk and grain densities show marked decreases to minima of 1.39 g/cm³ and 2.16

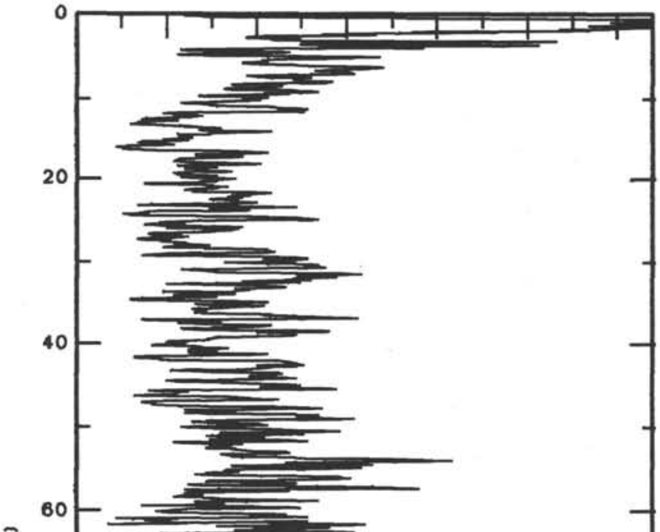

Figure 28. Volume magnetic susceptibility for Hole 721C.

g/cm^3, respectively. These decreases are attributed to the low grain density of the opal of the siliceous microfossils.

Lithologic Unit III

At the contact between Unit II and the underlying nannofossil chalk of lithologic Unit III (309.9 mbsf), the porosity and water content decrease abruptly in response to the disappearance of the siliceous microfossils. Coincident increases in wet-bulk and grain densities are also seen. Throughout lithologic Unit III (309.9-340.7 mbsf) the index properties profiles again resume the original gradients established in the nannofossil ooze of lithologic Unit I. Average porosity and water content values decrease from 52% to 49% and from 27% to 25%, respectively.

Lithologic Unit IV

As the section changes to a clay-bearing nannofossil chalk interbedded with mud turbidites in lithologic Unit IV (340.7-424.2 mbsf), the profiles of porosity, water content, and bulk density show similar gradients to those encountered in lithologic Unit I. They are, however, slightly offset toward higher densities and lower porosities. The porosity and water contents in the mud turbidites of Cores 117-721B-37X to -40X are slightly lower than in the adjacent more calcareous units. The overall gradients displayed in Unit IV are similar to those determined by Hamilton (1976). The porosity values are lower than the average values reported by Hamilton for both terrigenous and calcareous sediments but are in the range of reported values (Bryant et al., 1981).

Compressional-Wave Velocity

Compressional-wave velocities measured perpendicular to bedding on discrete samples in the Hamilton Frame Velocimeter show considerable variation at all sub-bottom depths (Fig. 35), but the values were found to match reasonably well with the data from the *P*-wave logger (Fig. 36). Throughout lithologic Unit I, the compressional-wave velocities increased gradually from 1500 m/s to 1560 m/s at 260 mbsf. The measured velocities are approximately 50 to 100 m/s lower than velocities predicted for calcareous sediments of equivalent density (Hamilton, 1978).

Within the siliceous nannofossil chalk of lithologic Unit II, the velocities dropped drastically to about 1530 m/s at the base of the sequence. This reversal in the velocity/depth gradient correlates with the gradient reversals seen in the index properties and is likely associated with the lower wet-bulk density.

Markedly higher compressional-wave velocities were measured in the nannofossil chalks of Unit III. At the contact between lithologic Units II and III, velocities increase abruptly to 1620 m/s. Within this unit the velocity values increase downsection to 1640 m/s.

Velocities continue to increase at a similar rate in the clay-bearing nannofossil chalk in the upper portion of Unit IV to (340.7-355 mbsf), where the velocity values average 1660 m/s. In the underlying terrigenous section, which comprises the lower portion of Unit IV, the velocity values apparently decrease slightly, but few measurements are available to confirm this trend.

GRAPE and *P*-Wave Logs

Overall, data collected by the GRAPE and *P*-wave logging systems are very good at Site 721 (Figs. 34 and 36). Excellent logs were obtained for sediments of lithologic Unit I, particularly over the interval cored with the APC. Cores from lithologic Units II and III commonly did not completely fill the core liners, and the lack of coupling between sediment and liner prevented *P*-wave signal transmission. Intervals for which the *P*-wave logs were not obtained should also be viewed as intervals in which the GRAPE underestimates the wet-bulk density. Full cores were more common for lithologic Unit IV, and moderately good GRAPE and *P*-wave logs were obtained. In all lithologic units a positive correlation exists between the GRAPE-determined wet-bulk density and the *P*-wave velocity.

The general pattern of density variation represented in the GRAPE records (Fig. 34) corresponds to that of wet-bulk density determined for discrete samples with two exceptions. The first discrepancy is in the interval 0-45 mbsf, where densities measured on discrete samples are approximately 0.10 g/cm^3 lower than the GRAPE density. Discrete-sample data in this interval display a large variation, and low values may be the product of sampling and measurement error or incorporation of water in the sediment during core splitting. The second feature of the GRAPE records that is not clearly evident in the discrete-sample data is the broad density minimum between 80 and 110 mbsf. This pattern is partially obscured in the discrete-sample

Table 8. XRD data from Hole 721C showing carbonate, quartz, dolomite, plagioclase feldspar, and combined kaolinite-chlorite peak areas extracted.

Core, section, interval (cm)	Depth (mbsf)	Kaolinite-chlorite	Quartz	Plagioclase feldspar	$CaCO_3$	Dolomite	Susceptibility	$CaCO_3$/quartz	$CaCO_3$ (wt %)
117-721C-									
1H-1, 30	0.30	0	196	25	3493	20	3.0	17.821	79.1
1H-2, 70	2.20	13	484	50	2830	48	9.3	5.847	70.5
1H-2, 110	2.60	59	655	128	3114	77	8.3	4.754	62.9
1H-3, 10	3.10	30	437	88	2621	24	6.0	5.998	68.3
2H-1, 65	4.25	16	213	59	2841	29	5.9	13.338	72.5
2H-1, 85	4.45	13	246	58	2788	12	2.9	11.333	75.3
2H-1, 110	4.70	28	400	506	2992	40	5.9	7.480	52.7
2H-1, 140	5.00	0	137	86	2088	16	2.8	15.241	
2H-2, 15	5.25	18	372	85	2016	55	8.4	5.419	64.6
2H-2, 50	5.60	24	458	110	2314	40	5.4	5.052	67.0
2H-2, 95	6.05	23	454	52	2841	61	4.6	6.258	67.2
2H-2, 145	6.55	28	645	146	1936	45	8.5	3.002	59.9
2H-3, 35	6.95	30	484	119	1673	52	6.7	3.457	58.0
2H-3, 50	7.10	27	645	139	1521	77	7.6	2.358	54.6
2H-3, 95	7.55	25	365	85	2927	27	4.7	8.019	69.5
2H-3, 120	7.80	20	357	110	1325	25	6.5	3.711	61.7
2H-4, 15	8.25	38	538	177	2894	52	5.3	5.379	62.3
2H-4, 40	8.50	23	279	52	3564	18	4.9	12.774	73.1
2H-4, 70	8.80	17	272	62	3446	31	5.7	12.669	76.4
2H-4, 100	9.10	10	151	26	3125	11	4.1	20.695	80.1
2H-4, 135	9.45	38	524	156	2694	35	6.7	5.141	64.9
2H-5, 5	9.65	21	376	125	3283	41	5.2	8.731	70.1
2H-5, 35	9.95	12	204	28	3422	0	3.4	16.775	80.2
2H-5, 50	10.10	26	266	64	2314	36	5.3	8.699	68.6
2H-5, 100	10.60	17	392	62	2391	30	4.3	6.099	70.6
2H-5, 125	10.85	19	289	83	3047	27	2.9	10.543	70.6
2H-6, 15	11.25	38	790	128	2611	49	5.2	3.305	63.2
2H-6, 50	11.60	38	497	106	2725	44	6.3	5.483	61.5
2H-6, 80	11.90	0	392	77	3457	17	4.8	8.819	70.3
2H-6, 100	12.10	0	240	36	3434	17	2.4	14.308	73.3
2H-6, 130	12.40	29	286	67	3446	20	5.6	12.049	79.8
2H-7, 20	12.80	10	156	35	3204	17	1.8	20.538	81.4
2H-7, 35	12.95	30	286	36	3612	14	2.8	12.629	76.6
2H-7, 60	13.20	18	210	188	3881	0	1.8	10.481	80.1

record by the scatter of data at shallow depths. The density minimum roughly coincides with a darkening of sediment color and an increase in the clay mineral abundance in the 80–110 mbsf interval.

The *P*-wave log pattern (Fig. 36) follows that of the GRAPE-determined density. A velocity minimum coincides with the broad density minimum centered at 90 mbsf. The *P*-wave logger velocities correspond approximately to those measured with the Hamilton Frame Velocimeter, although the Hamilton Frame data are more widely varying than the *P*-wave logger data. At depths less than 35 mbsf the velocities measured for discrete samples are significantly lower than the *P*-wave logs. Difficulties in measuring velocities of soft sediments with the Hamilton Frame may account for this discrepancy.

In lithologic Unit I, GRAPE and *P*-wave records display patterns of cyclic variation on the scale of tens of centimeters to meters. This variation is typified by that in the 0–50 mbsf interval (Fig. 37). The scale of the variation corresponds to the scale of color change, but the relationship between sediment color and relative density is not consistent. The GRAPE and *P*-wave records were further compared with the results of shipboard carbonate measurements, and a consistent relationship between sediment density and velocity and percent calcium carbonate is not present either. The lack of such a correlation may be partly the product of comparing the closely spaced (approximately 2 cm) data of the GRAPE and *P*-wave logs with the data from the more widely spaced (50 cm) carbonate samples. The small-scale variation displayed in Figure 37 is well-developed in all three holes drilled at Site 721, and individual peaks in the records can be correlated between holes. The density and velocity variations also display a strong positive correlation with variation in magnetic susceptibility and thus must be regarded as an expression of changes in sediment characteristics over relatively short intervals (see "Paleomagnetism" section, this chapter).

Vane Shear Strength

Vane shear strengths were measured in the nine APC cores recovered from each of the two holes (Fig. 35). Shear strengths increased from 14.6 kPa near the surface to a maximum value of 97.7 kPa at 81.75 mbsf. Shear strength measurements were attempted in Cores 117-721B-10X through -20X, but the sediment developed radial fractures prior to shear failure in all cases.

SEISMIC STRATIGRAPHY

The Owen Ridge is an asymmetric, linear feature in the western Arabian Sea that trends northeastward and dips gently to the west (Fig. 38). The ridge is uplifted lamprophyric basement overlain by claystones, chalks, and turbiditic sequences of Eocene to Miocene age that are, in turn, capped by Miocene and younger pelagic sediments (Whitmarsh et al., 1974; Whitmarsh, 1979). The seismic stratigraphy of the ridge is complex and includes irregular basement features, large-scale onlap of turbidite and other facies, numerous slump scars and large slump(?) canyons, and several prominent sub-bottom reflectors. To interpret the seismic stratigraphy of Site 721 and companion Site 722, we have used several single-channel seismic (SCS) profiles from the Leg 117 site survey by the *Robert Conrad* (see Mountain and Prell, this volume), in combination with the drilling results from Sites 721 and 722 (see "Lithostratigraphy" section,

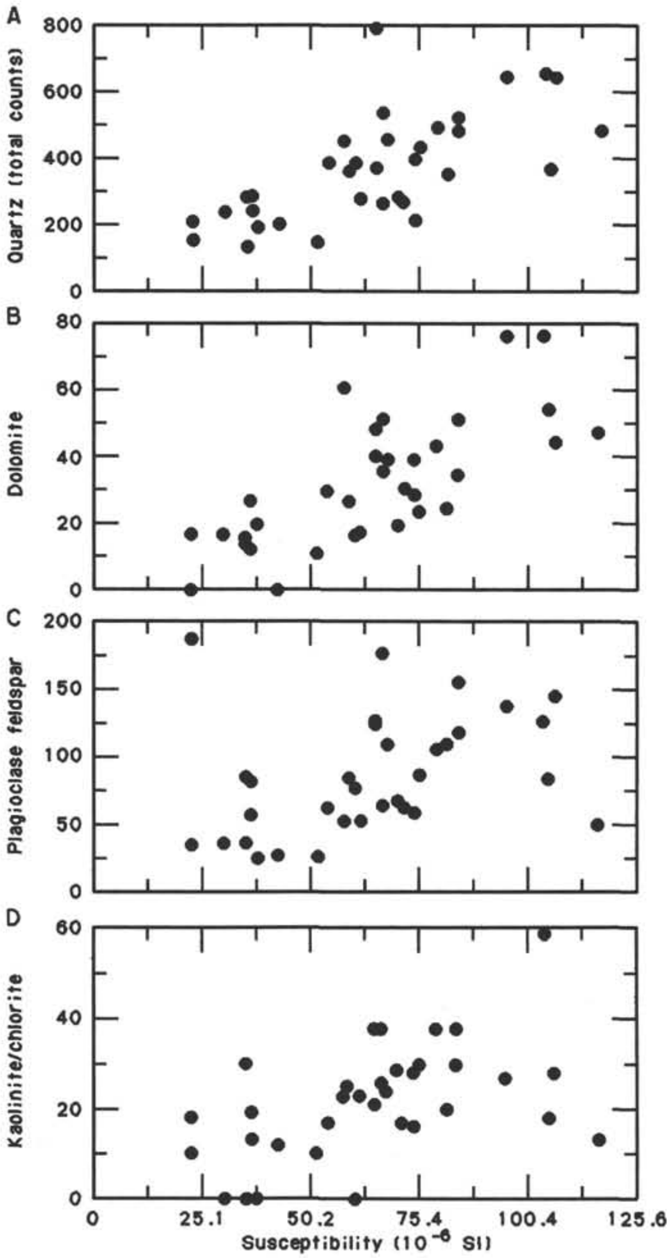

Figure 29. Plots of quartz, dolomite, plagioclase feldspar, and kaolinite-chlorite results from the X-ray-diffraction analyses of discrete samples taken from susceptibility maxima and minima of Hole 721C (0–~13 mbsf). Note the positive correlations of terrigenous components with susceptibility.

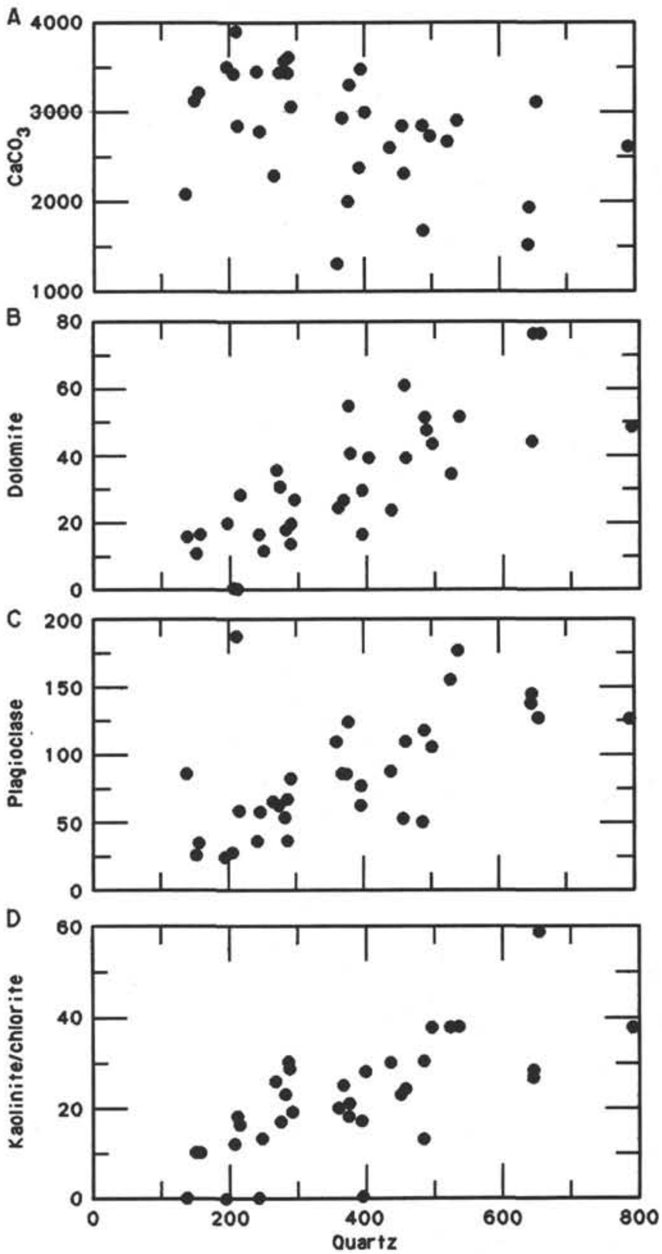

Figure 30. Plots of carbonate, dolomite, plagioclase feldspar, and kaolinite-chlorite vs. quartz as determined from the XRD analyses.

this chapter and "Site 722" chapter, this volume). Downhole logging data from Site 722 (see "Downhole Measurements" section, "Site 722" chapter, this volume), as well as the SCS data obtained during the site approaches by the *JOIDES Resolution* were also used for this synthesis. Figure 38 shows the location of the SCS tracks used in this discussion in relation to the bathymetry of the Owen Ridge (Sea Beam data from the site survey; Prell, unpubl. data).

The sedimentary sequence at Site 721 is complicated by several hiatuses and the seismic stratigraphy at this site must be compared to the more complete sedimentary and seismic section available at Site 722. Thus, we initially use SCS Line 38 and results of drilling and logging at Site 722 to associate reflector sequences with the lithologic section. Subsequently, we use RC2704 SCS lines 39 and 40 to project the reflector stratigraphy into the section recovered at Site 721. The detailed correlation of Site 722 with SCS profiles, lithology, logging data, and the synthetic seismogram are discussed in the "Seismic Stratigraphy" section, "Site 722" chapter (this volume). Here, we only summarize the identification and lithologic significance of the important reflectors within the cored section. The correlation of the major reflectors recognized at both Site 722 and Site 721 is shown in Figure 39. The reflectors are identified by an alpha-numeric code and are discussed in order of increasing depth.

Regional Seismic Stratigraphy

Reflector A is a high-amplitude return that is coincident with the top of the siliceous lithologic Unit II in Site 722. It can be easily traced through Line 39 to the the crest of the ridge (Line

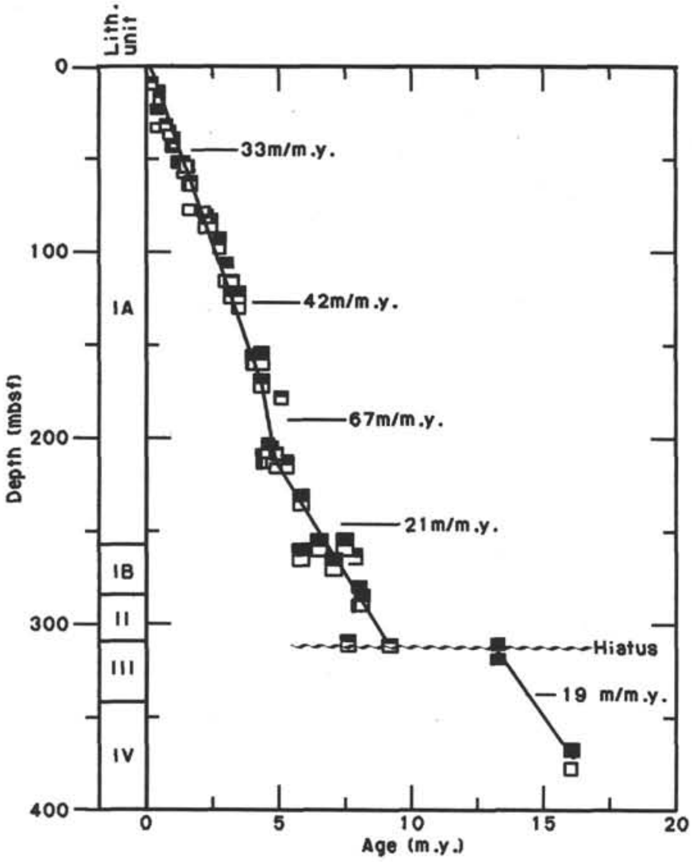

Figure 31. Age-depth plot of stratigraphic datums listed in Tables 4 and 5. The filled and open boxes are the upper and lower depths of each datum level, respectively. Indicated sedimentation rates are based on a best fit to all stratigraphic data. Sedimentation rates calculated between reliable nannofossil datum levels in the top 115 m are listed in Table 9 and shown in Figure 32.

40, Fig. 39). Reflector A cannot be traced directly into Site 721 (Line 40), but it is generally correlative with the irregular reflectors that mark the top of the siliceous facies in lithologic Unit II in Site 721 (see Fig. 40).

Reflector B is a series of reflectors that are associated with the siliceous and chalk units. B_1 marks the bottom of a package of four closely spaced conformable reflectors that have a distinctive pattern and are coincident with the lower part of siliceous lithologic Unit II in Site 722 (Fig. 39). B_1 is easily traced through Line 39 to the crest of the ridge (Line 40, Fig. 39), but B_1 is missing at Site 721 (Line 40, Fig. 39). B_2 is a low-amplitude reflector that correlates with the top of the chalks in the lower half of lithologic Unit III at Site 721. These chalks have higher velocity and higher density than the surrounding lithologies. B_2 becomes more reflective as it trends upslope through Line 39 to the crest of the ridge (Line 40) and to Site 721. The increase in amplitude between Site 722 and the crest of the ridge may be associated with the increased thickness of the lower chalk. The increased amplitude is probably related to the pronounced hiatus identified at this level in Site 721, which brings very-low-velocity siliceous sediments in contact with the much faster lower chalk unit. This hiatus and its corresponding high-amplitude reflector were not found at Site 722. Reflector B_3 has a variable amplitude and at Site 722 coincides with the boundary between the chalk (lithologic Unit III) and the turbiditic sediments of lithologic Unit IV (Fig. 39).

Reflector C is the uppermost strong return of a thick series of parallel reflectors that are generally correlated to turbidite deposits within lithologic Unit IV at both Sites 721 and 722 (Fig. 39). Reflector C is not, however, the top of lithologic Unit IV, which is marked by B_3.

Seismic Stratigraphy of Site 721

The relationship of the reflectors to the stratigraphic section at Site 721 is shown in a plot of traveltime (two-way) vs. depth (mbsf; Fig. 40). The correlation of traveltimes and lithologic features indicates average sediment velocities of 1.6–1.7 km/s. These average velocities are lower than the empirical time-depth relationships for carbonate-dominated sediments (Hamilton, 1979). Reflector C is clearly identified at about 0.48 s (Figs. 39 and 41) and is projected to be about 400 mbsf at Site 721. Reflectors B_3 and B_2 are observed at about 0.42 and 0.38 s, respectively, and are interpreted to represent the bottom and the top of the high-density chalk unit. Reflector B_2 also represents the base of a major hiatus that spans about 5 m.y. (from nannofossil Zone NN9 to NN5). Reflector B_1 is not observed at Site 721 as its associated sediments are missing within the hiatus. Identification of seismic reflector A is difficult at Site 721 because it is included in the slumped section. The time-depth relations (Fig. 40) indicate that both the top of the low-density siliceous facies and the top of the disturbed section (top of lithologic Unit II) are marked by reflectors at 0.365–0.350 s and 0.32 s, respectively. Alternatively, the deformed slump surface could be represented by the strong negative peak at about 0.33 s. The section above 0.32 s is characterized by conformable reflectors indicating a continuous pelagic deposition.

On a larger scale (about 20 km), seismic stratigraphy of the sediments capping the crest of the Owen Ridge reveals the origin of the hiatus found at Site 721. The sediment thickness at the Site 721 is about 1.62 s. The sediments overlie a strong irregular reflector that rises to the south and is interpreted as basement. Overlying basement is a zone of diffuse reflection from about

Table 9. Sedimentation and accumulation rate data for Site 721.

Depth interval (mbsf)	Age range (m.y.)	$CaCO_3$ ($\bar{x}$ %)	C_{org} ($\bar{x}$ %)	Dry-bulk density ($\bar{x}$ g/cm^3)	Sed. rate ($\bar{x}$ m/m.y.)	$CaCO_3$ acc. rate (g/cm^2/k.y.)	Non-$CaCO_3$ acc. rate (g/cm^2/k.y.)	C_{org} acc. rate (mg/cm^2/k.y.)
0–9.2	0–0.19	66.9	0.77	0.940	48.2	3.03	1.50	34.9
9.2–19.0	0.19–0.49	70.5	0.72	1.012	32.8	2.34	0.98	23.9
19.0–31.4	0.49–0.82	64.9	0.45	1.082	37.6	2.64	1.43	18.3
31.4–50.5	0.82–1.45	61.8	0.85	0.988	30.8	1.88	1.16	25.9
50.8–80.5	1.45–2.4	68.0	1.33	1.015	31.3	2.16	1.02	42.3
80.5–115.4	2.4–3.48	64.9	2.32	0.986	32.3	2.07	1.12	78.9
115.4–169.0	3.48–4.77	64.1	0.81	1.043	41.6	2.78	1.56	35.1
169.0–208.0	4.77–5.35	65.0	1.09	1.038	67.2	4.53	2.44	76.0
208.0–310.0	5.35–10.25	53.7	0.68	0.969	20.8	1.08	0.93	13.7
315.0–370.0	14.4–17.4	37.4	0.07	1.540	18.8	1.08	1.81	2.0

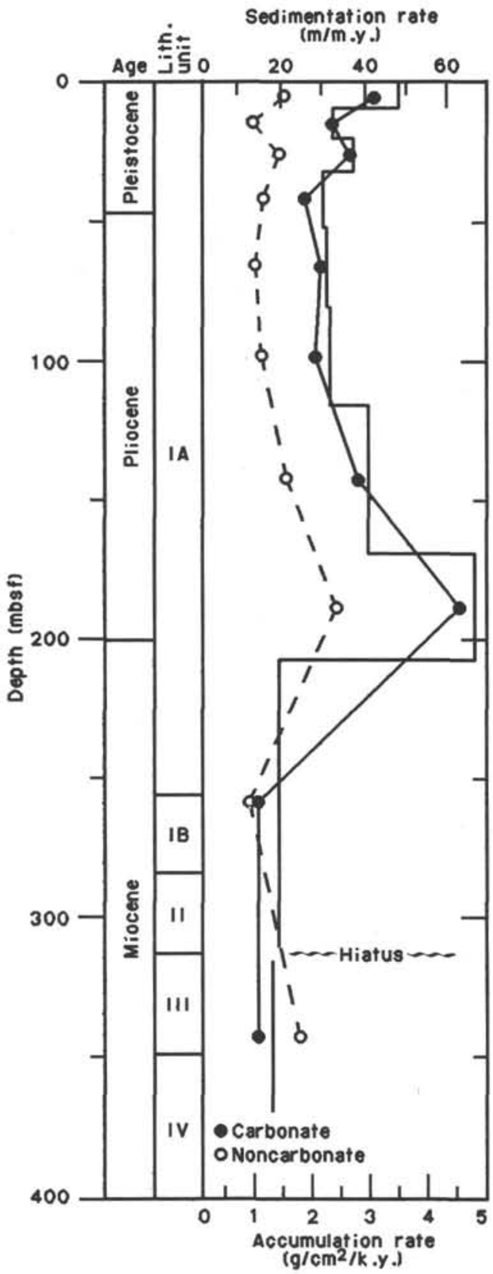

Figure 32. Sedimentation rate (m/m.y.; solid line), calcium carbonate accumulation rate (g/cm^2/k.y.; dots), and noncarbonate accumulation rate (g/cm^2/k.y.; circles) vs. depth at Site 721. Accumulation rates are plotted at the midpoint of the respective depth intervals.

1.62 to 1.26 sbsf. This diffuse zone is succeeded by a thick sequence of strongly reflective, largely conformable reflectors that are capped by seismic reflector C. This sequence is interpreted as the clastic-turbidite facies of Oligocene to Miocene age that was observed at DSDP Site 224 (Whitmarsh et al., 1974) and at the base of Site 721. The surface of the turbidite facies (reflector C) dips about 1° to the northwest. Near the crest of the ridge, about 5 km updip and south from Site 721, the stratigraphic section is relatively complete (Fig. 41) and almost identical to the section at Site 722 (Fig. 39). Below the crest, a slump fault cuts through the section and eliminates most of the sediments between seismic reflectors B_2 and A. The base of the slump coincides with the top of the chalk facies in lithologic Unit II at Site 721. The slump fault probably occurred in the siliceous low-density sediments of lithologic Unit II. Comparison of the seismic stratigraphy at Site 722, at the crest of the ridge, and at Site 721 indicates that about 90 m of sediment was lost by slumping at Site 721. The upper chalk (corresponding to reflector B_2) and top of the siliceous unit (reflector A) in Site 721 are 135 m thick, but only 51 m thick at Site 721. This estimated loss assumes that all of lithologic Unit I is present at Site 721, which may not be the case.

The age of the slump event is estimated to be late Miocene (about 7.7 Ma) on the basis of overlying sediments. The slump is clearly associated with the uplift, which created the inclined sediments, but it cannot be assigned to a specific uplift event. Conformable seismic reflectors below reflector C, inferred to be turbidites, exhibit a modest thickening from the crest of the ridge into the basin. They suggest that minor uplift may have occurred prior to reflector C time, about 17 Ma. However, no major uplift can have occurred prior to cessation of turbidite deposition at Sites 721 and 722. Post-cruise studies of the regional seismic stratigraphy combined with these drilling results should provide more detailed information about the timing of uplift of the Owen Ridge.

INORGANIC GEOCHEMISTRY

Introduction

Eighteen interstitial water samples collected by squeezing at Site 721 were analyzed for alkalinity, pH, salinity, Mg^{2+}, Ca^{2+}, Cl^-, SO_4^{2-}, PO_4^{3-}, NH_4^+, and silicate. Two additional samples were collected using the *in-situ* pore-water sampler; all the measurements listed above were made on these samples, with the single exception of sulfate and one phosphate determination. The first four squeezed samples collected at this site were taken from Hole 721A and the remainder from Hole 721B. The *in-situ* samples were taken from Hole 721C. The samples were obtained from different depths in the three holes, but because the stratigraphic correlation between the three was excellent, we have chosen to plot all the results on a common depth scale in Figure 42. All data are listed in Table 12.

Salinity, Chlorinity, and pH

The concentration profiles of chloride, salinity, and pH are shown in Figure 42. Although the distribution of chloride shows little variation with depth in the upper 300 m, the salinity decreases distinctly from about 34.3 g/kg in the topmost sample to ~32.2 g/kg at ~90 mbsf. This decrease reflects the loss of sulfate (and to some extent magnesium) from interstitial solution over this same depth interval. A slight, and apparently real, ~2% increase with depth of the chloride concentration occurs over the lowermost 110 m of the hole. The cause of this distribution is not clear but it may be related to uptake of water to the interlayer sites of clay minerals in the turbidites near the bottom of the hole. The slight increase in salinity and the presence of a small quantity of sulfate in the deepest sample (422 mbsf) are probably due to contamination with drill water; Core 117-721A-44X from which the sample was collected showed abundant evidence of drilling disturbance ("biscuiting").

The pH ranges between ~7.2 and ~8.0 over the cored section (Fig. 42). Lower values probably result from the production of H_2S which is abundant in the upper 300-350 m and dissociates to form HS^- and H^+. Because the carbonate oozes tend to be iron-depleted, sulfide precipitation is limited, allowing substantial H_2S to occur in the interstitial water. Of those pore waters collected by squeezing, the highest pH (7.94) was measured in the deepest sample which may have been contaminated with seawater. Both *in-situ* samples have slightly higher pH levels than the squeezed samples collected at similar depths (Table 12),

Table 10. Physical properties summary for Hole 721A.

Core, section, interval (cm)	Depth (mbsf)	Wet-bulk density (g/cm^3)	Porosity (%)	Water content (%)	Grain density (g/cm^3)	Dry-bulk density (g/cm^3)	Velocity (m/s)	Vane shear strength (kPa)
117-721A-								
1H-2, 38–40	1.88	1.553	66.3	43.7	2.393	0.873		
1H-2, 49–49	1.99							14.6
1H-4, 40–42	4.90	1.635	61.2	38.3	2.504	1.008		
1H-6, 40–42	7.90	1.646	65.4	40.7	2.579	0.977		
2H-2, 50–52	11.80	1.624	63.1	39.8	2.621	0.978		
2H-4, 40–40	14.70							23.8
2H-4, 50–52	14.80	1.722	62.4	37.1	2.691	1.083		
2H-6, 50–52	17.80	1.671	62.1	38.1	2.750	1.035		
3H-2, 50–52	21.50	1.559	64.7	42.5	2.635	0.896		
3H-4, 50–52	24.50	1.590	59.3	38.2	2.595	0.983		
3H-5, 43–43	25.93							17.6
3H-5, 80–83	26.30						[a]1465	
3H-6, 50–52	27.50	1.646	63.8	39.7	2.539	0.992		
4H-2, 50–52	31.20	1.665	64.3	39.6	2.675	1.006		
4H-5, 43–43	34.13							23.6
4H-5, 50–52	34.20	1.564	64.0	41.9	2.491	0.908		
4H-5, 80–83	36.00						[a]1527	
4H-6, 50–52	37.20	1.644	63.1	39.3	2.659	0.997		
5H-2, 47–49	40.87	1.670	62.0	38.0	2.686	1.035		
5H-5, 47–49	43.87	1.587	65.9	42.5	2.635	0.912		
5H-5, 60–60	44.00							44.7
5H-5, 80–83	45.70						[a]1539	
5H-6, 47–49	46.87	1.693	62.5	37.8	2.591	1.053		
6H-2, 45–47	50.45	1.677	62.2	38.0	2.660	1.040		
6H-5, 45–47	53.45	1.688	60.0	36.5	2.626	1.072		62.3
6H-6, 41–44	56.41						[a]1350	
6H-6, 45–47	56.45	1.712	61.0	36.5	2.683	1.087		
7H-2, 45–47	59.75	1.671	64.0	39.2	2.630	1.015		
7H-5, 45–47	62.75	1.698	63.3	38.2	2.539	1.049		72.3
7H-6, 41–44	65.71						[a]1297	
7H-6, 45–47	65.75	1.714	65.4	39.1	2.480	1.044		
8H-2, 45–47	69.25	1.677	63.0	38.5	2.593	1.032		
8H-5, 60–62	72.40	1.693	58.9	35.6	2.580	1.090		56.1
8H-6, 45–47	75.25	1.697	58.9	35.6	2.548	1.093		
8H-6, 48–51	75.28						[a]1521	
9H-2, 45–47	78.75	1.625	64.3	40.5	2.596	0.967		
9H-5, 45–47	81.75	1.643	62.4	38.9	2.520	1.003		97.7
9H-6, 45–47	84.75	1.659	60.0	37.1	2.462	1.044		

[a] Velocity measurement perpendicular to bedding.

but it is not clear whether or not the difference is related to a sampling artifact.

Sulfate and Alkalinity

Sulfate reduction at this site is complete by about 100 mbsf, and is pronounced in the top several meters (Fig. 42). The deepest sample contains >4 mmol/L SO_4^{2-} which is thought to represent contamination (see above). The turbidites near the base of the cored section contained abundant macroscopic pyrite as both discrete grains and veinlets (see "Lithostratigraphy" section, this chapter).

Titration alkalinity increases from ~5.5 mmol/L at 9 mbsf depth to a distinct maximum near 90 mbsf before decreasing steadily toward the bottom of the hole (Fig. 42). Above the maximum the increase with depth can be attributed to the production of HCO_3^- during sulfate reduction; the decrease at greater depths presumably reflects carbonate precipitation reactions. The reduction of about 25 mmol/L of sulfate over the top 100 m should be mirrored by an increase in alkalinity of about 50 mmol/L, 40 mmol/L more than is observed. The missing alkalinity must be consumed during the precipitation of authigenic carbonate phases. However, 40 mmol/L of alkalinity is only sufficient to precipitate <1% of authigenic carbonate, assuming a porosity of 50% and a grain density of 2.75 g/cm^3, neglecting additional supply via diffusion. It is unlikely that such a small change in mineralogy would be detected by lithological examination. The alkalinity measured in the upper *in-situ* pore-water sample (100 mbsf) is about 1 mmol lower than in the adjacent squeezed samples, which is well in excess of analytical uncertainty. The reason for the difference is not clear.

Calcium and Magnesium

Profiles of dissolved calcium and magnesium are shown in Figure 42. The calcium concentration decreases to a minimum of ~6 mmol/L at about 80 mbsf depth before increasing to ~12 mmol/L at the base of the hole. Mg^{2+} decreases relatively rapidly to about 31 mmol/L over the top 100 m and more gradually to a near-constant minimum of ~26 mmol/L in the lower 200 m. The curved segments of these profiles represent zones of production and consumption: precipitation of carbonate phases in the upper 100 m must be responsible for the Ca^{2+} and at least some of the Mg^{2+} decreases, while both carbonate precipitation and alteration reactions involving alumino-silicate phases can probably account for the addition of calcium to solution and magnesium uptake at greater depths. The extent of removal of Mg^{2+} from pore water in the upper 100 m greatly exceeds that observed for calcium. Although it is possible that Mg-rich calcite could be precipitating in this zone, such a reaction would be insufficient to account for the relative magnesium deficit. Therefore, Mg^{2+} is probably being adsorbed by clay minerals in addition to participating in carbonate authigenesis. Dolomitization of calcite would also consume Mg^{2+} and release Ca^{2+}, which would tend to reduce the net calcium depletion but enhance the removal of magnesium; this latter suggestion is consistent with

Table 11. Physical properties summary for Hole 721B.

Core, section, interval (cm)	Depth (mbsf)	Wet-bulk density (g/cm^3)	Porosity (%)	Water content (%)	Grain density (g/cm^3)	Dry-bulk density (g/cm^3)	Velocity (m/s)	Vane shear strength (kPa)
117-721B-								
1H-4, 48–52	4.98	1.578	62.2	40.4	2.604	0.940		15.0
2H-5, 68–70	16.08	1.648	62.1	38.6	2.601	1.012		19.5
2H-5, 72–75	16.12						[a]1466	
3H-2, 35–38	20.95						[a]1518	
3H-2, 41–43	21.01	1.714	61.7	36.9	2.740	1.082		25.2
5H-3, 47–50	41.97						[a]1528	
5H-3, 50–52	42.00	1.654	65.0	40.3	2.707	0.988		22.3
6H-3, 95–98	52.05						[a]1532	
6H-3, 104–106	52.14	1.649	63.3	39.3	2.600	1.001		20.0
7H-3, 70–72	61.10	1.599	63.4	40.6	2.464	0.950		70.8
7H-3, 72–75	61.12						[a]1517	
8H-4, 57–59	71.97						[a]1555	
8H-4, 60–62	72.00	1.694	58.8	35.6	2.543	1.092		43.8
9H-3, 70–72	80.10	1.663	63.2	39.0	2.634	1.015		67.3
10X-1, 70–72	86.70	1.632	63.1	39.6	2.519	0.986		
10X-3, 70–72	89.70	1.616	64.9	41.1	2.561	0.951		
10X-5, 66–69	92.66						[a]1546	
10X-5, 70–72	92.70	1.632	65.6	41.2	2.621	0.960		
11X-1, 70–72	96.30	1.779	71.0	40.9	2.698	1.052		
11X-3, 70–72	99.30	1.509	57.5	39.1	2.665	0.920		
11X-5, 68–71	102.28						[a]1476	
11X-5, 70–72	102.30	1.677	64.0	39.1	2.635	1.021		
12X-2, 40–42	107.10	1.652	62.4	38.7	2.549	1.013		
12X-2, 43–46	107.13						[a]1523	
13X-2, 40–42	116.70	1.699	62.1	37.4	2.654	1.064		
13X-4, 40–42	119.70	1.681	61.7	37.6	2.583	1.049		
13X-6, 40–42	122.70	1.726	62.0	36.8	2.719	1.091		
14X-2, 40–42	126.30	1.643	63.7	39.8	2.542	0.990		
14X-2, 44–47	126.34						[a]1526	
14X-4, 40–42	129.30	1.680	61.9	37.7	2.584	1.047		
14X-5, 40–42	130.80	1.720	61.7	36.7	2.584	1.088		
14X-5, 143–145	131.80							51.7
15X-2, 40–42	136.00	1.659	60.3	37.2	2.386	1.041		
15X-4, 40–42	139.00	1.759	60.4	35.2	2.748	1.141		
15X-6, 40–42	142.00	1.655	63.1	39.1	2.540	1.008		
16X-2, 40–42	145.70	1.719	61.1	36.4	2.541	1.093		
16X-4, 40–42	148.70	1.653	61.7	38.2	2.577	1.021		
16X-6, 40–42	151.70	1.680	63.5	38.7	2.552	1.030		
16X-6, 82–84	152.12							42.0
17X-2, 40–42	155.40	1.707	61.2	36.7	2.524	1.080		
17X-2, 44–47	155.44						[a]1454	
17X-4, 40–42	158.40	1.617	62.7	39.7	2.327	0.974		
17X-6, 40–42	161.40	1.629	64.8	40.8	2.427	0.965		
17X-6, 132–132	162.32							63.7
18X-2, 38–40	165.08	1.664	63.5	39.1	2.594	1.014		
18X-4, 46–48	168.16	1.679	63.3	38.6	2.638	1.030		
18X-6, 96–98	171.66	1.653	62.6	38.8	2.531	1.011		
19X-2, 40–42	174.80	1.621	63.4	40.0	2.495	0.972		
19X-4, 10–12	177.50	1.705	61.0	36.7	2.631	1.080		
19X-4, 19–21	177.59						[a]1562	
19X-6, 40–42	180.80	1.626	63.7	40.2	2.585	0.973		
20X-2, 40–42	184.50	1.703	61.6	37.0	2.631	1.072		
20X-4, 40–42	187.50	1.659	62.4	38.5	2.575	1.020		
20X-4, 50–53	187.60						[a]1531	
20X-6, 10–12	190.20	1.690	58.6	35.5	2.521	1.090		
21X-2, 52–54	194.32	1.656	61.1	37.8	2.556	1.030		
21X-4, 48–50	197.28						[a]1590	
22X-2, 40–42	203.90	1.692	63.2	38.3	2.676	1.045		

the substantially greater loss of Mg^{2+} from solution compared to calcium. Furthermore, reprecipitation as calcite of the Ca^{2+} released during dolomitization would consume dissolved bicarbonate, which would help to account for the missing alkalinity. Similar suites of reactions have been postulated to explain calcium and magnesium distributions observed at other sites where carbonate-rich hemipelagic sediments have been drilled (e.g., Gieskes, 1981).

Ammonia, Phosphate, and Silicate

As noted at Site 720, ammonia and phosphate are added to solution as products of the degradation of organic matter under anoxic conditions. Ammonia levels are relatively high, reaching a maximum of about 2.5 mmol/L at 180 mbsf; concentrations decrease to about 1 mmol/L toward the base of the cored section (Fig. 42). Ignoring the effect of methanogenesis, total depletion of sulfate as observed over the top 100 m at this site should be accompanied by the release to solution of about 4 mmol/L of ammonia if the initial organic substrate had a near-Redfield C:N ratio of 106:16. About half this predicted ammonia value is observed, indicating that the degrading organic matter is relatively nitrogen depleted or that ammonia has been removed from solution by ion exchange with clay minerals such as illite; with the limited information at hand, we cannot differentiate between these two possibilities.

Table 11 (continued).

Core, section, interval (cm)	Depth (mbsf)	Wet-bulk density (g/cm^3)	Porosity (%)	Water content (%)	Grain density (g/cm^3)	Dry-bulk density (g/cm^3)	Velocity (m/s)	Vane shear strength (kPa)
117-721B-								
22X-4, 28-30	206.78						[a]1568	
22X-4, 40-42	206.90	1.718	61.7	36.8	2.669	1.086		
22X-6, 40-42	209.90	1.753	58.6	34.3	2.632	1.152		
23X-2, 32-35	213.52						[a]1538	
23X-2, 37-39	213.57	1.743	57.3	33.7	2.605	1.156		
24X-2, 38-40	223.18						[a]1558	
24X-2, 43-45	223.23	1.522	54.4	36.6	2.649	0.965		
24X-4, 4-6	225.84	1.890	69.5	37.6	2.638	1.179		
25X-2, 46-48	232.46	1.659	60.2	37.1	2.548	1.043		
25X-4, 48-50	235.48	1.713	59.6	35.6	2.562	1.103		
25X-6, 50-52	238.50						[a]1584	
25X-6, 48-50	238.48	1.746	61.3	36.0	2.723	1.117		
26X-2, 46-48	242.06	1.673	61.2	37.5	2.561	1.046		
26X-3, 112-113	244.22						[a]1507	
26X-4, 70-72	245.30	1.617	64.9	41.1	2.572	0.952		
27X-2, 45-47	251.75	1.579	65.3	42.3	2.400	0.911		
27X-4, 42-45	254.72						[a]1549	
27X-4, 45-47	254.75	1.607	60.6	38.6	2.555	0.986		
28X-2, 48-50	261.58	1.632	66.0	41.5	2.647	0.955		
28X-4, 35-37	264.45						[a]1587	
28X-4, 50-52	264.60	1.694	63.0	38.1	2.607	1.049		
28X-6, 77-79	267.87	1.730	58.3	34.5	2.579	1.133		
29X-2, 48-50	271.38						[a]1577	
29X-2, 58-60	271.48	1.683	61.9	37.7	2.625	1.049		
30X-2, 41-43	281.11	1.805	57.2	32.5	2.705	1.219		
30X-4, 33-34	284.03						[a]1534	
30X-4, 34-35	284.04	1.478	73.7	51.1	2.576	0.723		
31X-2, 40-42	290.90	1.567	68.1	44.5	2.608	0.869		
31X-4, 40-42	293.90	1.534	66.4	44.3	2.425	0.854		
31X-6, 40-42	296.90	1.464	72.6	50.8	2.367	0.721		
32X-2, 42-44	300.72	1.398	73.4	53.8	2.284	0.646		
32X-4, 62-64	303.92	1.435	75.0	53.5	2.167	0.667		
32X-6, 61-63	306.91	1.518	73.8	49.8	2.567	0.762	[a]1519	
33X-1, 4-6	308.44	1.569	68.1	44.5	2.451	0.872	[a]1542	
33X-CC, 41-43	311.66	1.988	49.4	25.5	2.722	1.481	[a]1653	
34X-4, 138-141	323.88	1.975	52.0	27.0	2.713	1.443	[a]1647	
34X-6, 21-24	325.71						[a]1553	
34X-CC, 21-24	324.95	1.928	50.7	26.9	2.578	1.409		
35X-2, 65-67	329.85	1.984	51.4	26.5	2.757	1.457	[a]1675	
35X-4, 2-4	332.22	1.966	49.5	25.8	2.747	1.459	[a]1634	
36X-CC, 28-30	341.01	2.098	47.6	23.3	2.732	1.610	[a]1648	
37X-1, 86-88	347.86	1.948	52.8	27.8	2.760	1.406		
37X-4, 39-41	351.89	2.088	44.4	21.8	2.774	1.633	[a]1674	
37X-5, 72-74	353.72	2.004	48.6	24.8	2.703	1.506	[a]1668	
38X-2, 60-62	358.70	1.976	50.7	26.3	2.831	1.457		
38X-4, 60-62	361.70	2.272	36.1	16.3	2.723	1.902		
38X-6, 60-62	364.70	2.081	41.6	20.5	2.642	1.654		
40X-2, 90-92	378.30	2.105	38.5	18.8	2.693	1.710	[a]1541	
40X-4, 90-92	381.30	2.056	43.4	21.6	2.708	1.612		
40X-6, 90-92	384.30	2.084	43.2	21.3	2.794	1.641		
41X-2, 60-62	387.70	2.085	50.4	24.7	2.861	1.569		
41X-4, 100-102	391.10	1.963	45.4	23.7	2.671	1.497		
41X-6, 90-92	394.00	2.006	45.7	23.4	2.686	1.537	[a]1584	
42X-2, 40-42	397.10	1.975	44.8	23.2	2.680	1.516		
44X-2, 51-53	416.51	1.966	45.8	23.9	2.674	1.496		
44X-4, 49-51	419.49	1.979	46.0	23.8	2.711	1.507		
44X-6, 45-46	422.45						[a]1630	
44X-6, 50-52	422.50	2.038	42.1	21.2	2.633	1.607		

[a] Velocity measurement perpendicular to bedding.

Similar reasoning indicates that a significant amount of phosphate has been removed from pore water at depth (Fig. 42). Decomposition of organic matter having a Redfield-type molar N:P ratio of 16 would yield about 50 μmol/L of dissolved phosphate per millimol of ammonia. Only about a tenth of this concentration is observed at this site (Table 12). Such a deficit is commonly observed in drill holes of DSDP and ODP and must be due to the precipitation of authigenic apatite phases. Calcite surfaces provide preferential nucleation sites for the precipitation of microcrystalline apatite (Stumm and Morgan, 1970).

The dissolved silica profile at Site 721 denotes two zones of reactivity (Fig. 42). Dissolution of biogenic opal in the nannofossil oozes which characterize the upper 300–350 m is almost certainly responsible for the high concentrations of silicate in pore water in this zone. However, the levels measured in interstitial waters collected from the turbidite sequence in the lower 50 m are lower by a factor of five, and the concentration in the deepest sample (51 μmol/L) is less than one-half that in present-day Arabian Sea bottom water. Because sedimentation rates just above the turbidites in the lower part of the hole (see "Accumu-

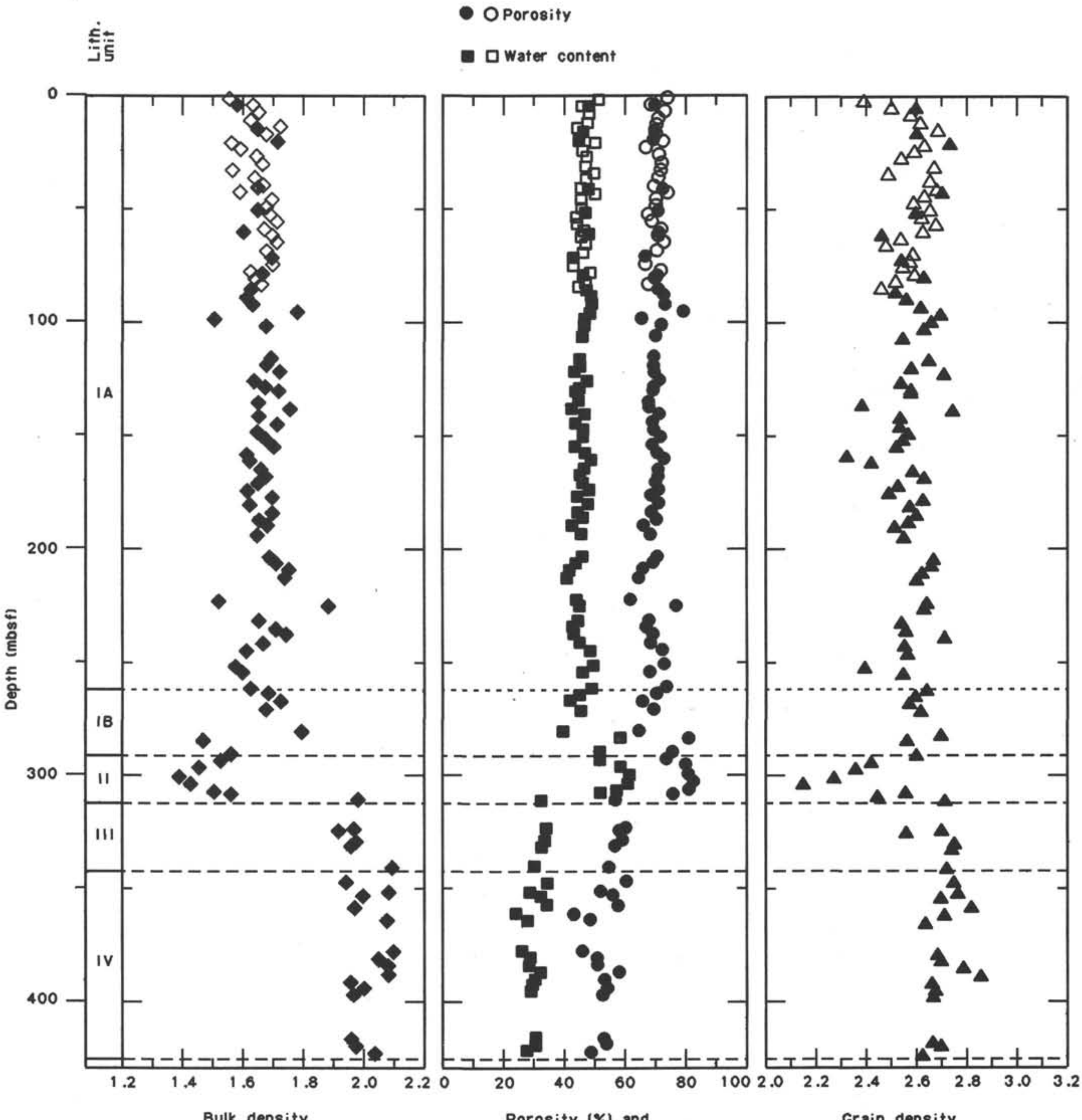

Figure 33. Index properties (wet-bulk density, porosity, water content, and grain density) measured on discrete samples from Holes 721A (open symbols) and 721B (solid symbols). Values are not corrected for sediment expansion.

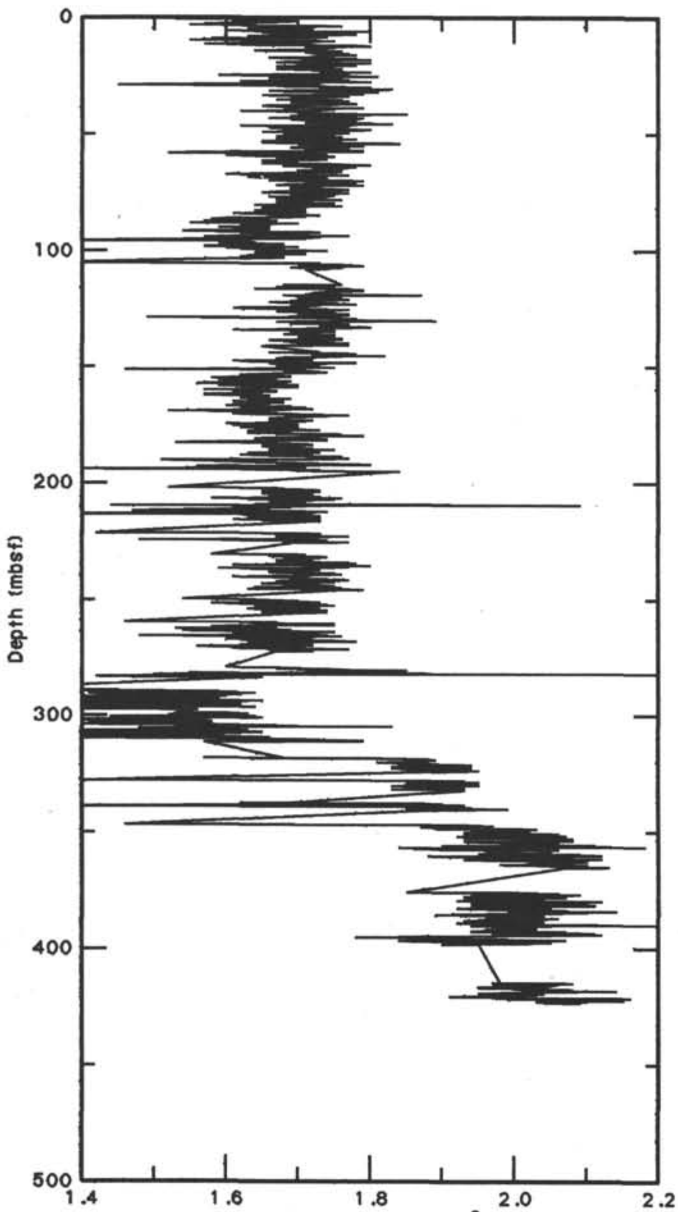

Figure 34. Wet-bulk density as measured by GRAPE for sediments in Hole 721B. The profile is based on 10-cm block averages of the data.

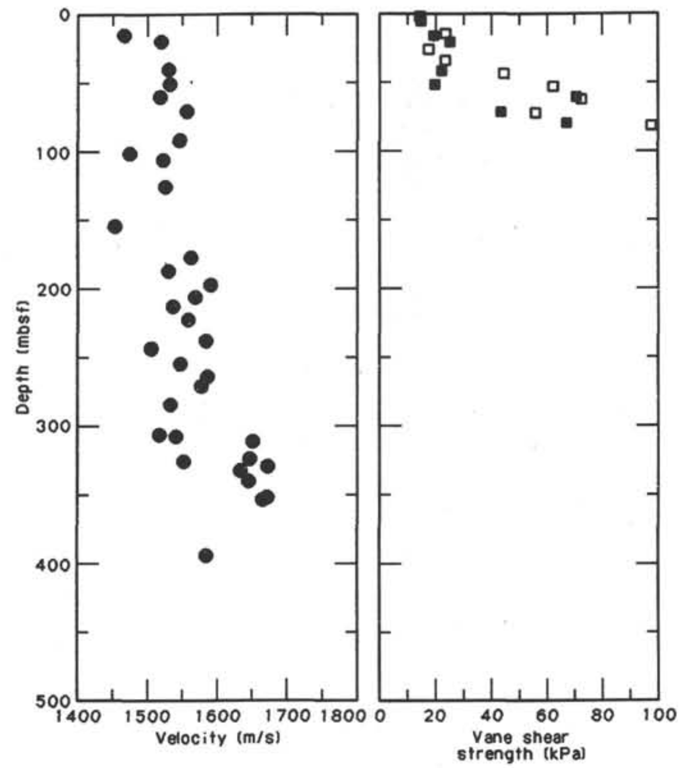

Figure 35. Compressional-wave velocity measured perpendicular to bedding in the Hamilton Frame Velocimeter and vane shear strength at Holes 721A (open symbols) and 721B (solid symbols).

lation Rates" section, this chapter) are about half the effective rate of diffusion of dissolved silica, the silica deficiency below 400 m depth must reflect SiO_2 precipitation rather than simply a paucity of dissolvable biogenic opal in the terrigenous deposits. Presumably, the dissolved silica distribution indicates that siliceous cementation is currently proceeding in the turbidite sequence. Indeed, both silica overgrowths on discoasters and replacement of discoaster calcite is observed in the turbidites (see "Lithostratigraphy" section, this chapter).

Sediment Mineralogy

The mineralogy of 16 sediment residues from Hole 721B remaining after interstitial water extraction was determined by X-ray diffractometry. Unoriented pressed-powder mounts were analyzed under standard operating conditions. No sample pretreatment was carried out. Relative abundances of illite, kaolinite, quartz, and dolomite (Fig. 43) were determined by correcting the net peak area counts for the effects of mineral mass absorption variation and changes in the calcite content (dilution)(MACC). The units expressed are therefore internally consistent among the four minerals, but have not been quantified with standards. The peak position used for the determination of illite may have a contribution from mica, and likewise chlorite may contribute to the kaolinite determination.

The general lithology of Site 721 is of pelagic nannofossil ooze overlying fine-grained muddy turbidites, with a sharp lithologic contrast between the two facies at 340 mbsf. Figure 43 suggests that both illite and kaolinite are abundant in the upper half of the core, with kaolinite being restricted to 110 mbsf. Over this interval kaolinite appears to be more abundant than illite. In contrast, quartz and dolomite occur throughout the cored section with quartz being apparently 2–3 times more abundant.

As indicated above, and in the "Lithostratigraphy" section (this chapter), the mineralogy of the nannofossil ooze is strikingly different from the fine-grained turbidites. In the latter, calcite is subordinate to quartz and significant concentrations of illite, chlorite, kaolinite, plagioclase feldspar, and pyrite were observed. Within the nannofossil ooze the proportion of terrigenous minerals per unit volume is controlled by variation in the terrigenous flux.

In order to assess the mode of occurrence of the dolomite at Site 721, the relative proportions of quartz and dolomite have been plotted together in Figure 44. A positive correlation is observed which argues in favor of a common source for the quartz and dolomite. If the dolomite was solely of authigenic origin, such a relationship would not be expected. A plausible source for both these minerals is the eolian transport of material to the Arabian Sea from adjacent landmasses.

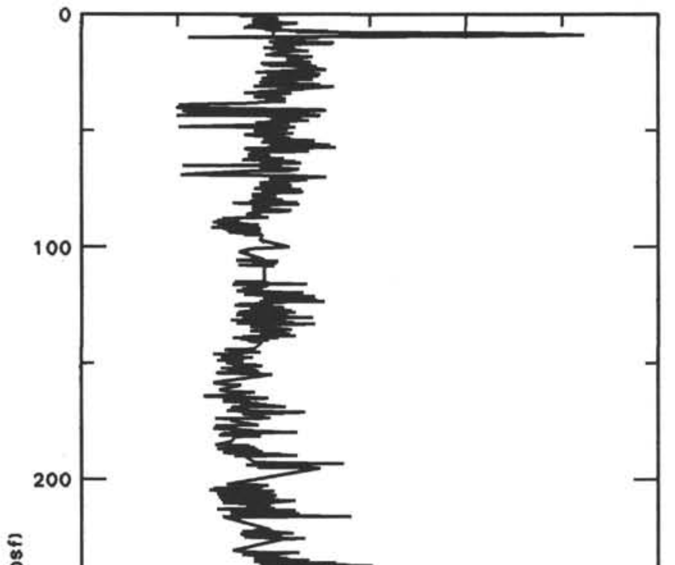

Figure 36. Compressional-wave velocity as the *P*-wave logger in Hole 721B. The profile is based on 5-cm block averages of the data.

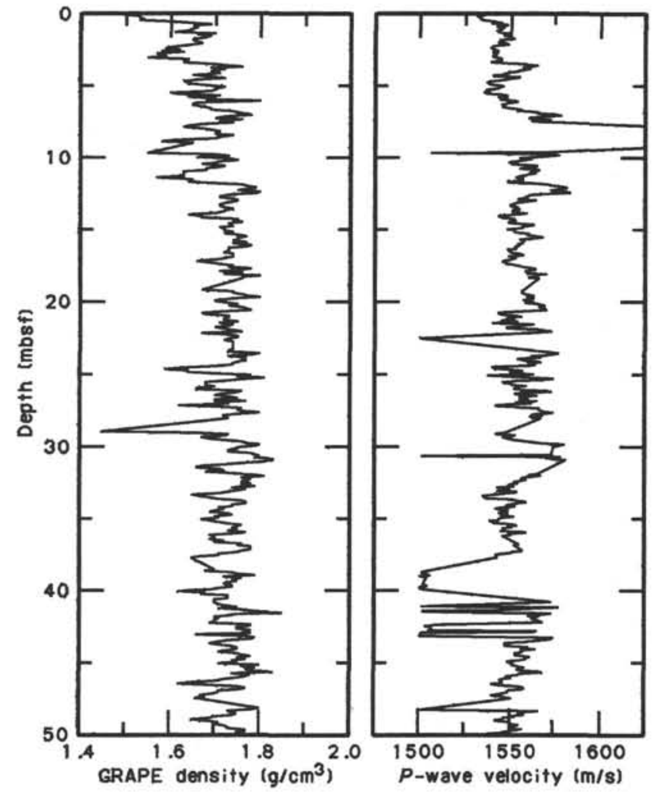

Figure 37. GRAPE wet-bulk density and *P*-wave logger compressional-wave velocity profiles for 0–50 mbsf in Hole 721B. The GRAPE and *P*-wave profiles are based on 10- and 5-cm block averages of the data, respectively.

Finally, four samples from Core 117-721B-18X (Samples 117-721B-18X-1, 150 cm; -1, 107 cm; -2, 20 cm; and -2, 61 cm) were examined in order to evaluate the mineralogical evidence for the high values of magnetic susceptibility (see "Paleomagnetism" section, this chapter). No unusual mineralogy was observed, and the main mineral was calcite.

ORGANIC GEOCHEMISTRY

The organic geochemical parameters routinely determined on sediments of Holes 721A and 721B were the abundance of organic carbon and pyrolysis characteristics. These parameters provide information on provenance of the organic matter and its maturity. Abundance of interstitial gas was determined in each core, and ratios of di- and triunsaturated C_{37} alkenones were measured in eight selected samples of Quaternary age to test their usefulness as indicators for variations in the sea-surface water temperatures. In general, organic matter is abundant in all levels of the cored interval of marine origin, and immature. Gas concentrations do not reach saturation levels and, as expected, the gas is exclusively of biogenic origin.

Organic Matter Abundance and Character

Sediments are generally rich in organic matter in the upper 310 m of the cored section, and values average 0.74% C_{org} in all samples of Holes 721A and 721B (Tables 3 and 13; Fig. 45). Notably, the maximum in C_{org} concentrations occurs between 40 and 200 mbsf. The eight samples selected for lipid analysis, after visual inspection of the upper three sections of Hole 721B, show an inverse correlation between organic carbon values and carbonate content. Layers with high organic carbon contents have low carbonate values and vice versa (see Table 3). The overall correlation coefficient ($r = 0.20$; all samples), however, shows that the organic carbon concentration does not correlate significantly with $CaCO_3$ content.

The organic matter is immature as shown by the uniformly low temperatures of maximum pyrolysis release of hydrocarbons, $T_{max} < 435°C$ (Table 13). The extremely low values measured in samples below 340 mbsf should be considered erroneous. Most samples plot in the lower part of the field of immature marine organic matter on the hydrogen index/oxygen index diagram (Fig. 46), but show a considerable scatter. Possible sources of CO_2 are admixtures of inert organic matter from terrigenous sources, CO_2 from carbonates which break down at temperatures below 390°C, or instrumental artifact (see "Explanatory Notes" chapter, this volume). A possible indicator for the origin of organic matter is the hydrogen index (HI) (Fig. 45). The good correlation of C_{org} concentrations with the HI indicates that increases in organic carbon concentrations are due to enhanced burial of marine, lipid-rich organic matter. This is

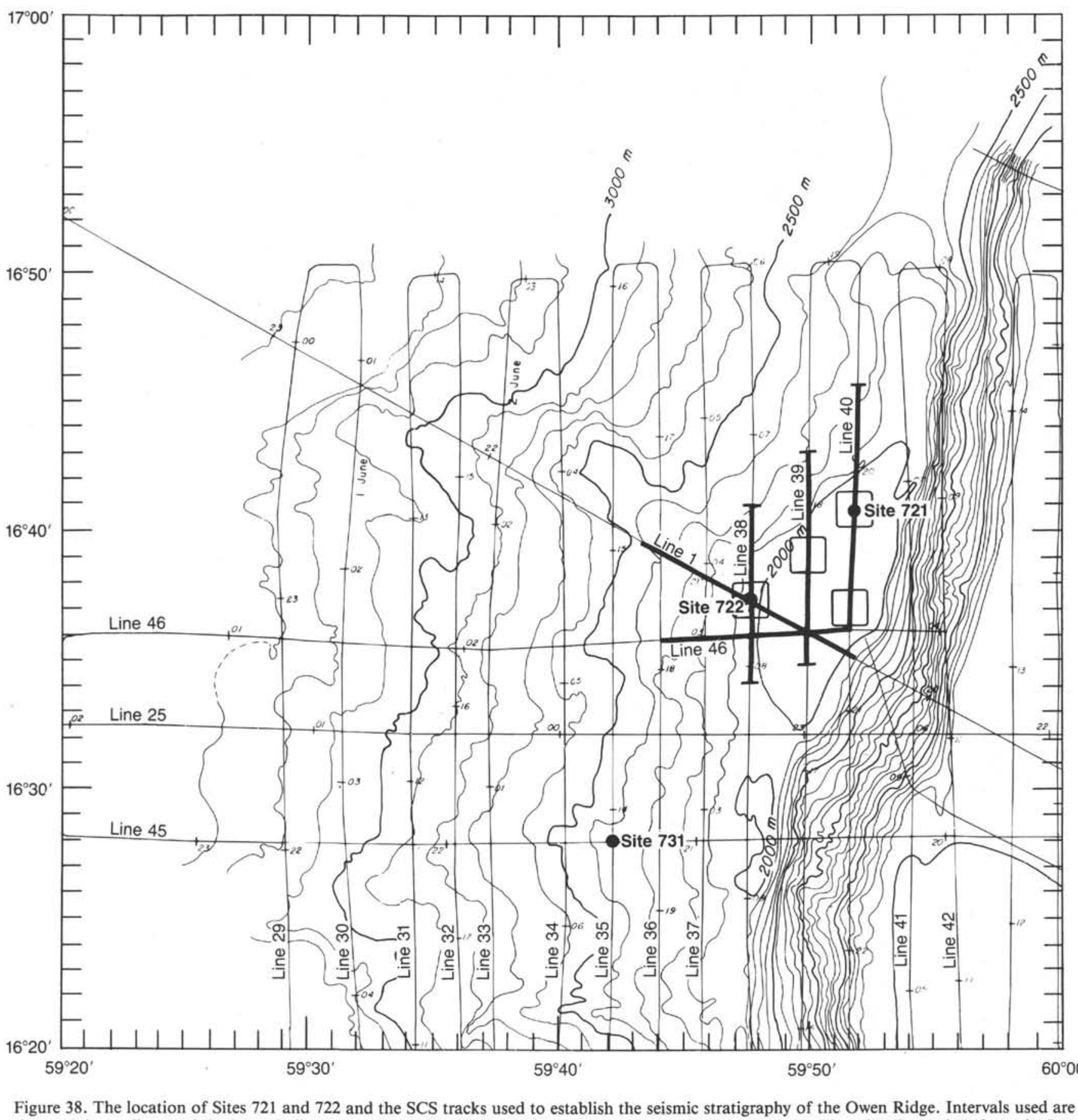

Figure 38. The location of Sites 721 and 722 and the SCS tracks used to establish the seismic stratigraphy of the Owen Ridge. Intervals used are shown as heavy lines and the boxes indicate portions of the tracks shown in Figure 39. The bathymetry is based on Sea Beam data from the Leg 117 site survey (RC2704, 1986).

somewhat surprising, as lipid-rich organic matter is considered to be the preferred substrate for microbial remineralization. Furthermore, benthic remineralization is believed to be more effective during times of low sedimentation rates, while burial of organic matter is more effective at high sedimentation rates (Müller and Suess, 1979). We would, therefore, expect lower HI values ratios in the intervals of low sedimentation rates between 41 and 170 mbsf. This is not the case, however, and with the data presently available, we are unable to decide whether we are dealing with an input signal (higher productivity and/or different organic matter source within the marine primary producers) or an enhanced preservation effect.

Hydrocarbon Gases

Samples for interstitial gas analysis with the headspace method were taken in each core of Hole 721A, and each core of Hole 721B starting from Core 117-721A-9H. Results are given in Table 14 and are shown vs. depth in Figure 47. As is usually observed in marine sediments containing more than baseline values of organic carbon (>0.2%), methane is generated in considerable quantities below the depth of sulfate depletion (see "Inorganic Geochemistry" section, this chapter) at approximately 100 mbsf. Values of methane per liter of wet sediment reach a maximum of 156 mL/L at 393 mbsf. Variability in the

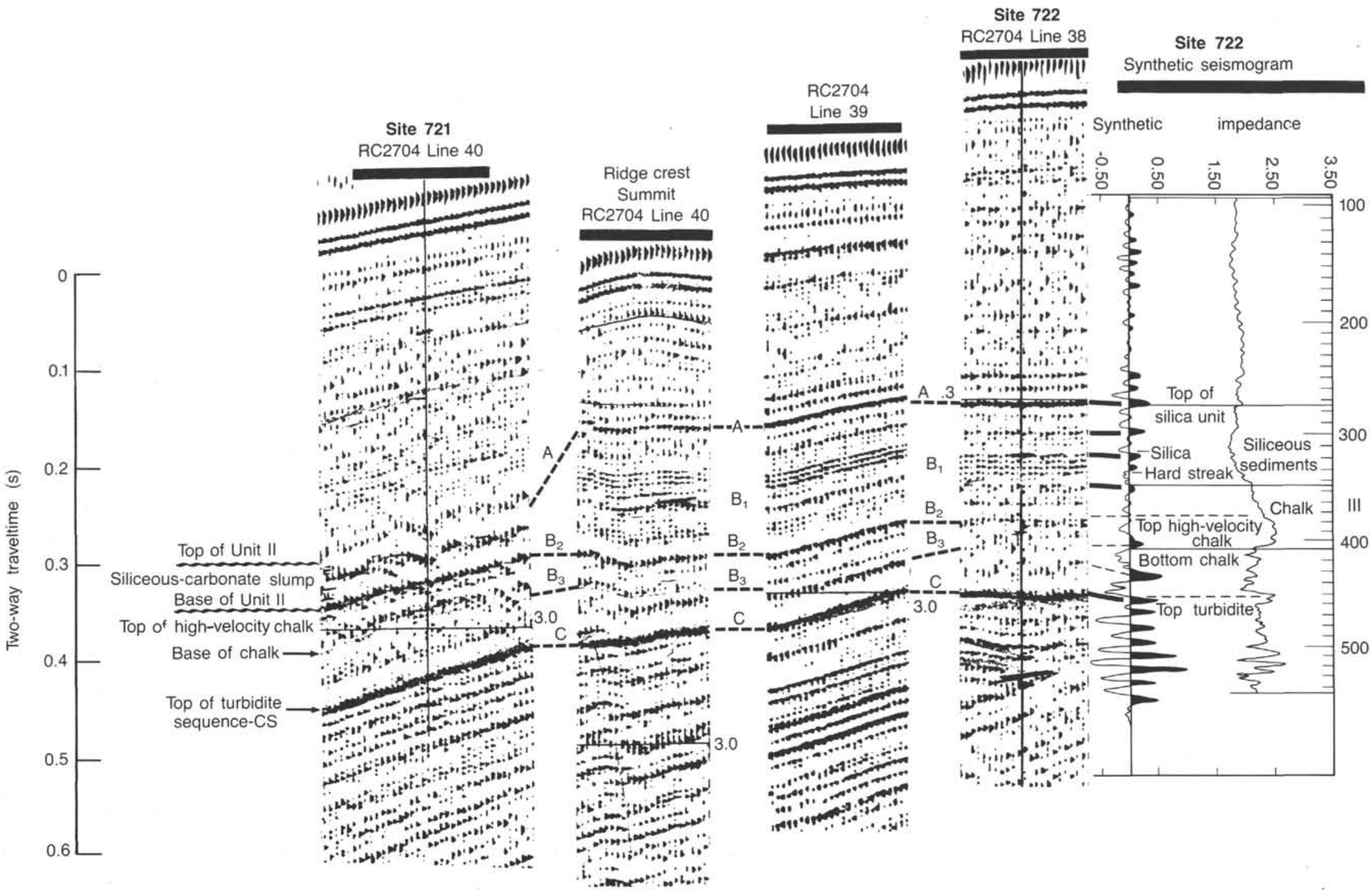

Figure 39. Correlation of reflectors (see text for discussion) between seismic profiles (see Fig. 38 for locations) and with the synthetic seismogram, which is based on logging data from Site 722 (see "Downhole Measurements" and "Seismic Stratigraphy" sections, "Site 722" chapter, this volume). Synthetic seismogram is scaled in mbsf and seismic profiles are in two-way traveltime (s). Profiles are aligned so that Reflector C is continuous; the position of 3.0 s below the sea surface is also shown.

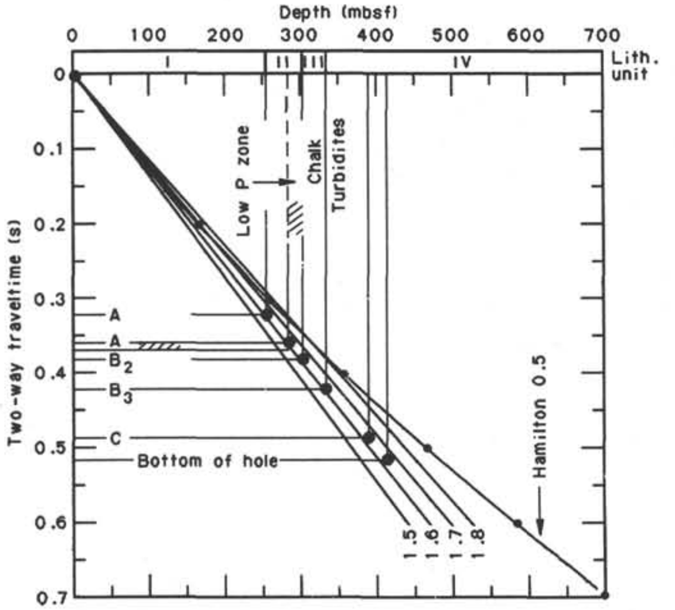

Figure 40. Plot of two-way traveltime (from SCS Line 40, see Figs. 39 and 41) and depth (mbsf) of lithologic features at Site 721. Reflectors are indicated on the traveltime axis and lithologic units and facies are shown on the depth axis. The wavy lines represent hiatuses. Diagonal straight lines correspond to time-depth curves for average velocities of 1.5, 1.6, 1.7, and 1.8 km/s. The slightly curved line is Hamilton's (1979) empirical curve for carbonate sediments.

concentrations downhole appear to be independent of organic matter abundance and quality (as expressed by the HI, Fig. 45), and below 200 mbsf the methane abundance levels out at values around 0.1 L/L. Insufficient gas was present in the sediments to cause the formation of gas pockets. The concentration of the C_{2+} gases is very low (only ethane could be detected) and attests to the immature nature of the organic matter in the Miocene to Holocene sediments cored at Site 721. Most likely the ethane is generated by microbial activity, and not by thermogenic cracking. Therefore, the C_1/C_2 ratios do not follow the exponential decrease with depth which one would expect by thermogenic cracking of kerogen (Claypool and Kaplan, 1974).

Lipid Analyses

An attempt was made to analyze the molecular distributions of extractable organic compounds in Quaternary sediments from Hole 721B, with emphasis on the occurrence of long-chain unsaturated ketones (alkenones). Variations in sea-surface water temperatures in the geological past are potentially recorded by these alkenones. Planktonic organisms that biosynthesize these compounds react to increasing water temperature with a decrease in the average degree of unsaturation (i.e., number of double bonds; Brassell et al., 1986; ten Haven et al., 1987). Brassell et al. (1986) defined an alkenone unsaturation index as:

$$U^{k}_{37} = \text{diunsaturated } C_{37} \text{ / diunsaturated + triunsaturated } C_{7} \text{ ketones}$$

This ratio can vary between 0 and 1, i.e., from cold to warm. Eight samples were selected from the upper three cores of Hole 721B. Depth, organic carbon and carbonate content of these samples are given in Table 15. The experimental procedure, as well as the gas chromatographic conditions are described in the "Explanatory Notes" chapter (this volume). The gas chromatograms of four sediment extracts are shown in Figure 48. The alkenones elute with retention times between 45 and 49 minutes. The first two eluting compounds are the di- and triunsaturated C_{37} ketones, respectively, followed by a group of C_{38} unsaturated ketones approximately 2 min later. Straight-chain alkanes are indicated with dots, and the numbers above the dots correspond to the number of carbon atoms of the molecules (the identification has been solely made on basis of retention times compared with a standard solution). The C_{17} straight-chain alkane (heptacosane) is the most prominent alkane, and abundances of C_{27} to C_{33} alkanes from cuticular waxes are low. These findings support a dominantly marine origin of the organic matter which has to be elucidated by shore-based investigation. An enlargement of the retention time range of alkenone elution is given in Fig. 49 for two extreme values, and the calculated U^{k}_{37} ratios are given in Table 15. The U^{k}_{37} ratios of sediments investigated here are high and in the range of data from the Sierra Leone Rise (0.88–0.97; Brassell et al., 1986). Our results point to "cool" sea-surface water temperatures in Samples 117-721B-1H-2, 100–103 cm, and 117-721B-2H-2, 17–20 cm, while higher sea-surface water temperatures are indicated in Sample 117-721B-2H-1, 87–90 cm. Using the calibration regression equation (U^{k}_{37} = 0.033T + 0.043) based on laboratory cultures (Prahl and Wakeham, 1987), absolute temperatures are 25.0°C and 28.5°C, respectively. The maximum difference in the U^{k}_{37} ratio (0.11) is the same as measured in samples of Leg 108 (offshore Morocco, Atlantic Ocean), covering a glacial/interglacial time span (Shipboard Scientific Party, 1988). In the Atlantic Ocean, glacial times are characterized by low $CaCO_3$ contents and high organic carbon contents, and vice versa for interglacial times. Surprisingly, a correlation seems to exist between the U^{k}_{37} ratio and the carbonate content of the sediments investigated from the Owen Ridge (Fig. 50). However, more samples need to be analyzed to prove whether this correlation is significant.

DOWNHOLE MEASUREMENTS

No logging was done at Site 721.

INTERHOLE CORRELATION

The upper part of lithologic Unit I recognized at Site 721 is characterized by cyclic changes in the nature of sediments. The changes can be detected not only by visual observation (i.e., color changes), but also by magnetic susceptibility (see "Paleomagnetism" section, this chapter) and $CaCO_3$ content (Fig. 5). Three holes were drilled by APC cores and collected sequences from the upper 100 mbsf within lithologic Unit I (Holes 721A, 721B, and 721C; Fig. 51). The correlation of the cycles among these holes provides valuable information on changes in the depositional environment and on gaps in the sections which are necessary for high-resolution studies. Uniformity and continuity of each layer gives information on differences in the sedimentation rates between the holes at Site 721. The essence of the interhole correlation process involves the determination of correlative lithologic marker layers which are then confirmed using the detailed whole-core magnetic susceptibility data; the process is summarized in the "Explanatory Notes" chapter (this volume).

The holes are located on the crest of the Owen Ridge and are aligned in a north-northeast direction. Hole 721B is 20 m west of Hole 721A, and Hole 721C lies 20 m south of Hole 721B. Hole 721A drilled to 86.4 mbsf with APC, and the recovery was almost perfect. Hole 721B is the deepest hole in Site 721 and reached 424.2 mbsf by APC and XCB drilling. Hole 721C was drilled by APC and XCB, and the bottom depth was 138.0 mbsf. The top of Hole 721C obtained the mud line, which was not recognized in Cores 117-721A-1H and 117-721B-1H, respectively.

Apart from visual correlation, physical and magnetic properties were used to correlate between the holes. The GRAPE

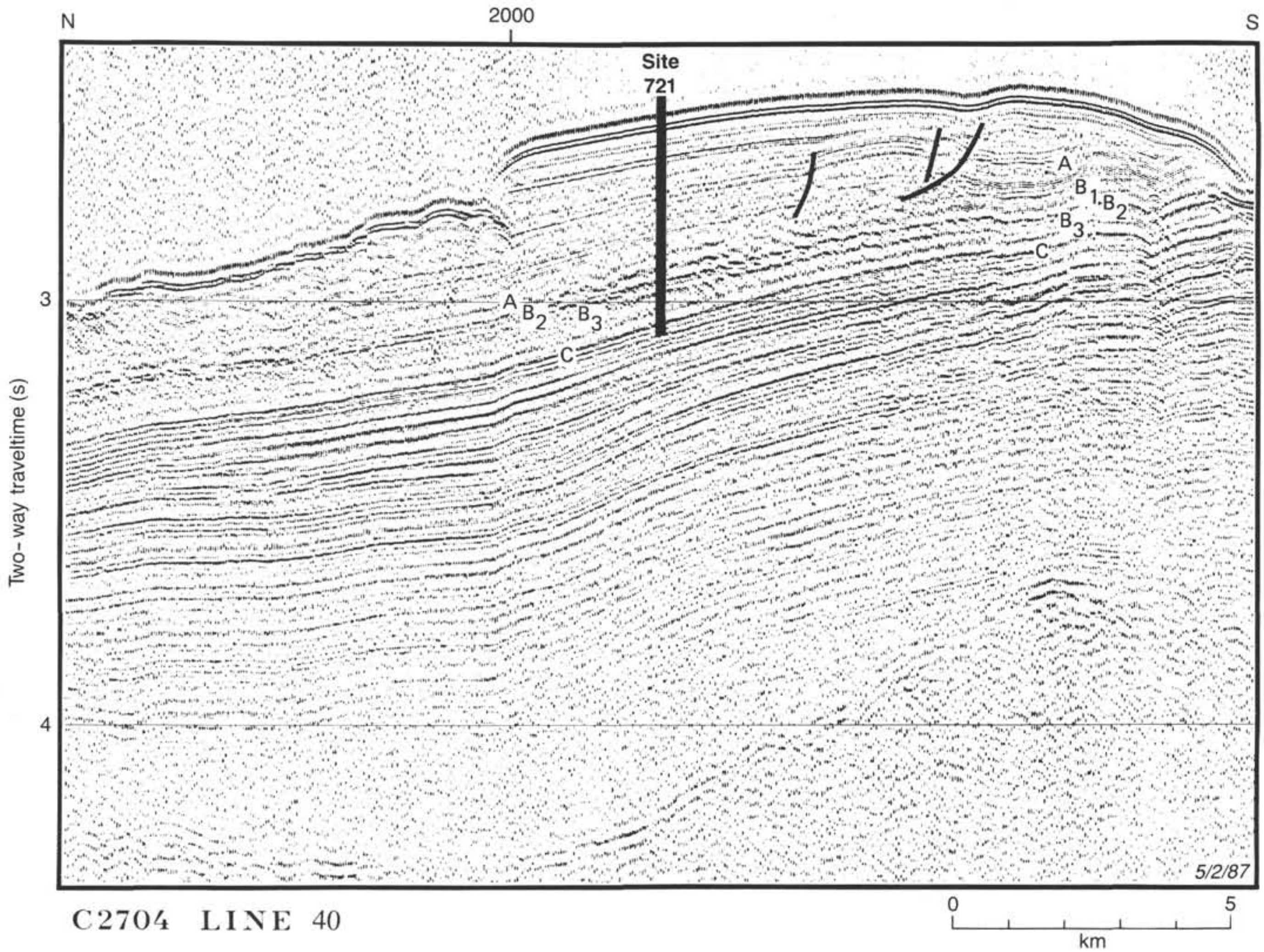

Figure 41. Seismic reflection profile (Line 40, see Fig. 38) across Site 721 to the crest of the Owen Ridge. The location and recovered interval of Site 721 are shown, along with the reflector identifications and interpreted faults.

density and magnetic susceptibility of the sediments were measured at 1.2- and 5-cm intervals before splitting the sections. Lithologic descriptions and photographs were obtained on the split sections.

Visual correlation of the cores relied on the core photographs. Several distinct and traceable layers were determined in each core and were notated as a_0, a_1, ·····, n_2, n_3 (Table 16). The marker layers were defined on the cored sediments of Hole 721A above 91.7 mbsf (i_4) and on Hole 721B below 94.25 mbsf (i_5).

Figure 52 shows an example of the correlations by visual and magnetic susceptibility methods. The figure shows the correlative interval with layer f_1 and f_2: Samples 117-721A-6H-1, 110 cm, to 117-721A-6H-2, 120 cm (49.70–51.20 mbsf); Samples 117-721B-6H-4, 100 cm to 117-721B-6H-5, 100 cm (53.60–55.10 mbsf); 117-721C-7H-2, 0–150 cm (53.50–55.00 mbsf). Visual lithologic correlations were based on the color pattern and bioturbation features. Light-colored intervals typically correspond to lower susceptibility while dark intervals correspond to higher susceptibility and lower $CaCO_3$ content. In this way the lithologic marker layer correlations were verified using the magnetic susceptibility data, which are quantitative.

The results of the layer-by-layer correlation allow us to calculate true thickness between these layers coinciding with and cut by core boundaries. Occasionally core tops were expanded by water uptake during drilling, and in such instances the apparent thickness of the sediment layer divided by the core boundary is assumed to be thicker than the original length. In some instances, the top part of the core was missing. In this case apparent thickness is assumed to be thinner than the original length. Fortunately, the three holes were staggered, so that they have different horizons at core boundaries as shown in Table 16. The original thickness of layers coinciding with core tops or bottoms can be obtained by comparing thickness of the correlative layer in the continuous section of the other holes. The differences in Hole 721B can be calculated by referring to Hole 721A and 721B. Unfortunately, the core boundaries in Hole 721A and 721C are located almost in the same horizons. The differences between these two were calculated by referring to the correlative intervals of Hole 721B. Table 17 shows the differences between the depth calculated by the ODP core log data and assigned depth, and depth calculated by the layer-by-layer correlation method. The reliability of this method to produce corrected depths is high; computation of corrected depths have errors less

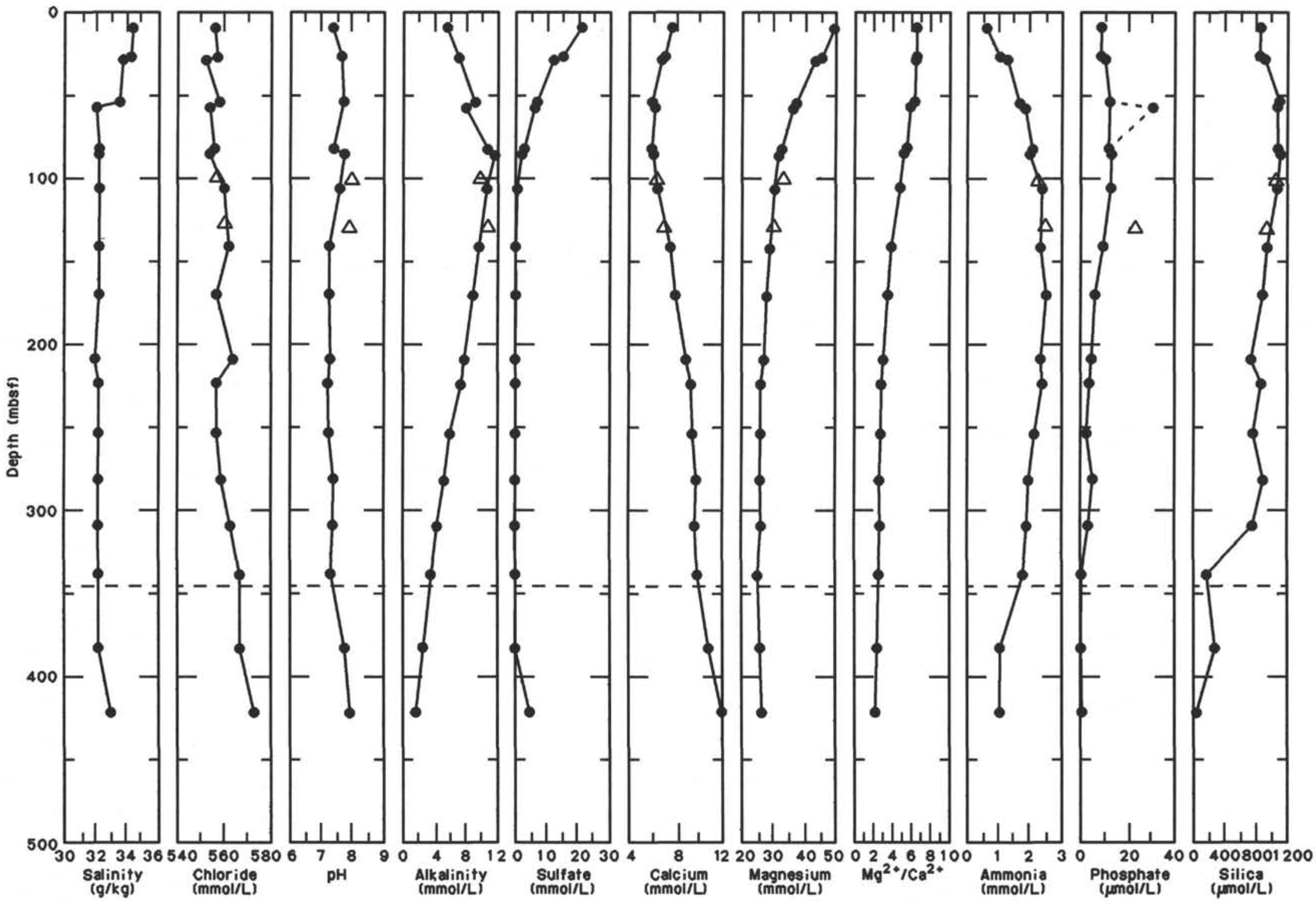

Figure 42. Concentration profiles vs. depth for Site 721. Dots = squeezed pore waters; triangles = *in-situ* pore-water samples obtained with the Barnes water sampler. The horizontal dashed line indicates the break in lithology between the biogenic ooze (Unit III) and the turbidites (Unit IV).

Table 12. Summary of interstitial water geochemical data for Holes 721A and 721B.

Hole, core, section (cm)	Depth (mbsf)	Vol. (mL)	pH	Alk. (mmol/L)	Sal. (g/kg)	Mg (mmol/L)	Ca (mmol/L)	Cl (mmol/L)	SO_4 (mmol/L)	PO_4 (μmol/L)	NH_4 (mmol/L)	SiO_2 (μmol/L)	Mg/Ca
117-													
721A-1H-6, 145-150	8.95	43	7.38	5.47	34.3	49.25	7.61	556	20.9	8.7	0.60	855	6.47
721B-3H-5, 145-150	26.55	45	7.66	6.99	34.2	45.35	7.01	557	15.0	8.6	1.03	846	6.47
721A-3H-6, 145-150	28.45	35	—	—	33.7	43.16	6.75	552	12.0	10.3	1.26	914	6.39
721B-6H-4, 145-150	54.05	55	7.74	9.02	33.5	37.42	5.94	558	6.8	12.4	1.66	1100	6.30
721A-6H-6, 145-150	57.45	40	—	7.88	32.0	36.29	6.20	554	6.1	30.7	1.84	1075	5.85
721B-9H-4, 145-150	82.35	48	7.42	10.72	32.2	32.77	5.93	556	2.75	12.0	2.07	1083	5.53
721A-9H-6, 145-150	85.75	48	7.76	11.56	32.2	31.81	6.10	554	2.01	13.2	1.99	1117	5.21
721C-12I-1, 0-1	100.00	15	8.02	9.75	32.3	33.39	6.08	556	0	—	2.19	1024	5.49
721B-12X-1, 145-150	106.65	40	7.61	10.55	32.2	30.54	6.42	560	0.5	12.9	2.37	1075	4.76
721C-15I-1, 0-1	129.00	15	7.84	10.57	31.7	30.37	6.92	559	0.0	23.2	2.48	948	4.39
721B-15X-5, 145-150	141.55	37	7.28	9.58	32.2	29.26	7.54	562	0	9.7	2.32	948	3.88
721B-18X-5, 145-150	170.65	32	7.28	8.87	32.2	28.18	7.99	557	0.2	6.3	2.51	889	3.53
721B-22X-5, 145-150	209.45	37	7.31	7.77	32.0	27.44	8.89	564	0	4.9	2.34	745	3.09
721B-24X-2, 140-150	224.20	73	7.23	7.36	32.2	26.31	9.31	557	0	3.8	2.39	872	2.83
721B-27X-3, 145-150	254.25	31	7.26	5.90	32.2	26.26	9.44	557	0	2.6	2.14	770	2.78
721B-30X-2, 140-150	282.10	50	7.42	5.20	32.2	26.14	9.79	559	0	5.3	1.96	897	2.67
721B-33X-1, 140-150	309.80	58	7.41	4.34	32.2	26.58	9.67	563	0	3.6	1.91	762	2.75
721B-36X-1, 140-150	338.80	30	7.33	3.60	32.2	25.49	9.89	567	0	0.5	1.79	178	2.58
721B-40X-5, 140-150	383.30	21	7.78	2.59	32.2	26.13	10.83	567	0	0.4	1.07	280	2.41
721B-44X-5, 140-150	421.90	30	7.94	1.63	33.0	26.74	11.96	573	4.6	0.8	1.06	51	2.24

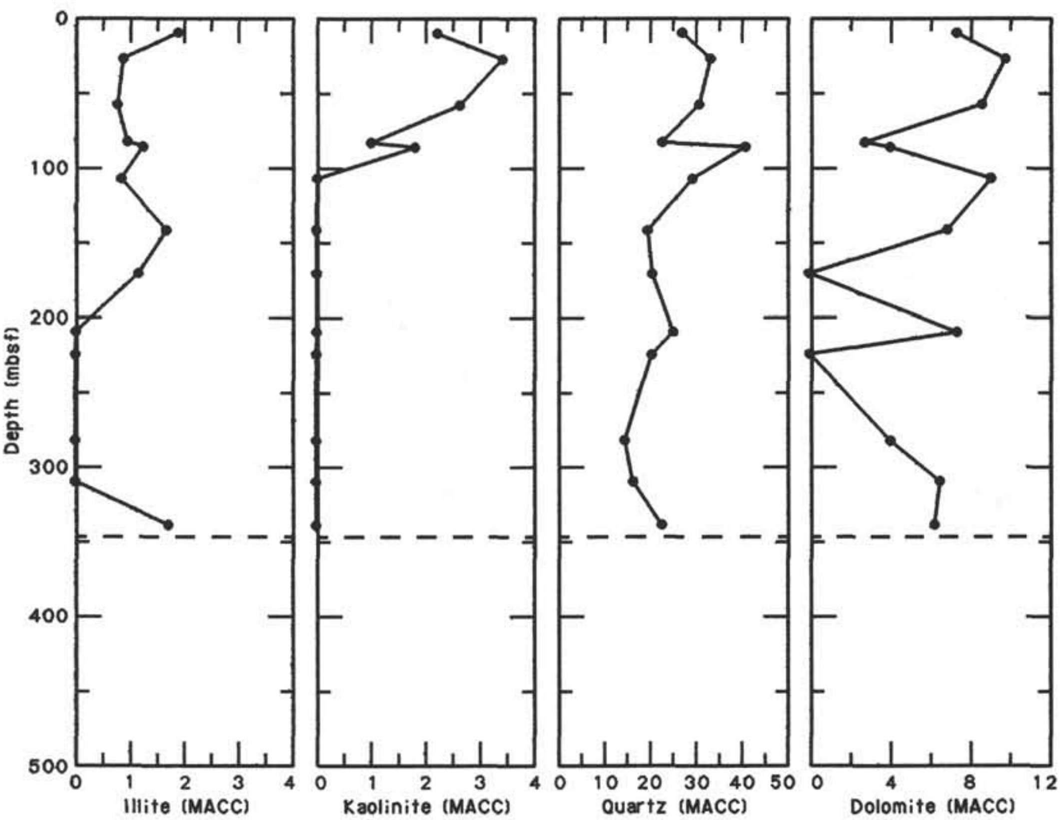

Figure 43. Qualitative distributions of illite, kaolinite, quartz, and dolomite in Site 721 sediments, corrected for dilution by calcium carbonate and differential mass absorption effects (MACC). Chlorite may contribute to the kaolinite peak. The abscissae show relative scales only and are not meant to imply absolute concentrations. The concentration of detrital clays and quartz in the turbidite facies greatly exceeds the levels in the nannofossil oozes and are thus not plotted.

than 20 cm. Using this correction offset for the calculation of true thickness, the thicknesses between a_2 and i_4 can be calculated as 87.95 m in 721A, 87.65 m in 721B, and 85.95 m in 721C. The sediments in Hole 721C are apparently 2.0 m thinner than in Hole 721A and 721B.

Hole 721C recovered the mud line in the first core. It appears that Hole 721B also has recovered the mud line, because the subsurface depth of a_0 is 10 cm deeper than Hole 721C. Hole 721A, however, missed the top 2.75 mbsf based on the correlation of horizon a_1. This estimate is substantiated by correlating

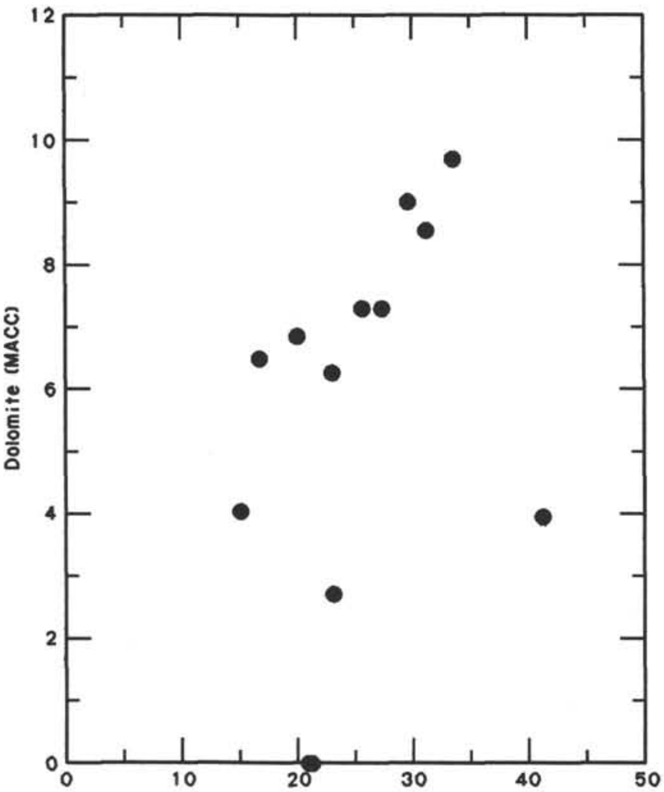

Figure 44. Correlation between the mass-absorption and carbonate-corrected (MACC) relative concentrations of dolomite and quartz in Site 721 sediments.

$CaCO_3$ data from Hole 721A and from a piston core (RC27-61) taken during the site survey (Fig. 53). Based on the calcium carbonate profile correlations, at least 2.25 m is missing from the top of 721A. A correlation of the piston core to trigger cores implies that 20 cm is missing from the top of RC27-61. Thus, the top of Hole 721A begins at least 2.45 m (2.25 ± 0.20 m) below the mud line. The 30-cm difference between the estimate of missing section based on the correlation to Hole 721B and the estimate based on carbonate profiles could be due to stretching of the sediments in the soupy section at the top of Core 117-721B-1H and differences in sedimentation rate between the two locations.

Hole 721B contains the most complete sediment record for the top 100 mbsf at Site 721. The correction factors in Table 17 are utilized to correct the ODP CORELOG data to provided a continuous sediment section for Site 721 (Table 18).

SUMMARY AND CONCLUSIONS

The primary reason for coring at Site 721 was to recover a continuous high-resolution section of pelagic sediments of late Neogene age from the crest of the Owen Ridge. These sediments have been deposited well above the carbonate lysocline and beyond the zone of lateral bottom transport from the continental margin. Study of this sedimentary sequence was expected to identify the initiation, and document the history, of monsoonal upwelling in the Arabian Sea (Kutzbach, 1981; Prell and Kutzbach, 1987). The detailed biotic, chemical, and sedimentologic records obtained from these sediments can provide data to test the hypothesis that much of the short-term variability (10^3 yr) of monsoonal upwelling is forced by changes in solar radiation related to cyclical variations in the earth's orbit (the Milankovitch mechanism). Long-term trends of the intensity of the monsoon related to the uplift of the Himalayas may also be imprinted on the long paleoenvironmental record from the ridge (Hahn and Manabe, 1975). In addition, the age and character of the sediments at Site 721 could be used to reconstruct the depositional and tectonic uplift history of the Owen Ridge.

The preliminary shipboard findings at Site 721 pertinent to the above objectives are summarized in Figure 54 and include the identification of:

1. The appearance of siliceous facies in the lower part of the upper Miocene.
2. The appearance of cold "upwelling" faunas in the middle upper Miocene.
3. Well-defined sedimentary cycles that are defined by changes in sediment color, magnetic susceptibility, and physical properties. The cycles have distinct periodicities, which are consistent with the Milankovitch frequencies, and individual cycles can be correlated in detail between holes.
4. High accumulation rates in the upper Miocene, which are followed by low rates in the lower Pliocene, and increasing rates during the Pliocene-Pleistocene.
5. The cessation of turbidite deposition on the ridge crest in the lower to middle Miocene.
6. The covariation of quartz and dolomite in the clastic fraction of the sediments.
7. Generally high values of marine-derived organic carbon and its relatively pristine character.

The major themes that are relevant to the interpretation of the depositional history of Site 721 combine such phenomena as the uplift of the Owen Ridge, the onset and preservation of siliceous fossils and the appearance of distinct upwelling faunas, and the pattern of high-frequency variability in the abundance of various sedimentary components. Below, we briefly address these themes.

Uplift of the Owen Ridge

The uplift history of Owen Ridge is indicated by variations in the lithofacies, i.e., by the gradation of turbiditic facies, and by phases of nondeposition or erosion. The lower Miocene section at Site 721 is characterized by silty turbidites that grade upward to muddy turbidites. The turbidites are typically low in organic carbon and carbonate, and frequently display concentrations of sand- to silt-sized pyrite (placers?) at their bases. Preservation of planktonic fossils is poor and opaline silica is sparse (Fig. 54). This sequence was laid down in an active deep-water turbidite depositional environment before the Owen Ridge was uplifted. In the upper part of lithologic Unit IV, the grain size of basal layers decreases, and finer-grained muddy turbidites are intercalated with pelagic nannofossil chalks. This trend of finer, more distal(?), and fewer turbiditic deposits is also shown in the decrease in magnetic susceptibility, bulk density (Fig. 54), and *P*-wave velocity. The source of the fine mud turbidites and their pyrite bed load is unknown. A shelf origin is assumed in spite of their low organic carbon content. We interpret the fining-upward sequence as an indicator of progressive uplift of the site above the surrounding seafloor. Thus, the coarser bed load of the turbidite flows would not reach the site. Seismic reflection profiles of the region indicate some onlap to the reflectors that are equivalent to the turbidites in Unit IV, so that some uplift probably occurred prior to the deposition of the deepest sediments recovered at Site 721. The upper limit of the turbiditic sequence is marked by a prominent seismic reflector (C) that can be mapped over much of the Owen Ridge and in the adjacent Owen Basin (Mountain and Prell, 1987).

The uppermost lower and middle Miocene deposits recovered at Site 721 were entirely composed of nannofossil chalk

Table 13. Results of Rock-Eval pyrolysis of samples from Holes 721A and 721B.

Hole, core, section, interval (cm)	Depth (mbsf)	T_{max} (°C)	S_1	S_2	S_3	S_2/S_3	TOC	HI	OI
117-									
721A-1H-6, 144–145	8.94	406	0.00	0.55	1.71	0.32	0.56	98	305
721A-2H-6, 149–150	18.79	411	0.00	0.51	1.38	0.36	0.38	134	363
721A-2H-7, 25–27	19.05	418	0.00	0.99	1.33	0.74	1.01	98	131
721A-3H-6, 119–120	28.19	390	0.00	0.20	1.31	0.15	0.30	66	436
721A-4H-5, 0–1	35.20	412	0.00	0.74	1.64	0.45	0.66	112	248
721A-5H-4, 149–150	44.89	417	0.00	2.11	1.83	1.15	1.04	203	176
721A-6H-6, 119–120	57.19	423	0.00	1.70	1.51	1.12	0.88	193	171
721A-7H-5, 149–150	65.29	419	0.00	2.77	1.80	1.53	1.04	266	173
721A-8H-5, 149–150	74.79	418	0.00	3.52	2.00	1.76	1.45	242	137
721A-9X-6, 119–120	85.48	416	0.00	14.72	3.36	4.38	3.68	400	91
721B-1H-2, 100–103	2.50	417	0.01	2.79	3.20	0.87	1.29	216	248
721B-1H-4, 80–83	5.30	405	0.02	0.78	2.11	0.36	0.43	181	490
721B-1H-5, 24–27	6.24	414	0.02	2.41	2.55	0.94	1.21	199	210
721B-2H-1, 87–90	10.27	407	0.02	0.91	2.04	0.44	0.46	197	443
721B-2H-2, 17–20	11.07	414	0.01	1.70	2.29	0.74	1.91	89	119
721B-3H-3, 10–13	22.20	417	0.02	1.52	1.98	0.76	0.74	205	267
721B-9H-4, 144–145	82.34	421	0.00	6.17	2.66	2.31	1.95	316	136
721B-10X-4, 149–150	91.99	419	0.00	1.82	1.73	1.05	0.96	189	180
721B-11X-2, 149–150	98.59	420	0.00	12.06	3.24	3.72	3.07	392	105
721B-12X-1, 144–145	106.64	422	0.00	2.93	1.91	1.53	1.56	187	122
721B-13X-4, 149–150	120.79	414	0.00	0.80	1.47	0.54	0.60	133	245
721B-14X-1, 149–150	125.89	396	0.00	0.46	1.88	0.24	1.37	33	137
721B-15X-2, 119–120	136.79	419	0.00	3.81	1.93	1.97	0.66	577	292
721B-16X-5, 149–150	151.29	422	0.00	1.92	1.65	1.16	0.70	274	235
721B-17X-5, 149–150	160.99	422	0.00	8.65	2.57	3.36	0.57	1517	450
721B-18X-5, 119–120	170.39	418	0.00	2.81	1.86	1.51	1.49	188	125
721B-19X-5, 149–150	180.39	418	0.00	1.11	1.60	0.69	1.97	56	81
721B-20X-5, 149–150	190.09	409	0.03	1.01	1.70	0.59	0.92	109	184
721B-21X-2, 0–1	193.80	420	0.00	3.74	1.90	1.96	0.28	1335	678
721B-22X-3, 0–1	205.00	420	0.00	2.55	1.65	1.54	0.78	326	211
721B-24X-3, 0–1	224.30	417	0.00	1.47	1.67	0.88	0.56	262	298
721B-25X-5, 0–1	236.50	413	0.00	0.62	1.75	0.35	0.37	167	472
721B-27X-3, 119–120	253.99	352	0.00	0.13	1.02	0.12	0.25	52	408
721B-28X-5, 0–1	265.60	415	0.02	1.80	1.70	1.05	0.80	225	212
721B-29X-2, 0–1	270.90	408	0.02	0.88	1.46	0.60	0.43	204	339
721B-31X-3, 149–150	293.49	411	0.04	1.74	1.62	1.07	0.85	204	190
721B-32X-2, 149–150	301.79	413	0.05	3.81	1.63	2.33	1.47	259	110
721B-33X-1, 114–115	309.54	418	0.07	4.46	2.02	2.20	1.60	278	126
721B-36X-1, 114–115	338.54	264	0.03	0.29	0.61	0.47	0.37	78	164

Note: Samples are mainly headspace residues. For a detailed description of parameters, see "Explanatory Notes" chapter (this volume).

(Unit III) that is characterized by high carbonate content (76%) and poor opal preservation (Fig. 54). Thus, by this time, the site had been uplifted well above the influence of turbidite deposition and was accumulating pelagic sediments. However, much of the middle Miocene section is missing. A significant hiatus (from nannofossil Zone NN9 to NN5) occurs at about 311 mbsf and correlates to seismic reflector B_2 (see "Seismic Stratigraphy," this chapter). Lithologic Unit II lies above the reflector B_2 and is composed of siliceous nannofossil oozes and chalks that are disturbed by slumping. The lower part of this unit is characterized by low bulk and grain densities and high porosities that reflect the greater biogenic silica content (Fig. 54). This stratigraphic interval appears to be the locus of the slump fault that removed most of the middle Miocene. The top of lithologic Unit II may also marked by a hiatus, but of much smaller extent than the basal hiatus. On the basis of biostratigraphy and comparison to other seismic sections on the Owen Ridge, we estimate that about 90 m of the middle Miocene is missing at Site 721. The slump of the sediments is, no doubt, related to the inclination caused by the uplift of the Owen Ridge, but the specific event cannot yet be attributed to a discrete uplift phase. Another phase of uplift, indicated by low accumulation rates (see below), may have occurred in the early Pliocene.

The Onset of Upwelling Faunas and Opal Deposition

If late Neogene uplift and orbital changes have affected the monsoon as outlined in the "Introduction, Background, and Major Objectives for Leg 117" chapter (this volume), the sediments at Site 721 should record both increased productivity and distinct faunas due to the upwelling. The sediments should also reflect increased eolian transport (although some of the transport may occur during the winter season). Furthermore, variations in source area of the eolian components may result in differing mineralogy and chemistry. Thus, the cyclic variations in sediment composition related to changes in solar radiation should have specific frequencies, the Milankovitch spectrum, that may be quantitatively identified in the sediments of Site 721.

The first indication of enhanced productivity at Site 721 is the appearance of the siliceous facies of lithologic Unit II in the upper Miocene (Fig. 54). Both radiolarians and diatoms appear at the base of this unit, but the species are tropical in nature. At the same time, organic carbon increases from less than 0.1% in Units III and IV to almost 2.0% in the base of the siliceous Unit II. As previously noted, this interval is also characterized by low bulk and grain densities and low velocities due to the admixture of siliceous fossils. Unfortunately, the base of the siliceous fa-

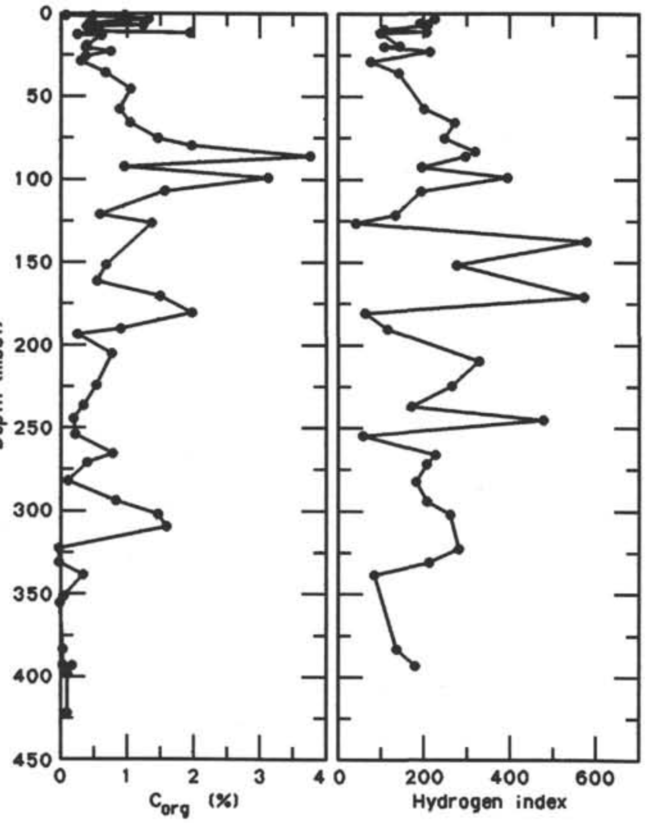

Figure 45. Downhole plots of C_{org} and hydrogen index values in Holes 721A and 721B. High values of HI are considered to be an attribute of lipid-rich, undegraded marine organic matter.

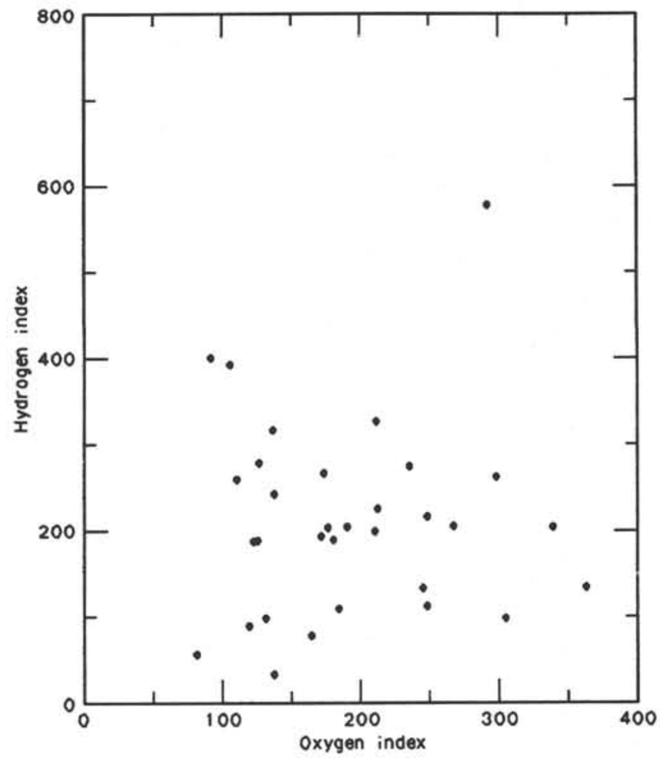

Figure 46. Plot of the hydrogen index vs. oxygen index (OI) of samples from Holes 721A and 721B. Samples plot mainly in the section for immature marine organic matter rich in relatively labile oxygen-rich functional groups.

cies (the boundary between lithologic Units II and III) corresponds to the basal hiatus of Unit II, so that the true age of the onset of siliceous deposition on the Owen Ridge is not recognized at Site 721. The siliceous facies (Unit II) grades upward to foraminifer-nannofossil ooze (chalk) with deformation and slump features (Unit II) and eventually to foraminifer-bearing and foraminifer-nannofossil ooze with alternating light and dark bands (Unit I). The different plankton assemblages undergo dramatic, but not simultaneous, changes in the upper Miocene. The first indication of upwelling is the appearance of a radiolarian fauna in the middle Miocene. This assemblage contains typical tropical species, but younger radiolarian faunas contain more robust, cool-water forms and lack many tropical forms. A distinctive upwelling planktonic foraminiferal fauna appears in the early late Miocene with the simultaneous appearance of *Globoratalia bulloides*, *Globoratalia menardii*, and *G. tumida*, and the *Neogloboguadrina* lineage of *N. acostaensis* and *N. dutertrei* at the boundary between lithologic Units II and I (Fig. 54). Finally, in the early Pliocene, cold-water forms of calcareous nannoplankton appear at Site 721. This sequence of assemblages may indicate an ecologic response to the evolution of monsoonal upwelling. However, detailed study of the faunal and floral variations will be needed to establish the oceanographic significance of this sequence.

Another possible indication of changes in monsoonal upwelling is the variation in accumulation rates, especially biogenic rates. The percent carbonate content of Unit I is relatively high (average about 60% with variations from 80% to 40%) and shows no long-term trends. However, the carbonate and noncarbonate accumulation rates show significant fourfold variations since the late Miocene. The carbonate accumulation rates increase from about 1 g/cm²/k.y. to over 4 g/cm²/k.y. in the middle of the upper Miocene and then decrease to about 2 g/cm²/k.y. in the uppermost Miocene and lower Pliocene (Fig. 54). From the lower Pliocene to the present, both carbonate and noncarbonate accumulation rates show variability around a long-term increase. The accumulation of organic carbon shows a similar pattern in the upper Miocene and lower Pliocene, but is highest in the upper Pliocene and decreases toward the present.

The high carbonate and carbon accumulation rates associated with the appearance of upwelling faunas clearly indicate that the monsoonal upwelling system was active in the late Miocene. However, other areas of the world ocean also have high accumulation rates in the late Miocene (Prell et al., 1982; Theyer et al., 1985). Thus, the question of global vs. regional causes of high productivity in the western Arabian Sea must be considered before the apparent upwelling phase of the late Miocene can be solely attributed to the relatively local monsoonal mechanism. Even so, the onset of monsoonal upwelling may occur in the middle Miocene; an interval that is largely missing at Site 721. The long-term increase in carbonate accumulation rates from the late Pliocene to the present may also reflect an increase in the intensity of monsoonal upwelling and eolian transport brought about by continued uplift of the Himalaya (Mercier et al., 1987). This long-term trend would be consistent with the gradual modification of surface boundary conditions due to tectonic mechanisms rather than with the short-term orbital, Milankovitch mechanism. The persistent continued abundance of upwelling faunas support this speculation, but the decrease in organic carbon accumulation raises questions about the variability of upwelling productivity. Alternatively, some of the intervals of low accumulation rate on the Owen Ridge may reflect changes in the depositional environment due to phases of local

Table 14. Concentrations of methane (C_1) and ethane (C_2) per liter of wet sediment in cores of Holes 721A and 721B. Also given is the ratio of C_1/C_2, an indicator of gas provenance and maturation state of organic matter.

Hole, core, section, interval (cm)	Depth (mbsf)	C_1 (μL/L)	C_2 (μL/L)	C_3 (μL/L)	C_1/C_2
117-					
721A-1H-6, 149–150	8.99	19			
721A-2H-6, 149–150	18.49	25			
721A-3H-6, 119–120	28.19	60			
721A-4H-5, 0–1	35.20	80			
721A-5H-4, 149–150	44.89	195			
721A-6H-6, 119–120	57.19	832			
721A-7H-6, 149–150	66.79	1488			
721A-8H-5, 149–150	74.79	2940	3		1131
721A-9H-6, 119–120	85.49	5421	6		847
721B-9H-4, 144–145	82.34	3766	3		1107
721B-10X-5, 149–150	93.49	4694	3		1618
721B-11X-3, 149–150	100.09	5280	5		
721B-12X-1, 144–145	106.64	4886			16286
721B-13X-4, 149–150	120.79	17625	3		5334
721B-14X-3, 149–150	128.89	19434	4		4983
721B-15X-6, 119–120	142.79	10138	3		3620
721B-16X-5, 149–150	151.29	35094	1		70188
721B-17X-5, 149–150	160.99	6426	5		1338
721B-18X-5, 119–120	170.39	35334	5		7852
721B-19X-5, 149–150	180.39	60006	5		12501
721B-20X-5, 149–150	190.09	98506	10		10261
721B-21X-2, 0–1	193.80	72608	5		16135
721B-22X-6, 0–1	209.50	74096	5		16466
721B-24X-3, 0–1	224.30	85872	5		17174
721B-25X-5, 0–1	236.50	96243	5		17823
721B-26X-3, 149–150	244.59	96960	6		16160
721B-27X-3, 119–120	253.99	111981	6		19307
721B-29X-2, 0–1	270.90	62406	4		15602
721B-30X-2, 114–115	281.84	83380	4		20845
721B-31X-3, 149–150	293.49	106544	4		23676
721B-32X-2, 149–150	301.69	89502	5		15983
721B-33X-1, 114–115	309.54	106584	7		14024
721B-34X-4, 0–1	322.50	94345	3		29483
721B-35X-2, 149–150	330.69	68718			
721B-36X-1, 114–115	338.54	119994	3		39998
721B-37X-3, 149–150	351.49	92963			
721B-40X-5, 114–115	383.04	126298			
721B-41X-5, 149–150	393.09	156886			
721B-42X-2, 149–150	398.19	125027			
721B-44X-5, 114–115	421.64	45767	2		20803

Note: Values are expressed in μL/L (volume gas/volume wet sediment).

uplift. In summary, the record at Site 721 gives ample evidence of large changes in productivity and upwelling-related faunas. The discrimination between regional vs. global causes, and the specific relationship between productivity and upwelling remain subjects for post-cruise research.

Short-term Variability and Sedimentary Cycles

The major characteristic of the Pliocene and Pleistocene sediments at Site 721 is a strong cyclicity that is documented by changes in sediment color, magnetic susceptibility, wet-bulk density, and carbonate content. If the intensity of monsoonal upwelling and eolian transport is controlled largely by variations of solar radiation, a strong cyclicity is expected in the sediments of the Owen Ridge. Preliminary analysis of over 20,000 magnetic susceptibility measurements in three holes reveal a dominant periodicity of about 1 m in length, which represents about 25 k.y. Other periodicities of about 1–2 m, 3–4 m, and 12–14 m suggest the presence of periodicities near 41 k.y., 100 k.y., and 400 k.y., respectively. These periodicities match those expected for the Milankovitch mechanism and suggest that it is a major cause of variations in monsoon intensity. A similar conclusion was reached by calculating the Walsh spectrum of sediment color changes that were classified as dark, medium, and light. Using a linear sedimentation rate over the past 2.95 m.y., we found the same periodicities that were observed in the magnetic susceptibility data. Here, we should note that these periodicities are not unique to the monsoon mechanism and that much post-cruise research is needed to identify the true monsoon spectrum. However, the sediment cycles are thought to reflect both changes in oceanic productivity/preservation and changes in the input of eolian material. Preliminary analysis of the mineralogy of the clastic fraction reveals that the concentrations of quartz and dolomite covary and are in phase with the susceptibility data. This association of minerals is consistent with an eolian source. The subject of the exact origin of the susceptibility cycles, which have been used for detailed cross-correlation between cores, and their significance with respect to monsoonal climate changes will be the major focus of the post-cruise research.

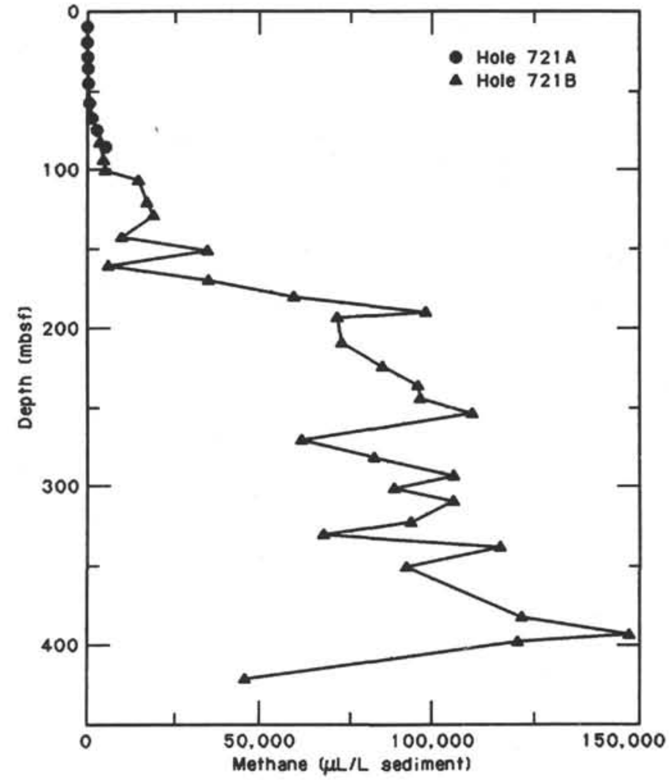

Figure 47. Downhole concentrations of methane in sediments from Holes 721A and 721B. The steep increase in concentrations below 100 mbsf coincides with the depletion of interstitial sulfate, which results in a predominance of fermentation reactions as the main mode of microbial organic matter degradation.

Table 15. Depth, organic carbon and $CaCO_3$ content, and U^k_{37} ratios of sediments from Hole 721B.

Core, section, interval (cm)	Depth (mbsf)	Organic carbon (%)	$CaCO_3$ (%)	U^k_{37}
117-721B-				
1H-1, 50–53	0.50	0.07	77.1	[a]n.k.
1H-2, 100–103	2.50	1.29	64.8	0.88
1H-4, 80–83	5.30	0.43	70.8	0.97
1H-5, 24–27	6.24	1.21	65.5	0.95
2H-1, 87–90	10.27	0.46	78.1	0.98
2H-2, 17–20	11.07	1.91	61.3	0.87
2H-3, 27–30	12.67	0.60	72.2	0.92
3H-3, 10–13	22.20	0.74	64.5	0.92

[a] n.k. = no ketones detected.

REFERENCES

Aubry, M.-P., 1984. *Handbook of Cenozoic Calcareous Nannoplankton, Book 1: Ortholithae (Discoasters)*: New York (Micropaleontology Press).

Bé, A.W.H., 1977. An ecological, zoogeographic and taxonomic review of Recent planktonic Foraminifera. *In* Ramsay, A. (Ed.), *Oceanic Micropalaeontology* (Vol. 1): London (Academic Press), 1-100.

Berggren, W. A., Kent, D. V., Flynn, J. J., and Van Couvering, J. A., 1985a. Cenozoic geochronology. *Geol. Soc. Am. Bull.*, 96:1407-1418.

Berggren, W. A., Kent, D. V., and Van Couvering, J. A., 1985b. The Neogene: Part 2, Neogene geochronology and chronostratigraphy. *In* Snelling, N. J. (Ed.), *The Chronology of the Geological Record*: Geol. Soc. Mem. (London), 10:211-260.

Brassell, S. C., Eglinton, G., Marlowe, I. T., Sarnthein, M., and Pflaumann, U., 1986. Molecular stratigraphy: a new tool for climatic assessment. *Nature*, 320:129-133.

Bryant, W. R., Bennett, R. H., and Katherman, C. E., 1981. Shear strength, consolidation, porosity, and permeability of oceanic sediments. *In* Emiliani, C. (Ed.), *The Oceanic Lithosphere: The Sea* (Vol. 7): New York (Wiley), 1555-1616.

Claypool, G. E., and Kaplan, I. R., 1974. The origin and distribution of methane in marine sediments. *In* Kaplan, I. R. (Ed.) *Natural Gases in Marine Sediments*: New York (Plenum), 94-129.

Corliss, B. H., 1979. Taxonomy of Recent deep-sea benthonic Foraminifera in the southeast Indian Ocean. *Micropaleontology*, 25:1-19.

Gardner, J. V., 1982. High-resolution carbonate and organic-carbon stratigraphies for the late Neogene and Quaternary from the eastern equatorial Pacific. *In* Prell, W. L., Gardner, J. V., et al., *Init. Repts. DSDP*, 68: Washington (U.S. Govt. Printing Office), 347-364.

Gieskes, J. M., 1981. Deep sea drilling interstitial water studies: implications for chemical alteration of the ocean crust, Layers I and II. *In* Warme, J. E., Douglas, R. C., and Winterer, E. L. (Eds.), *The Deep Sea Drilling Project: A Decade of Progress*, Soc. Econ. Paleontol. Mineral. Spec. Publ., 32:149-168.

Hahn, D. G., and Manabe, S., 1975. The role of mountains in the South Asian monsoon circulation. *J. Atmos. Sci.*, 32:1515-1541.

Hamilton, E. L., 1976. Variations of density and porosity with depth in deep-sea sediments. *J. Sediment. Petrol.*, 46:280-300.

________, 1978. Sound velocity-density relations in sea-floor sediments and rocks. *J. Acoust. Soc. Am.*, 63:366-377.

________, 1979. Sound velocity gradients in marine sediments. *J. Acoust. Soc. Am.*, 65:909-922.

Honjo, S., 1982. Seasonality and interaction of biogenic and lithogenic particulate flux at the Panama Basin. *Science*, 218:883-884.

Johnson, D. A., and Nigrini, C. A., 1985. Synchronous and time-transgressive Neogene radiolarian datum levels in the equatorial Indian and Pacific Oceans. *Mar. Micropaleontol.*, 9:489-523.

Johnson, D. A., Nigrini, C. A., Caulet, J.-P., Schneider, D., and Kent, D., in press. Pliocene-Pleistocene radiolarian events and magnetostratigraphic calibrations for the tropical Indian Ocean. *Mar. Micropaleontol.*

Kutzbach, J. E., 1981. Monsoon climate of the early Holocene: climate experiment with the earth's orbital parameters for 9000 years ago. *Science*, 214:59-61.

Mead, G. A., 1985. Recent benthic Foraminifera in the Polar Front region of the southwest Atlantic. *Micropaleontology*, 31:221-248.

Mercier, J.-T., Armijo, R., Tapponnier, P., Carey-Gailhardis, E., and Lin, H.T., 1987. Change from late Tertiary compression to Quaternary extension in Southern Tibet during the India-Asia collision. *Tectonics*, 6:275-304.

Mountain, G., and Prell, W. L., 1987. Leg 117 ODP site survey: a revised history of Owen Basin. *Eos, Trans. Am. Geophys. Union*, 68: 424.

Müller, P. J., and Suess, E., 1979. Productivity, sedimentation rate, and sedimentary organic matter in the oceans—I. Organic carbon preservation. *Deep-Sea Res.*, Part A, 26:1347-1362.

Nigrini, C. A., 1974. Cenozoic Radiolaria from the Arabian Sea, DSDP Leg 23. *In* Davies, T. A., Luyendyk, B. P., et al., *Init. Repts. DSDP*, 26: Washington (U. S. Govt. Printing Office), 1051-1121.

Perch-Nielsen, K., 1985. Cenozoic calcareous nannofossils. *In* Bolli, H., Saunders, J., and Perch-Nielsen, K. (Eds.), *Planktonic Stratigraphy*: Cambridge (Cambridge University Press), 427-554.

Pisias, N. G., and Prell, W. L., 1985. High resolution carbonate records from the hydraulic piston cored section of Site 572. *In* Mayer, L., Theyer, F., et al., *Init. Repts. DSDP*, 85: Washington (U.S. Govt. Printing Office), 711-722.

Prahl, F. G., and Wakeham, S. G., 1987. Calibration of unsaturation patterns in long-chain ketone compositions for paleotemperature assessment. *Nature*, 330:367-369.

Prell, W. L., 1984a. Variation of monsoonal upwelling: a response to changing solar radiation. *In* Hansen, J. E., and Takahashi, T. (Eds.), *Climatic Processes and Climate Sensitivity*: Washington (American Geophysical Union), Geophys. Monogr. 29, Maurice Ewing Series, 5:48-57.

________, 1984b. Monsoonal climate of the Arabian Sea during the late Quaternary: a response to changing solar radiation. *In* Berger, A., and Imbrie, J. (Eds.), *Milankovitch and Climate*: Dordrecht (D. Reidel), 349-366.

Prell, W. L., Gardner, J. V., et al., 1982. *Init. Repts. DSDP*, 68: Washington (U.S. Govt. Printing Office).

Prell, W. L., and Kutzbach, J. E., 1987. Monsoon variability over the past 150,000 years. *J. Geophys. Res.*, 92:8411-8425.

Saito, T., Burckle, L. H., and Hays, J. D., 1975. Late Miocene to Pleistocene biostratigraphy of equatorial Pacific sediments. *In* Saito, T., and Burckle L. H. (Eds.), *Late Neogene Epoch Boundaries*: New York (Micropaleontology Press), 226-244.

Sato, T., Takayama, T., Kato, M., Kudo, T., and Kameo, K., in press. Calcareous microfossil biostratigraphy of the uppermost Cenozoic formations distributed in the coast of the Japan Sea. Part 4: Conclusion. *Sekiyu Gijutsu Kyokaishi.*

Shipboard Scientific Party, 1988. Site 658. *In* Ruddiman, W., Sarntheim, M., et al., *Proc. ODP, Init. Repts.*, 108: College Station, TX (Ocean Drilling Program), 105-219.

Stumm, W., and Morgan, J. J., 1970. *Aquatic Chemistry*: New York (Wiley).

Takayama, T., and Sato, T., 1987. Coccolith biostratigraphy of the North Atlantic Ocean, Deep Sea Drilling Project Leg 94. *In* Ruddiman, W. E., Kidd, R. B., Thomas, E., et al., *Init. Repts. DSDP*, 94, Pt. 2: Washington (U.S. Govt. Printing Office), 651-702.

ten Haven, H. L., Baas, M., Kroot, M., de Leeuw, J. W., Schenck, P. A., and Ebbing, J., 1987. Late Quaternary Mediterranean sapropels: III. Assessment of source of input and palaeotemperature as derived from biological markers. *Geochim. Cosmochim. Acta*, 51: 803-810.

Theyer, F., Mayer, L. A., Barron, J. A., and Thomas, E., 1985. The equatorial Pacific high-productivity belt: elements for a synthesis of Deep Sea Drilling Project Leg 85 results. *In* Mayer, L., Theyer, F., et al., *Init. Repts. DSDP*, 85: Washington (U.S. Govt. Printing Office), 971-985.

van Morkhoven, F. P., Berggren, W. A., and Edwards, A. S., 1986. Cenozoic cosmopolitan deep-water benthic Foraminifera. *Bull. Cent. Rech. Explor.-Prod. Elf-Aquitaine, Mem.*, 11.

Weedon, G. P., 1986. Hemipelagic shelf sedimentation and climatic cycles: the basal Jurassic (Blue Lias) of South Britain. *Earth Planet. Sci. Lett.*, 76:321-325.

Whitmarsh, R. B., 1979. The Owen Basin off the southeast margin of Arabia and the evolution of the Owen Fracture Zone. *Geophys. J. R. Astron. Soc.*, 58:441-470.

Whitmarsh, R. B., Weser, O. E., Ross, D. A., et al., 1974. *Init. Repts. DSDP*, 23: Washington (U.S. Govt. Printing Office).

Ms 117A-106

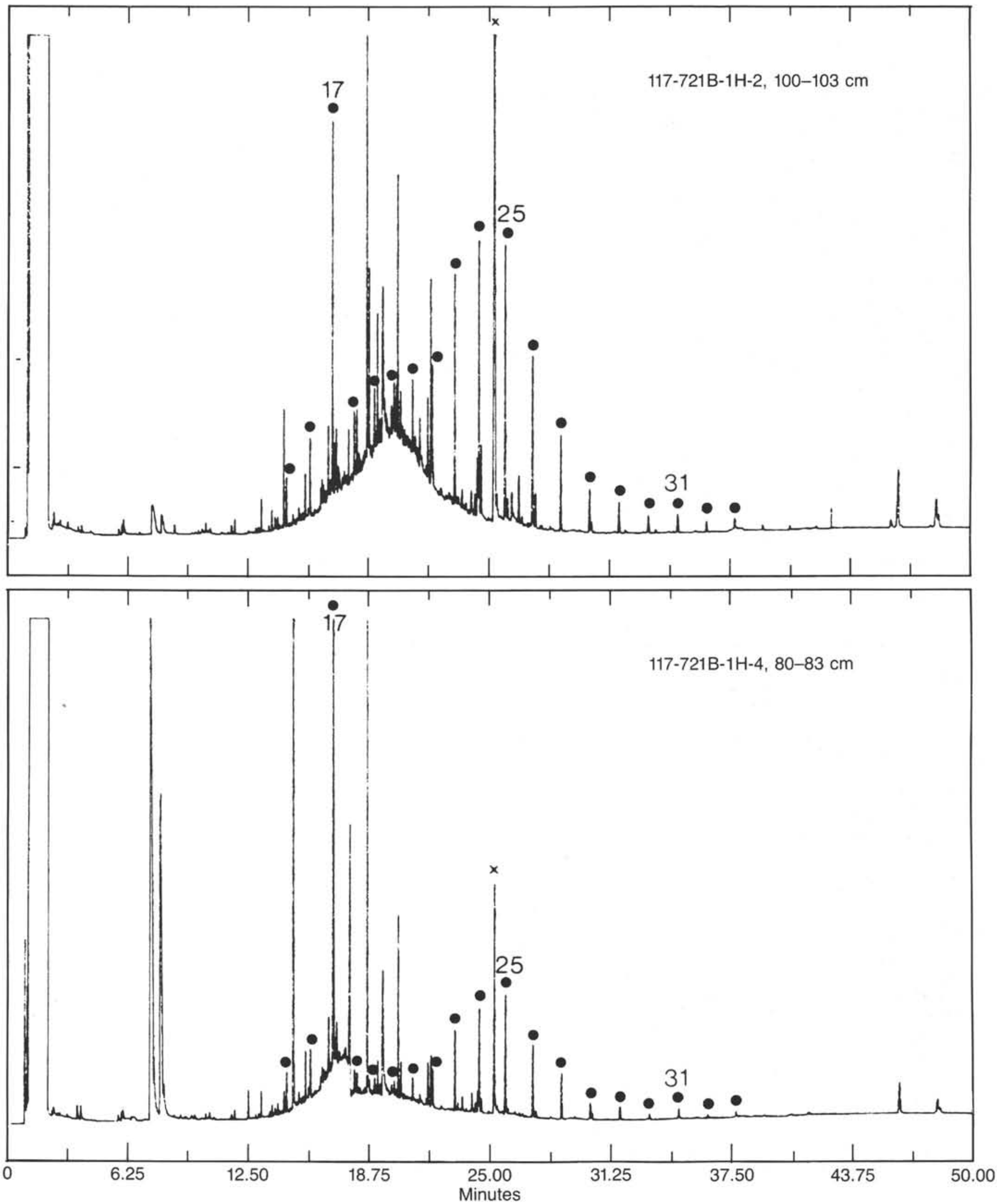

Figure 48. Gas chromatograms of extracts of four samples from Hole 721B. Dots indicate straight chain alkanes, and the number above the dots correspond with the number of carbon atoms. The cross (×) indicates a phtalate ester (contaminant), which is known to elute between C_{24} and C_{25}. Identifications of compounds are tentative.

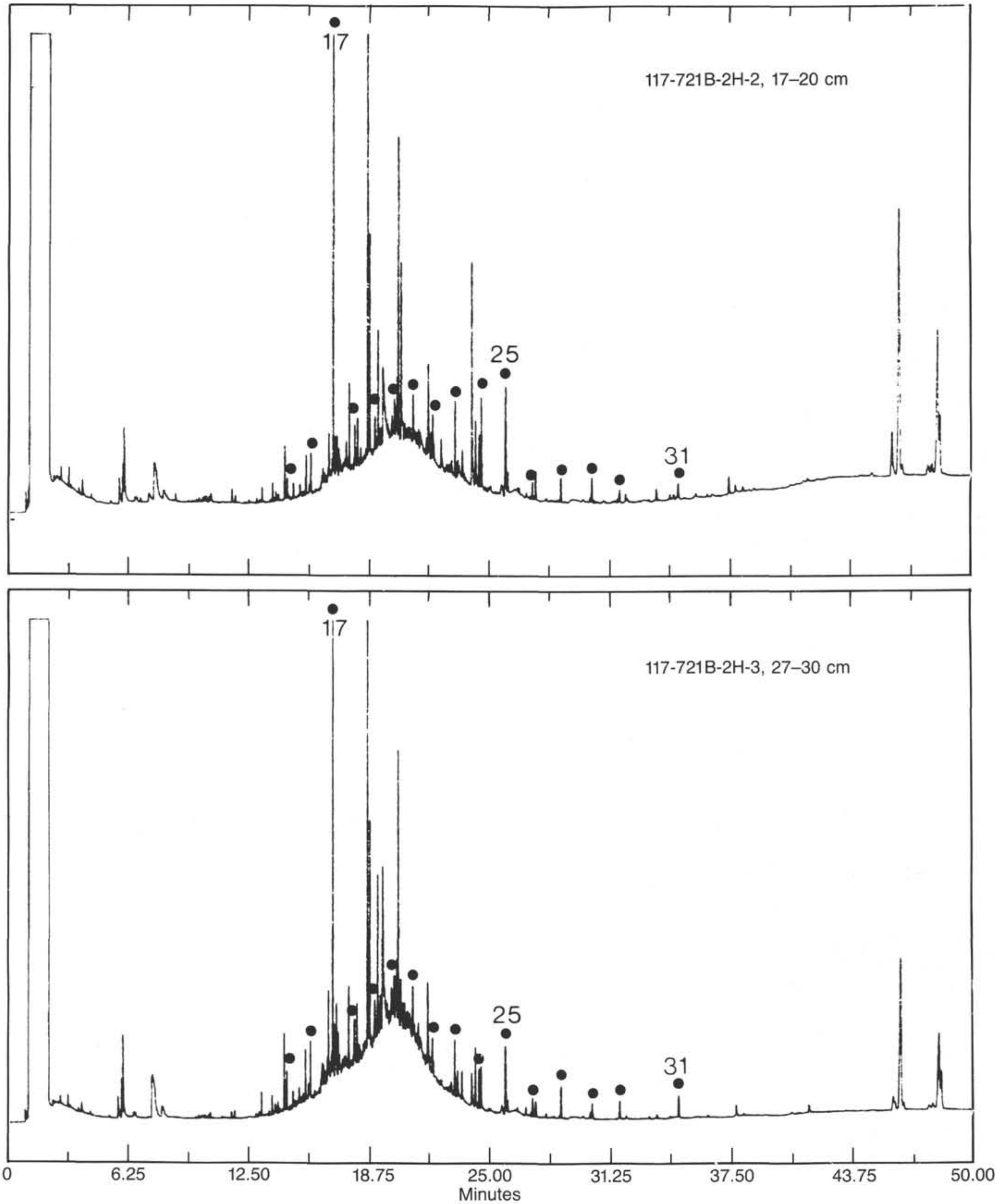

Figure 48 (continued).

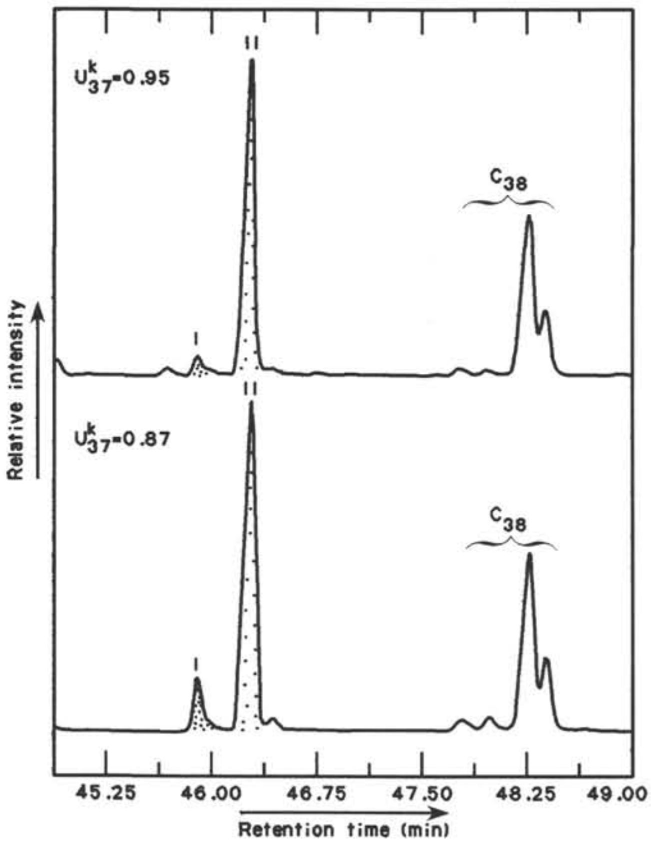

Figure 49. Detail of gas chromatogram of Sample 117-721B-1H-5, 24–27 cm (top), and Sample 117-721B-2H-2, 17–20 cm (bottom), showing the distribution of the C_{37} and C_{38} alkenones. Peak I is the triunsaturated C_{37} alkenone; Peak II is the diunsaturated C_{37} alkenone.

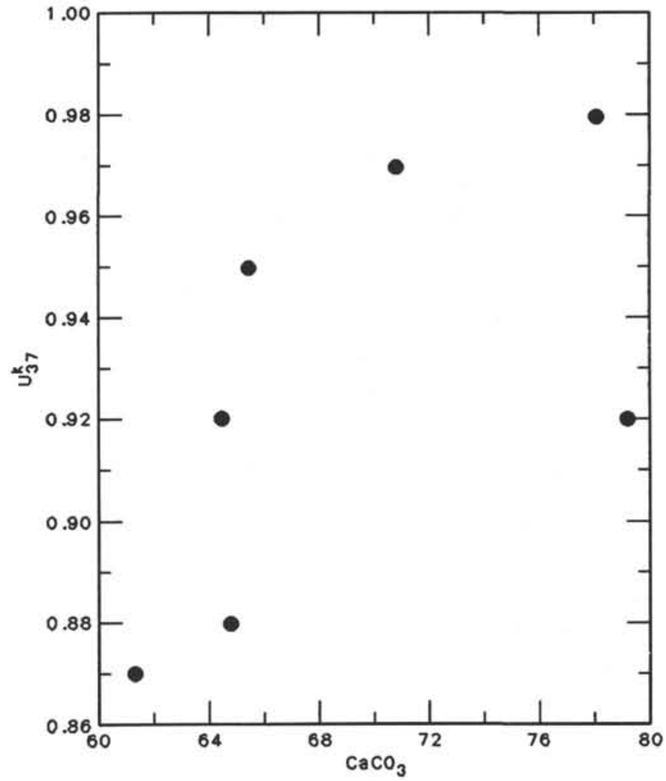

Figure 50. Crossplot of U^k_{37} vs. $CaCO_3$. Correlation coefficient r = 0.77.

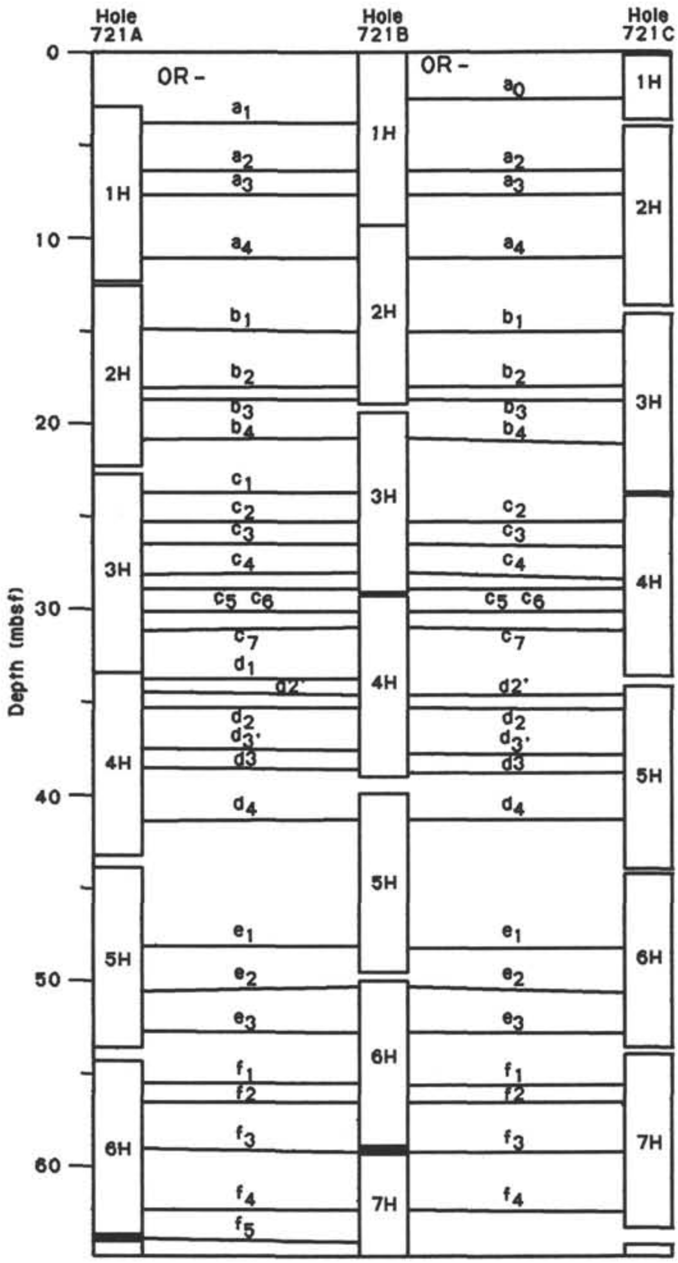

Figure 51. Correlation of Holes 721A, 721B, and 721C based on marker layers.

Table 16. Stratigraphic depths of the marker layers at Site 721.

	Hole 721A		Hole 721B			Hole 721C		
	Core, section, interval (cm)	Depth (mbsf)	Core, section, interval (cm)	Depth (mbsf)	Holes 721A–721B	Core, section, interval (cm)	Depth (mbsf)	Holes 721C–721B
117-721A-								
OR-a_0			1H-2, 105	2.55		1H-2, 95	2.45	-0.10
a_1	1H-1, 115	1.15	1H-3, 90	3.90	-2.75			
a_2	1H-3, 70	3.70	1H-5, 45	6.45	-2.75	2H-2, 95	6.05	-0.40
a_3	1H-4, 45	4.95	1H-6, 32	7.82	-2.87	2H-3, 65	7.25	-0.57
a_4	1H-6, 90	8.40	2H-2, 25	11.15	-2.75	2H-5, 105	10.65	-0.50
b_1	2H-2, 90	12.20	2H-4, 135	15.25	-3.05	3H-1, 100	14.30	-0.95
b_2	2H-4, 100	15.30	2H-6, 115	18.05	-2.75	3H-3, 95	17.25	-0.80
b_3	2H-5, 15	15.95	2H-7, 40	18.80	-2.85	3H-4, 20	18.00	-0.80
b_4	2H-6, 85	18.15	3H-1, 140	20.50	-2.35	3H-5, 100	20.30	-0.20
c_1	3H-1, 100	20.50	3H-3,130	23.40	-2.90			
c_2	3H-2, 100	22.00	3H-4, 130	24.90	-2.90	4H-1, 140	24.40	-0.50
c_3	3H-3, 80	23.30	3H-5, 105	26.15	-2.85	4H-2, 125	25.75	-0.40
c_4	3H-4, 90	24.90	3H-6, 110	27.70	-2.80	4H-3, 145	27.45	-0.25
c_5	3H-5, 25	25.75	3H-7, 50	28.60	-2.85	4H-4, 55	28.05	-0.55
c_6	3H-5, 135	26.85	4H-1, 75	29.55	-2.70	4H-5, 35	29.35	-0.20
c_7	3H-6, 85	27.85	4H-2, 20	30.50	-2.65	4H-5, 120	30.20	-0.30
d_1	4H-1, 40	29.60	4H-4, 0	33.30	-3.70			
$d_{2'}$	4H-1, 100	30.20	4H-4, 70	34.00	-3.80	5H-1, 50	33.20	-0.80
d_2	4H-2, 40	31.10	4H-4, 145	34.75	-3.65	5H-1, 130	34.00	-0.75
$d_{3'}$	4H-3, 105	33.25	4H-6, 85	37.15	-3.90	5H-3, 70	36.40	-0.75
d_3	4H-4, 60	34.30	4H-7, 30	38.10	-3.80	5H-4, 0	37.20	-0.90
d_4	4H-6, 45	37.15	5H-1, 125	39.75	-2.60	5H-5, 105	39.75	0.00
e_1	5H-3, 130	43.20	5H-6, 75	46.75	-3.55	6H-3, 110	46.50	-0.25
e_2	5H-5, 70	45.60	6H-1, 35	48.45	-2.85	6H-5, 60	49.00	-0.55
e_3	5H-6, 130	47.70	6H-2, 130	50.90	-3.20	6H-H, 130	51.20	0.30
f_1	6H-1, 130	49.80	6H-4, 115	53.75	-3.95	7H-2, 15	53.65	-0.10
f_2	6H-2, 75	50.75	6H-5, 60	54.70	-3.95	7H-2, 110	54.60	-0.10
f_3	6H-4, 30	53.30	6H-7, 15	57.25	-3.95	7H-4, 80	57.30	0.05
f_4	6H-6, 60	56.60	7H-3, 45	60.85	-4.25	7H-6, 100	60.50	-0.35
f_5	6H-7, 70	58.20	7H-4, 65	62.55	-4.35			
g_1	7H-2, 25	59.55	7H-5, 45	63.85	-4.30	8H-1, 130	62.60	-1.25
g_2	7H-4, 65	62.95	8H-1, 85	67.75	-4.80	8H-4, 25	66.05	-1.70
g_3	7H-5, 30	64.10	8H-2, 50	68.90	-4.80	8H-4, 140	67.20	-1.70
g_4	7H-6, 50	65.80	8H-3, 70	70.60	-4.80	8H-6, 10	68.90	-1.70
h_1	8H-3, 140	71.70	8H-7, 50	76.40	-4.70	9H-4, 105	76.35	-0.05
h_2	8H-4, 50	72.30	9H-1, 35	76.75	-4.45	9H-5, 15	76.95	0.20
h_3	8H-5, 70	74.00	9H-2, 60	78.50	-4.50	9H-6, 25	78.55	0.05
h_4	8H-7, 50	76.80	9H-4, 40	81.30	-4.50			
i_1	9H-1, 45	77.25	9H-5, 45	82.85	-5.60	10H-1, 135	81.65	-1.20
i_2	9H-3, 40	80.20	9H-7, 40	85.80	-5.60	10H-3, 115	84.45	-1.35
i_*	9H-4, 140	82.70	10X-2, 50	88.00	-5.30	10H-5, 70	87.00	-1.00
i_3	9H-6, 100	85.30	10X-4, 25	90.75	-5.45	10H-7, 60	89.90	-0.85
i_4	9H-7, 65	86.45	10X-4, 120	91.70	-5.25	11X-1, 70	90.60	-1.10
i_5			10X-6, 75	94.25		11X-3, 40	93.30	-0.95
j_1			11X-1, 120	96.80		11X-4, 90	95.30	-1.50
j_2			11X-2, 130	98.40		11X-5, 100	96.90	-1.50
j_3			11X-3, 70	99.30		12X-1, 85	100.35	1.05
j_4			11X-4, 65	100.75		12X-2, 90	101.90	1.15
j_5			11X-5, 90	102.50		12X-3, 125	103.75	-1.25
k_1			12X-1, 55	105.75		12X-4, 130	105.30	-0.45
l_1			13X-1, 60	115.40		13X-1, 90	110.00	-5.40
l_2			13X-2, 60	116.90		13X-2, 55	111.15	-5.75
l_3			13X-4, 40	119.70		13X-4, 15	113.75	-5.95
l_4			13X-6, 30	122.30		14X-2,45	120.65	-1.65
m_1			14X-2, 115	127.05		14X-4, 40	123.60	-3.45
m_2			14X-3, 120	128.60		14X-5, 55	125.25	-3.35
m_3			14X-4, 70	129.60		15X-1, 60	128.90	-0.70
n_1			15X-1, 75	134.85		15X-4, 140	134.20	-0.65
n_2			15X-2, 135	136.95		15X-6, 45	136.25	-0.70
n_3			15X-3, 130	138.40				

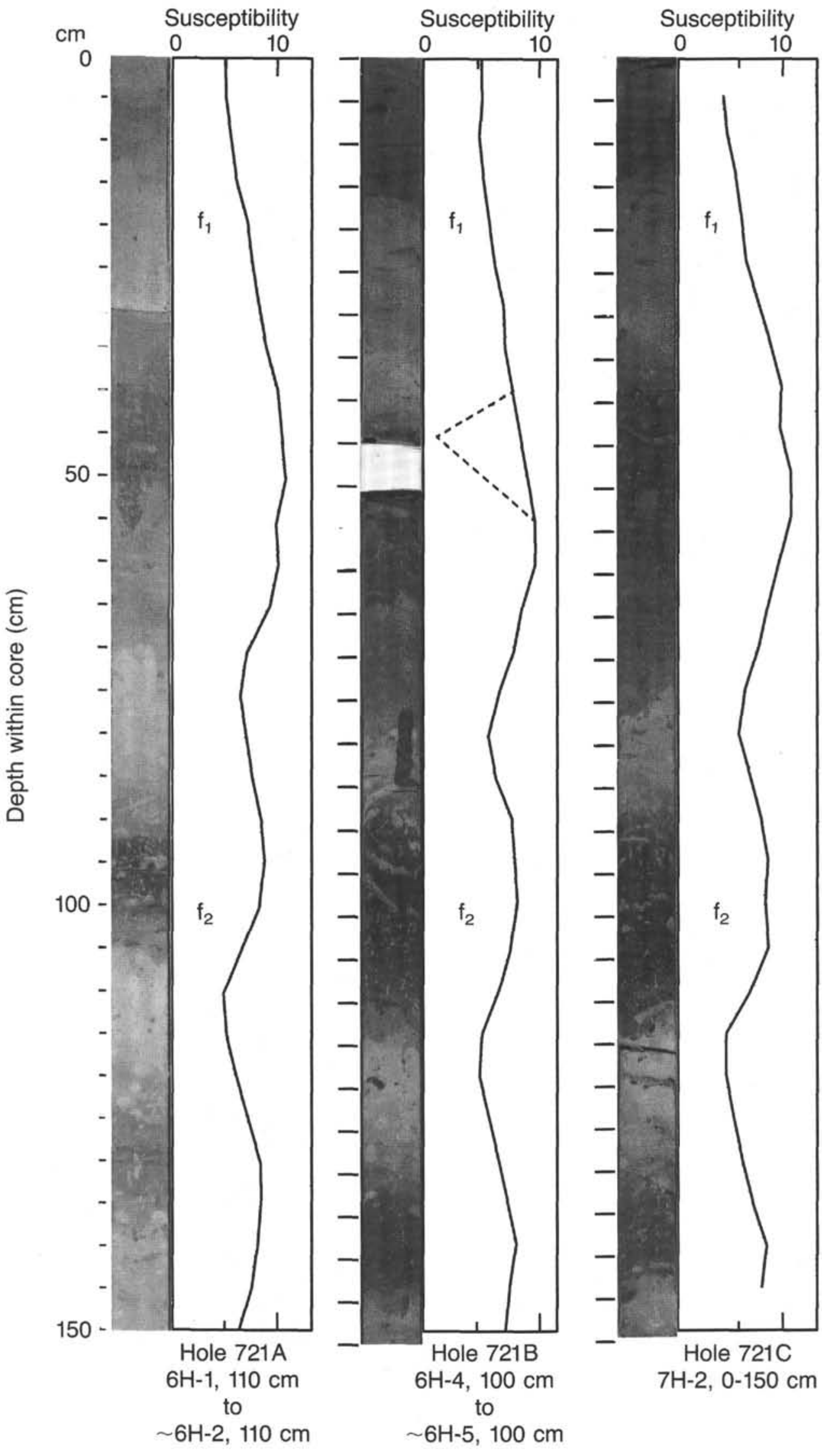

Figure 52. Example of the correlations by visual and magnetic susceptibility methods. The correlative interval corresponds to layer f_1 and f_2.

Table 17. Correction factor for stratigraphic depth calculation from depth based on ODP CORELOG data.

	Hole 721A			Hole 721B				Hole 721C		
Core	ODP, top depth (mbsf)	Difference	Corrected top depth (mbsf)	ODP top depth (mbsf)	Difference	Offset (m)	Corrected top depth (mbsf)	ODP top depth (mbsf)	Difference	Corrected top depth (mbsf)
1	0.0	2.8	2.8	0.0	0.0		0.0	0.0	0.1	0.1
2	9.8	0.1	12.7	9.4	0.0	0.0	9.4	3.6	0.4	4.1
3	19.5	0.5	22.9	19.1	0.5	0.6	19.6	13.3	0.4	14.2
4	29.2	1.0	33.6	28.8	0.2	0.2	29.5	23.0	0.2	24.1
5	38.9	[a]1.0-0.3	44.0	38.5	[a]1.2-0.3	0.9	40.1	32.7	0.5	34.3
6	48.5	0.8	54.4	48.1	0.4	0.4	50.1	42.4	0.2	44.2
7	57.8	0.1	63.8	57.4	−0.3	−0.3	59.1	52.0	0.3	54.1
8	67.3	0.0	73.3	66.9	−0.5	−0.4	68.2	61.3	0.9	64.3
9	76.8	1.1	83.9	76.4	0.2	0.2	77.9	70.8	−1.7	72.1
10				86.0	0.3	0.3	87.8	80.3	1.5	83.1
11				95.6		−0.4	97.0	89.9	0.1	92.8
12				105.2		−1.7	104.9	99.5	−2.7	99.7
13				114.8		−5.7	109.1	109.1		109.1
14				124.4		−1.7	117.0	118.7	−4.0	114.7
15				134.1		0.0	126.7	128.3	−2.7	121.6

Note: Difference is between the depth calculated by the ODP CORELOG data and assigned depth, and depth calculated by the layer-by-layer correlation method. Offset = correction factor for stratigraphic depth calculation.
[a] Corrected for void at Core 721A-4H-5, 0–30 cm.

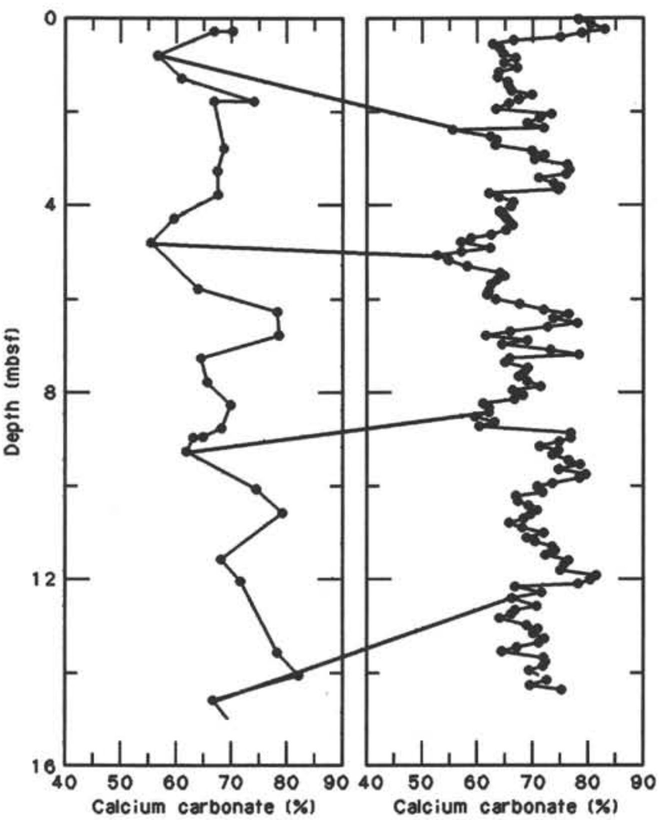

Figure 53. Correlation of calcium carbonate profiles from Hole 721A on left and site survey piston core RC2761 on right (Prell, unpubl. data).

Table 18. Depth of the marker layers in Hole 721B, based on the correction factor of Table 17. Depth based on ODP CORELOG data.

	Hole 721A			Hole 721B			Hole 721C		
	Core, section, interval (cm)	Curated depth (mbsf)	Corrected depth (m)	Core, section, interval (cm)	Curated depth (mbsf)	Corrected depth (m)	Core, section, interval (cm)	Curated depth (mbsf)	Corrected depth (m)
OR-a_0				1H-2, 105	2.55	2.55	1H-2, 95	2.45	2.55
a_1	1H-1, 115	1.15	3.95	1H-3, 90	3.90	3.90			
a_2	1H-3, 70	3.70	6.50	1H-5, 45	6.45	6.45	2H-2, 95	6.05	6.55
a_3	1H-4, 45	4.95	7.75	1H-6, 32	7.82	7.82	2H-3, 65	7.25	7.75
a_4	1H-6, 90	8.40	11.20	2H-2, 25	11.15	11.15	2H-5, 105	10.65	11.15
b_1	2H-2, 90	12.20	15.10	2H-4, 135	15.25	15.25	3H-1, 100	14.30	15.20
b_2	2H-4, 100	15.30	18.20	2H-6, 115	18.05	18.05	3H-3, 95	17.25	18.15
b_3	2H-5, 15	15.95	18.85	2H-7, 40	18.80	18.80	3H-4, 20	18.00	18.90
b_4	2H-6, 85	18.15	21.05	3H-1, 140	20.50	21.00	3H-5, 100	20.30	21.20
c_1	3H-1, 100	20.50	23.90	3H-3, 130	23.40	23.90			
c_2	3H-2, 100	22.00	25.40	3H-4, 130	24.90	25.40	4H-1, 140	24.40	25.50
c_3	3H-3, 80	23.30	26.70	3H-5, 105	26.15	26.65	4H-2, 125	25.75	26.85
c_4	3H-4, 90	24.90	28.30	3H-6, 110	27.70	28.20	4H-3, 145	27.45	28.55
c_5	3H-5, 25	25.75	29.15	3H-7, 50	28.60	29.10	4H-4, 55	28.05	29.15
c_6	3H-5, 135	26.85	30.25	4H-1, 75	29.55	30.25	4H-5, 35	29.35	30.45
c_7	3H-6, 85	27.85	31.25	4H-2, 20	30.50	31.20	4H-5, 120	30.20	31.30
d_1	4H-1, 40	29.60	34.00	4H-4, 0	33.30	34.00			
$d_{2'}$	4H-1, 100	30.20	34.60	4H-4, 70	34.00	34.70	5H-1, 50	33.20	34.80
d_2	4H-2, 40	31.10	35.50	4H-4, 145	34.75	35.45	5H-1, 130	34.00	35.60
$d_{3'}$	4H-3, 105	33.25	37.65	4H-6, 85	37.15	37.85	5H-3, 70	36.40	38.00
d_3	4H-4, 60	34.30	38.70	4H-7, 30	38.10	38.80	5H-4, 0	37.20	38.80
d_4	4H-6, 45	37.15	41.55	5H-1, 125	39.75	41.35	5H-5, 105	39.75	41.35
e_1	5H-3, 130	43.20	48.30	5H-6, 75	46.75	48.35	6H-3, 110	46.50	48.30
e_2	5H-5, 70	45.60	50.70	6H-1, 35	48.45	50.45	6H-5, 60	49.00	50.80
e_3	5H-6, 130	47.70	52.80	6H-2, 130	50.90	52.90	6H-6, 130	51.20	53.00
f_1	6H-1, 130	49.80	55.70	6H-4, 115	53.75	55.75	7H-2, 15	53.65	55.75
f_2	6H-2, 75	50.75	56.65	6H-5, 60	54.70	56.70	7H-2, 110	54.60	56.70
f_3	6H-4, 30	53.30	59.20	6H-7, 15	57.25	59.25	7H-4, 80	57.30	59.40
f_4	6H-6, 60	56.60	62.50	7H-3, 45	60.85	62.55	7H-6, 100	60.50	62.60
f_5	6H-7, 70	58.20	64.10	7H-4, 65	62.55	64.25			
g_1	7H-2, 25	59.55	65.55	7H-5, 45	63.85	65.55	8H-1, 130	62.60	65.60
g_2	7H-4, 65	62.95	68.95	8H-1, 85	67.75	69.05	8H-4, 25	66.05	69.05
g_3	7H-5, 30	64.10	70.10	8H-2, 50	68.90	70.20	8H-4, 140	67.20	70.20
g_4	7H-6, 50	65.80	71.80	8H-3, 70	70.60	71.90	8H-6, 10	68.90	71.90
h_1	8H-3, 140	71.70	77.70	8H-7, 50	76.40	77.70	9H-4, 105	76.35	77.65
h_2	8H-4, 50	72.30	78.30	9H-1, 35	76.75	78.25	9H-5, 15	76.95	78.25
h_3	8H-5, 70	74.00	80.00	9H-2, 60	78.50	80.00	9H-6, 25	78.55	79.85
h_4	8H-7, 50	76.80	82.80	9H-4, 40	81.30	82.80			
i_1	9H-1, 45	77.25	84.35	9H-5, 45	82.85	84.35	10H-1, 135	81.65	84.45
i_2	9H-3, 40	80.20	87.30	9H-7, 40	85.80	87.30	10H-3, 115	84.45	87.25
i^*	9H-4, 140	82.70	89.80	10H-2, 50	88.00	89.80	10H-5, 70	87.00	89.80
i_3	9H-6, 100	85.30	92.40	10H-4, 25	90.75	92.55	10H-7, 60	89.90	92.70
i_4	9H-7, 65	86.45	93.55	10H-4, 120	91.70	93.50	11X-1, 70	90.60	93.50
i_5				10H-6, 75	94.25	96.05	11X-3, 40	93.30	96.20
j_1				11H-1, 120	96.80	98.20	11X-4, 90	95.30	98.20
j_2				11H-2, 130	98.40	99.80	11X-5, 100	96.90	99.80
j_3				11H-3, 70	99.30	100.70	12X-1, 85	100.35	100.55
j_4				11H-4, 65	100.75	102.15	12X-2, 90	101.90	102.10
j_5				11H-5, 90	102.50	103.90	12X-3, 125	103.75	103.95
k_1				12H-1, 55	105.75	105.45	12X-4, 130	105.30	105.50
l_1				13H-1, 60	115.40	109.70	13X-1, 90	110.00	110.00
l_2				13H-2, 60	116.90	111.20	13X-2, 55	111.15	111.15
l_3				13H-4, 40	119.70	114.00	13X-4, 15	113.75	113.75
l_4				13H-6, 30	122.30	116.90	14X-2, 45	120.65	116.65
m_1				14H-2, 115	127.05	119.65	14X-4, 40	123.60	119.60
m_2				14H-3, 120	128.60	121.20	14X-5, 55	125.25	121.25
m_3				14H-4, 70	129.60	122.20	15X-1, 60	128.90	122.20
n_1				15H-1, 75	134.85	127.45	15X-4, 140	134.20	127.50
n_2				15H-2, 135	136.95	129.55	15X-6, 45	136.25	129.55
n_3				15H-3, 130	138.40	131.00			

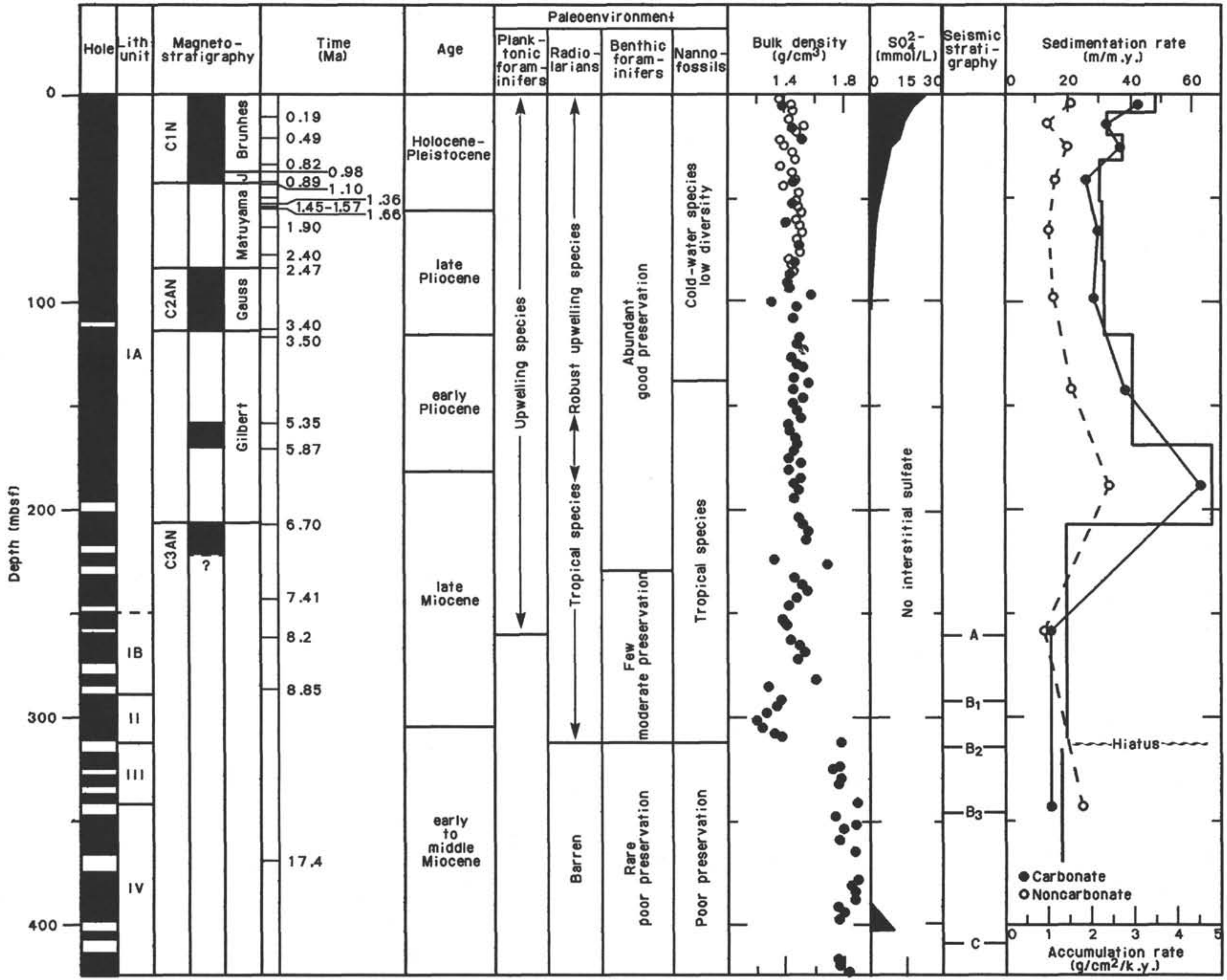

Figure 54. Summary chart outlining preliminary shipboard findings at Site 721.